

Ultimate toughness of amorphous polymers

Citation for published version (APA):

Sanden, van der, M. C. M. (1993). *Ultimate toughness of amorphous polymers*. [Phd Thesis 1 (Research TU/e / Graduation TU/e), Chemical Engineering and Chemistry]. Technische Universiteit Eindhoven.
<https://doi.org/10.6100/IR406651>

DOI:

[10.6100/IR406651](https://doi.org/10.6100/IR406651)

Document status and date:

Published: 01/01/1993

Document Version:

Publisher's PDF, also known as Version of Record (includes final page, issue and volume numbers)

Please check the document version of this publication:

- A submitted manuscript is the version of the article upon submission and before peer-review. There can be important differences between the submitted version and the official published version of record. People interested in the research are advised to contact the author for the final version of the publication, or visit the DOI to the publisher's website.
- The final author version and the galley proof are versions of the publication after peer review.
- The final published version features the final layout of the paper including the volume, issue and page numbers.

[Link to publication](#)

General rights

Copyright and moral rights for the publications made accessible in the public portal are retained by the authors and/or other copyright owners and it is a condition of accessing publications that users recognise and abide by the legal requirements associated with these rights.

- Users may download and print one copy of any publication from the public portal for the purpose of private study or research.
- You may not further distribute the material or use it for any profit-making activity or commercial gain
- You may freely distribute the URL identifying the publication in the public portal.

If the publication is distributed under the terms of Article 25fa of the Dutch Copyright Act, indicated by the "Taverne" license above, please follow below link for the End User Agreement:

www.tue.nl/taverne

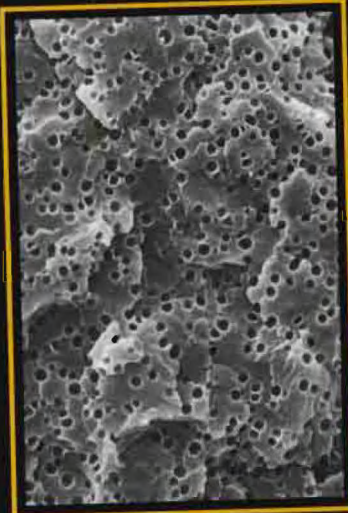
Take down policy

If you believe that this document breaches copyright please contact us at:

openaccess@tue.nl

providing details and we will investigate your claim.

Ultimate Toughness of Amorphous Polymers



M.C.M. van der Sanden

Ultimate Toughness
of
Amorphous Polymers

CIP-DATA KONINKLIJKE BIBLIOTHEEK, DEN HAAG

Sanden, Marcellus Cornelis Maria van der

Ultimate toughness of amorphous polymers / Marcellus
Cornelis Maria van der Sanden. - Eindhoven : Eindhoven

University of Technology

Thesis Eindhoven. - With ref.

ISBN 90-386-0013-5

Subject headings: polymers ; toughness.

Cover: Scanning electron micrograph of a fracture surface of a (high-density) polystyrene foam obtained via thermally induced phase separation (solvent: n-butanol)

Omslag: Elektronen mikroskopie opname van een breukvlak van een (hogedichtheid) polystyreen schuim verkregen via thermisch geïnduceerde fase-scheiding (oplosmiddel: n-butanol)

Ultimate Toughness
of
Amorphous Polymers

PROEFSCHRIFT

ter verkrijging van de graad van doctor aan de Technische Universiteit Eindhoven, op gezag van de Rector Magnificus, prof.dr. J.H. van Lint, voor een commissie aangewezen door het College van Dekanen in het openbaar te verdedigen op maandag 13 december 1993 om 16.00 uur

door

Marcellus Cornelis Maria van der Sanden

Geboren te Valkenswaard

Dit proefschrift is goedgekeurd door

de promotoren:

prof.dr.ir. H.E.H. Meijer

prof.dr. P.J. Lemstra

Contents

Chapter 1 Introduction

1.1	Ultimate Properties	1
1.2	Molecular Network Structure	3
1.3	Natural Draw Ratio	7
1.4	Deformation Mechanisms	8
	1.4.1 Crazeing	8
	1.4.2 Shear Yielding	10
	1.4.3 Crazeing versus Shear Yielding	11
1.5	Natural Draw Ratio versus Local Strain	12
1.6	Toughness Improvement in Practice	14
	1.6.1 Plasticization	14
	1.6.2 Rubber Modification	15
1.7	Scope of the Thesis	18
1.8	References	21

Chapter 2 The Concept of a Critical Thickness

2.1	Introduction	23
2.2	Experimental	24
	2.2.1 Sample preparation	24
	2.2.2 Mechanical testing	26
	2.2.3 Scanning electron microscopy	26
2.3	Results and Discussion	26
	2.3.1 The structure of multilayered tapes of PS/PE	26
	2.3.2 Mechanical properties of PS tapes	28
	2.3.3 Rubber-modified PS	31
2.4	Conclusions	35
	2.4.1 Local thickness	35
	2.4.2 Influence of network density	36
2.5	References	38

Chapter 3 Influence of Entanglement Density

3.1	Introduction	39
3.2	Experimental	40
	3.2.1 Materials	40
	3.2.2 Sample preparation	40
	3.2.3 Mechanical testing	41
	3.2.4 Dynamic mechanical thermal analysis	42
	3.2.5 Scanning electron microscopy	42
	3.2.6 D.s.c. measurements	43
3.3	Results and Discussion	43
	3.3.1 Characterization of layered PS-PPE/PE tapes and (rubber-modified) PS-PPE blends	43
	3.3.2 Mechanical properties of multilayered PS-PPE/PE tapes	48
	3.3.3 Mechanical properties of rubber-modified PS-PPE blends	49
	3.3.4 Fracture surfaces	53
3.4	Theoretical Considerations	54
	3.4.1 Macroscopic strain	54
	3.4.2 Critical microscopic thickness	55
3.5	Conclusions	60
3.6	References	61

Chapter 4 Influence of Crosslink Density

4.1	Introduction	63
4.2	Experimental	65
	4.2.1 Materials	65
	4.2.2 Sample preparation	65
	4.2.3 Crosslink density	66
	4.2.4 Mechanical properties	67
	4.2.5 Microscopy	68
4.3	Results and Discussion	68
	4.3.1 Crosslink density	68
	4.3.2 Morphology	71
	4.3.3 Strain to break	71
	4.3.4 Fracture toughness	74

4.3.5	Impact toughness	76
4.3.6	Optical microscopy	80
4.3.7	Critical ligament thickness	81
4.4	Conclusions	84
4.5	References	86
 Chapter 5 Influence of Strain rate and Temperature		
5.1	Introduction	87
5.2	Experimental	91
5.2.1	Materials	91
5.2.2	Sample preparation	91
5.2.3	Mechanical testing	91
5.3	Results and Discussion	92
5.3.1	Unnotched samples	92
5.3.2	Notched samples	94
5.4	Conclusions	105
5.5	References	106
 Chapter 6 A Critical Examination of Multilayered Structures		
6.1	Introduction	107
6.2	Experimental	109
6.2.1	Materials	109
6.2.2	Sample preparation	110
6.2.3	Interlayer adhesion	110
6.2.4	Microscopy	111
6.2.5	Mechanical testing	111
6.2.6	Microscopy during tensile testing	112
6.3	Results and Discussion	112
6.3.1	Interfacial adhesion	112
6.3.2	Mechanical testing	113
6.3.3	Microscopy during tensile testing	116
6.3.4	Modelling of the first transition	119
6.3.5	Increase in interlayer adhesion	120
6.3.6	Modelling of the second transition	121

6.4	Conclusions	124
6.5	References	126
Appendix 6.A	The derivation of the critical thickness in films from craze growth analysis according to Kramer	127
Chapter 7	Critical Thickness of Diluted Entanglement Networks	
7.1	Introduction	129
7.2	Experimental	130
	7.2.1 Materials	130
	7.2.2 Sample preparation	131
	7.2.3 Scanning electron microscopy	131
	7.2.4 Mechanical testing	131
7.3	Results and Discussion	131
	7.3.1 Network density and natural draw ratio	131
	7.3.2 Slow-speed tensile testing	133
7.4	Conclusions	135
7.5	References	137
Chapter 8	Influence of Dispersed Rubbery Phase	
8.1	Introduction	139
8.2	Experimental	140
	8.2.1 Materials	140
	8.2.2 Sample preparation	141
	8.2.3 Microscopy	141
	8.2.4 Irradiation	141
	8.2.5 Dynamic mechanical thermal analysis	142
	8.2.6 Molar mass measurements	142
	8.2.7 Mechanical testing	142
8.3	Results	143
	8.3.1 Slow-speed tensile testing	144
	8.3.2 Notched, high-speed tensile testing	145
8.4	Discussion	154
	8.4.1 An illustrative example	157

8.5	Conclusions	159
8.6	References	161
Chapter 9	The Influence of Network and Microscopic Structure	
9.1	Introduction	163
9.2	The Phenomenon of a Material-Specific Critical Thickness	164
9.3	Polystyrene Sub-micron Engineering Foam	168
	Summary	171
	Samenvatting	175
	Acknowledgements	178
	Curriculum Vitae	181

Chapter 1

Introduction

1.1 Ultimate Properties

The main feature which sets polymers apart from other materials are the constituting elements: long chain macromolecules. The main characteristic of the macromolecular chain is that the chemical bonding is strong and directional along the chain whereas usually only weak secondary (e.g. Van der Waals) interactions exist between the chains in the case of apolar polymers and occasionally hydrogen-bonding for example in polyamides.

Polymeric materials were usually not associated with impressive mechanical properties for engineering purposes. In fact, the generic term "plastic" for (thermoplastic) polymeric materials is indicative for the generally expected mechanical performance.

However, in the past two decades impressive progress has been made in exploiting the intrinsic properties of the macromolecular chain in producing high-strength/high-stiffness structures viz. fibres and tapes. Amongst the various developments in the area of these so-called high-performance fibres, two major routes can be discerned which are completely different in respect of the base materials, respectively rigid chain molecules as opposed to flexible macromolecules. The prime examples of rigid chain polymers are the aromatic polyamides, notably poly(p-phenylene terephthalamide), PPTA. Fibres based on aligned PPTA macromolecules are produced by DuPont (Kevlar[®]) and AKZO (Twaron[®]) with Young's moduli of 90 GPa and tensile strengths of 3 GPa. The prime example of a high-performance fibre based on flexible macromolecules is (high molecular weight) polyethylene. High-strength polyethylene fibres are produced by DSM (Dyneema[®]) via solution-spinning of ultra-high-molecular-weight polyethylene followed by an (ultra)drawing process. The paramount factors controlling drawability and related tensile properties are understood in molecular terms. Upon dissolution of ultra-high-molecular weight polyethylene, the long chain macromolecules become disentangled and the

disentangled structure is retained upon quenching/crystallization in the gel or solid state. Ultra-drawing in the solid state, in a temperature range close to but below the melting point, is feasible since the polyethylene crystals do not resist deformation and the number of entanglements which act as physical crosslinks on the time scale of the drawing operation have been removed to a large extent during the dissolution procedure. The maximum draw ratio, λ_{\max} , is related to the square root of the molecular weight between entanglements M_e , $\lambda_{\max} \propto M_e^{1/2}$, whereas M_e is inversely proportional to the polymer volume fraction ϕ in solution, see equation (1.1) for the dependence of λ_{\max} on M_e and ϕ ¹.

$$\lambda_{\max} \propto (M_e / \phi)^{1/2} \quad (1.1)$$

In contrast with the ultimate properties like stiffness and strength, the **ultimate toughness** of polymeric materials, another important engineering property, is poorly understood as demonstrated by numerous papers with conflicting views and often system related specific results which lack generality.

Toughness can be considered, in a first approximation, as the work to break during (tensile) deformation viz. the area of the stress-strain curve during loading the specimen to failure. In this respect, toughness should be related to the deformation of an entanglement network rather similar to tensile drawing for obtaining high-strength/high-modulus oriented fibrous structures.

In contrast with crystallizable polymers like polyethylene and polypropylene, the entanglement network in the case of amorphous polymers can not be changed via a dissolution procedure. Disentangling can be achieved by dissolving the amorphous polymer but the disentangled state cannot be made permanent via crystallization and, consequently, upon removal of solvent, re-entanglement occurs. Hence, in the case of amorphous, glassy polymers, the entanglement network is dictated by the macromolecular chemical structure (see section 1.2). Information concerning the entanglement network structure in the solid state can be obtained via equilibrium rheological measurements since the molecular weight between entanglement nodes, M_e , can be derived from the rubber plateau modulus in the melt ² (see section 1.2). In this respect, polystyrene can be considered as a rather loose network, the value for M_e is appr. 20 kg mol⁻¹ to be compared with polycarbonate and polyethylene, M_e is appr. 2 kg mol⁻¹ ³.

Transferring the basic principles of drawing (disentangled) semi-crystalline polymers (read: polyethylene) one would expect polystyrene to be a rather tough polymer in comparison with polycarbonate. The maximum or **natural** draw ratio can be estimated from M_e and is expected to be appr. 4 or an elongation at break of about 300% ⁴. In the early eighties, Kramer et al. ⁵ performed pioneering and elegant experiments which showed that the maximum extension ratios in craze fibrils and shear deformation zones in amorphous glassy polymers, including polystyrene and polycarbonate, corresponded with the natural draw ratio calculated from M_e using equation (1.1), $\phi = 1$. These important experiments demonstrate that the basic principles viz. the maximum draw ratio is determined by fully stretching the molecular strands between entanglement nodes, can be applied during deformation of glassy amorphous polymers.

In actual practice, however, polystyrene is the paradigm of a **brittle** polymer with a **macroscopic elongation at break** of 1-3% whereas polycarbonate is considered to be a tough engineering plastic. This paradox initiated the present study and is the main issue for this thesis.

1.2 Molecular Network Structure

Using small-angle neutron scattering, Kirste et al. ⁶ demonstrated that the conformation of macromolecules of amorphous polymers in the glassy state is equal to its conformation in a Theta solvent (and in the melt), i.e. the so-called unperturbed chain.

From viscosity measurements performed on melts of polystyrene it is known that above a certain critical molecular weight of polystyrene the viscosity suddenly strongly increases: see *figure 1.1* ⁷.

This effect is attributed to *entanglement coupling*; above a certain critical molecular weight (M_{cr}) entanglements are formed. The formation of entanglements above the critical molecular weight can also be noticed in an evaluation of the storage modulus, G' , of narrow-distribution polystyrenes with varying molecular weight as a function of the reduced frequency (see *figure 1.2*) ⁸.

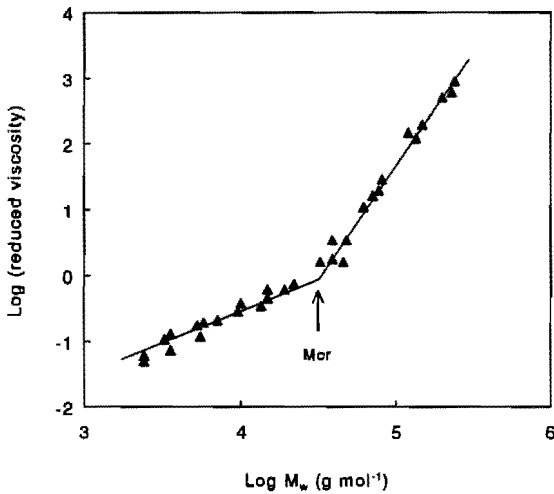


Figure 1.1 Log-log plot of reduced melt viscosity as a function of weight-average molar mass for polystyrene (reproduced with permission from reference 7)

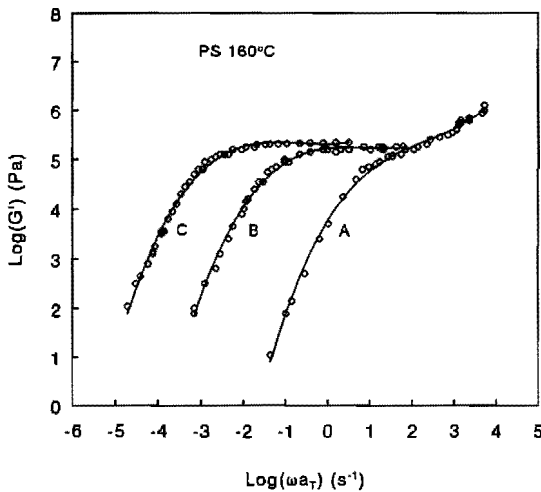


Figure 1.2 Storage modulus of narrow-distribution polystyrenes, plotted logarithmically against frequency reduced to 160°C as a function of the viscosity-average molecular weight: (A) 59; (B) 215; (C) 580 kg mol⁻¹ (reproduced with permission from reference 8)

The storage modulus reveals a plateau region above the glass transition. The so-called rubbery plateau becomes more pronounced with an increasing molecular weight, i.e.

longer relaxation times of the polymer chains. However, the height of this plateau, G_{N0} , remains unchanged upon increasing the molecular weight above the critical value. Similar to the rheological behaviour of crosslinked rubbers above their glass transition temperature, G_{N0} can be related to an average molecular weight between nodes of enhanced friction (i.e. entanglements in the case of thermoplastic polymers; and crosslinks for chemically cured thermosets).

Also in the glassy state the effect of entanglement coupling can be noticed. In *figure 1.3* the dependence of the fracture stress upon molar mass is shown for poly(methyl methacrylate) according to Vincent ⁹.

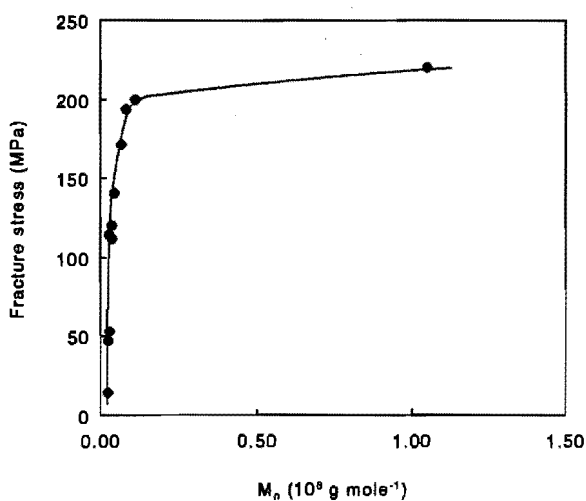


Figure 1.3 Dependence of fracture stress, σ_f , of poly(methyl methacrylate) upon number-average molar mass measured at -196°C (reproduced with permission from reference 9)

At a number-average molecular weight of approximately 50 kg mol^{-1} a rather abrupt increase in fracture stress can be observed. The molecular weight at which this sudden increase in fracture stress occurs is experimentally found to be correlated with the value of M_e ¹⁰.

Wu ^{3,11,12} proposed a correlation between chain stiffness (characteristic ratio, C_∞) and average molecular weight between entanglement nodes, M_e . Although the theoretical evaluation and interpretation of the data is highly speculative with respect to the

physical reality (especially the assumption of a binary hooking type of entanglement nodes; see discussion in reference ¹³), the experimentally determined correlation between the entanglement molecular weight, M_e , and C_∞ is clearly demonstrated. In Wu's analysis M_e is expressed in terms of the number of real and virtual skeletal bonds within an entanglement strand (N_v). In *figure 1.4* this number of statistical units in an entanglement strand, N_v , is shown versus the characteristic ratio.

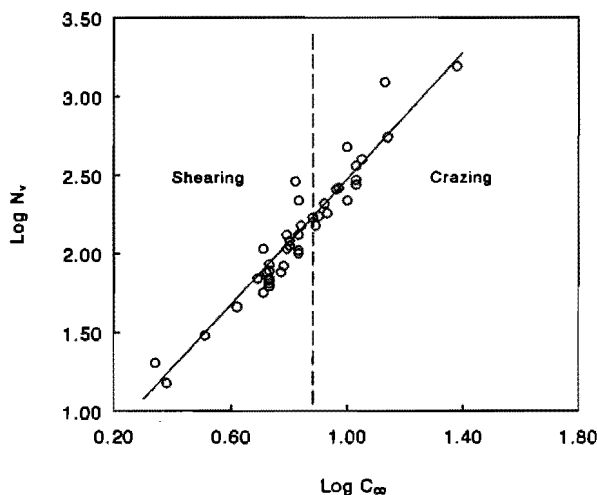


Figure 1.4 $\text{Log } N_v$ versus $\text{log } C_\infty$ plot for 44 polymers (reproduced with permission from reference 3)

N_v and, consequently, also M_e prove to be proportional to the square of the characteristic ratio:

$$N_v \propto C_\infty^2 \quad (1.2)$$

and:

$$M_e \propto C_\infty^2 \quad (1.3)$$

Polystyrene possesses a relatively stiff chain due to the presence of the large phenyl rings that hinder the rotational movement within the backbone of the polymer chain ($C_\infty = 10.8$) and, consequently, its molecular weight between entanglements is estimated to be 20 kg mol^{-1} . Polycarbonate of bisphenol-A, on the other hand, has a very flexible backbone and possesses very low values of C_∞ (2.4) and M_e (2 kg mol^{-1}).

1.3 Natural Draw Ratio

In section 1.2 it has been pointed out that the molecular conformation of amorphous glassy polymers can be characterized by a certain average molecular weight between network nodes. These network nodes can be both physical and chemical of nature. Following the principles of network drawing, as discussed in section 1.1, a theoretical maximum draw ratio of a single strand in the polymer network, assuming no chain slippage or breakage takes place, can be given by ^{4,5}:

$$\lambda_{max} = \frac{l_e}{d} \quad (1.4)$$

where l_e is the chain contour length and d the root-mean-square end-to-end distance between junction points in the network (i.e. mesh size). According to Kramer ^{4,5} the value of l_e is given by:

$$l_e = \frac{l_o M_e}{M_o} \quad (1.5)$$

where l_o and M_o are the average projected length of a chain segment along the chain and its molecular weight respectively. The value of d is related to the polymer network structure via ^{4,5}:

$$d = k (M_e)^{1/2} \quad (1.6)$$

where k is a constant that can be determined from neutron scattering measurements of the radius of gyration of molecular coils in the glass.

Combining equations (1.4), (1.5) and (1.6) results in:

$$\lambda_{max} = \frac{l_o}{k M_o} M_e^{1/2} \quad (1.7)$$

which can be related to the network density via:

$$v_e = \frac{\rho N_A}{M_e} \quad (1.8)$$

resulting in:

$$\lambda_{max} = \frac{\rho^{1/2} N_A^{1/2} l_o}{k M_c v_c^{1/2}} \quad (1.9)$$

in which ρ is the density and N_A is Avogadro's number. Equation (1.7) is a more detailed version of equation (1.1).

Typical values of the theoretical draw ratio of amorphous glassy polymers vary from 4.8 for poly(tert-butylstyrene)¹⁴, i.e. a elongation to break of 380%, to less than 1.2¹⁵, i.e. a elongation to break of 20%, for a densely crosslinked thermosetting polymer. For the latter type of amorphous polymers equations (1.7) and (1.9) are still applicable if ' M_c ' and ' v_c ' are replaced by ' M_c ' (i.e. the molecular weight between crosslinks) and ' v_c ' (i.e. crosslink density) respectively.

1.4 Deformation Mechanisms

The experimentally derived (macroscopic) elongation to break is often much lower than the theoretical value, λ_{max} . The macroscopic elongation to break of polystyrene for instance is only 1-3% compared to the 300% as expected from its network density (see section 1.1). The reason for this contradiction is related to the fact that deformation is only occurring localized in the sample in the so-called deformation areas. Two types of localized deformation mechanisms are known for the group of amorphous glassy polymers: crazing and shear yielding (see section 1.4.3 for a classification).

1.4.1 Crazing

A craze can be described as a micro-crack bridged by polymer fibrils. Within the craze structure many microvoids can be found. These microvoids develop in a plane perpendicular to the maximum principle stress. In contrast to a true crack, crazes are load bearing due to the presence of bridging fibrils. The thickness of these fibrils strongly depends on the type of polymer, e.g. air grown crazes in PS have typical fibril diameters of 5 to 20 nm¹⁶. In *figure 1.5* a transmission electron micrograph of a craze structure in styrene-acrylonitrile copolymer is shown.

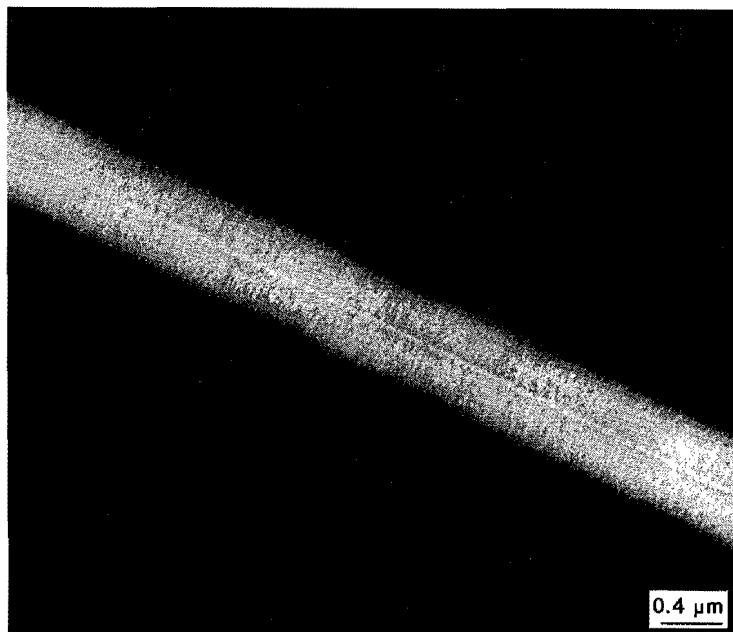


Figure 1.5 Transmission electron micrograph of a craze in styrene-acrylonitrile copolymer (reproduced with permission from reference 17)

The craze structure consists of numerous fibrils running across from one craze interface to the other. These main fibrils are interconnected by somewhat thinner, so-called cross-tie fibrils¹⁸. Since crazing involves the formation of microvoids, crazing is always accompanied by an increase in volume and is favoured by a large dilatational component of the stress tensor¹⁹. This latter condition can often be found ahead of a crack tip or in the vicinity of dust or other foreign particles, sharp edges and other types of inhomogeneities. Several types of crazes are reported in literature varying in coarseness of the microfibrillar structure, as reviewed extensively by Michler²⁰⁻²². In principle, the size of crazes is not limited since the growth of a craze occurs via drawing unfibrillated polymeric material from the bulk into the craze structure⁴. Therefore, a classification of crazes by length or thickness as proposed by Michler²⁰⁻²², is irrelevant in retrospect. Only, in front of a crack tip the maximum thickness of a craze is limited due to the presence of cross-tie fibrils as explained by Brown²³.

Recently, several studies have been reported in literature on the prediction of the macroscopic G_{Ic} fracture toughness from a molecular point of view where localized

deformation is considered^{23,24}. Brown²³ calculated the fracture toughness of polymers that tend to form crazes ahead of a crack tip. He derived an analytical equation for the value of G_{Ic} that scales with the square of the breaking force of the chain molecules and the square of the density of entangled strands at the crack-tip interface.

1.4.2 Shear Yielding

Shear yielding involves plastic deformation that can be either in a very localized form, or in a homogeneous manner, and occurs without any volume change. Localized shear deformation arises from instabilities during homogeneous yielding that are induced by geometric irregularities²⁵⁻²⁷ (neck formation as a consequence of slight variations in cross sectional area) and/or the supposed intrinsic strain softening character of the polymeric material. Recently, new insights were obtained concerning the supposed intrinsic strain softening character of polymeric materials and it was demonstrated that necking is caused by a mechanical (and to a lesser extent: thermal) runaway of (initially) small instabilities due to the strong non-linear strain rate dependence of the yield stress²⁸. Shear yielding preferentially occurs in relatively densely entangled (or: crosslinked) polymers (see section 1.4.3) and is favoured when conditions that tend to promote crazing are suppressed (e.g. appliance of hydrostatic pressure). *Figure 1.6* shows an optical micrograph of a polycarbonate sample viewed between crossed polars uniaxially deformed just past the yield point at room temperature.

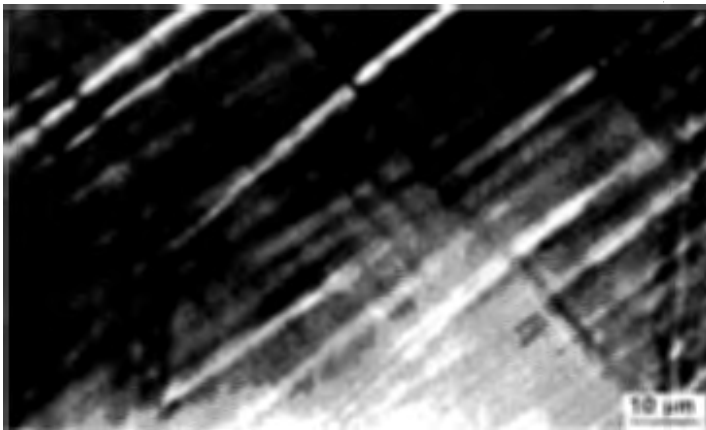


Figure 1.6 Microshear bands in a polycarbonate sample that has been uniaxially deformed just past yield at room temperature viewed between crossed polars (load direction: horizontal)

At an angle of approximately 45°C (direction of maximum shear stress) sharp shear bands are visible. Various types of shear bands are listed in literature termed microshear bands or diffuse zones. According to Bowden et al. the differences in shear band structure mainly arise from their differences in growth speed ²⁹.

1.4.3 Crazeing versus Shear Yielding

Wu proposed ¹¹ that polymers that tend to deform by crazeing possess network densities lower than 9×10^{25} chains m^{-3} (or: values of $C_w \geq 7.5$) and polymers that deform by shear yielding have network densities above the value of 9×10^{25} chains m^{-3} (i.e. $C_w \leq 7.5$; see vertical line in *figure 1.4*). This classification arises from a comparison of the craze initiation stress with the shear band initiation stress for a large number of amorphous glassy polymers. At a network density of approximately 9×10^{25} chains m^{-3} the craze initiation stress roughly equals the shear band initiation stress, below this network density the craze initiation stress is lower than the yield stress and crazeing prevails.

A physical explanation for this network density dependent transition in the deformation mechanism, occurring at a network density of 9×10^{25} chains m^{-3} , has been proposed by Kramer et al. ⁴. They ascribed this transition to the fact that an increasing network density results in a higher surface tension which hampers the void formation process of crazeing. Henke ¹⁵ confirmed this hypothesis by inducing a transition from crazeing to shear yielding in polystyrene (PS; a typical craze deforming polymer) at room temperature as a result of electron beam irradiation of the material. The electron beam irradiation induces crosslinking (at very high irradiation doses because PS is relatively inert to electron beam irradiation) of the polystyrene resulting in an increased network density (i.e. the total of physical entanglements and chemical crosslinks).

The experimental observations of a crazeing-shear yielding transition depending on the entanglement density of the amorphous glass are also, at least qualitatively, confirmed by calculations performed by Termonia and Walsh ³⁰. They modelled the deformation behaviour and mechanical properties of polymeric glasses by taking into account the role of the interactive forces between macromolecular chains as well as chain slippage through entanglements. The network structure can deform elastically (0 - 2% elongation) and plastically. Plastic deformation occurs via stretching or slippage

(disentanglement) of the entanglement strands, depending on the strain rate and local stress state. Via a two-dimensional Monte Carlo simulation the minimum energy state is retained after each increment in strain. These calculations clearly demonstrate a transition from a crazing to shearing mode of deformation with an increasing network density. This transition is visualized if the network structure is observed after a certain deformation. If crazing prevails 'holes' can be observed in the molecular network. These holes are either the result of disentanglement, or are due to chain breakage. At higher network densities, shear yielding is observed as indicated by the absence of 'holes' in the network structure, instead homogeneous deformation is observed. It has to be noted that these model calculations have to be interpreted only qualitatively, since the thickness of the calculated fibrils differs considerably from the experimentally determined values.

The applicability of the network density classification proposed for the transition from crazing to shear deformation according to Wu ¹¹ is very limited since the transition is highly influenced by the testing conditions applied. For instance, straining of a typical shear deforming polymer like polycarbonate at elevated temperatures, instead of room temperature, results in a transition from shear yielding to crazing. This is explained by Donald ³¹ in terms of disentanglement crazing: high temperatures enhance the disentanglement process during deformation resulting in a less densely entangled network structure that tends to deform by crazing.

1.5 Natural Draw Ratio versus Local Strain

Kramer et al. compared the theoretical extension ratio of the molecular network of a large group of amorphous polymers (λ_{max} ; see equation (1.7) or (1.9)) with the local extension ratio in a craze or shear deformation zone ^{14,15,32,33} using the technique introduced by Lauterwasser and Kramer ¹⁶. The extension ratios in a craze fibril or within a shear deformation zone can be determined from optical densitometry of transmission electron micrographs of these structures. *Figure 1.7* summarizes some of the results of their studies: the craze fibril extension ratio, λ_{craze} , and the extension ratio in a shear deformation zone, λ_{DZ} , are plotted versus the natural draw ratio (which is a network characteristic for a polymer).

In *figures 1.7a* and *1.7b* data are presented obtained from measurements on entangled thermoplastic polymers. Similar results are published by Kramer et al. on chemically

crosslinked polymers¹⁵.

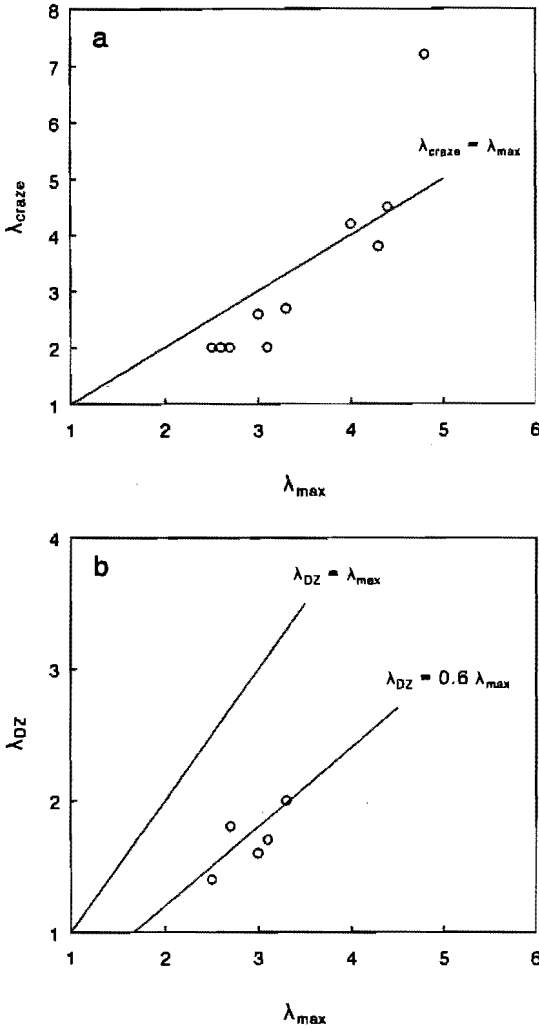


Figure 1.7 (a) Craze fibril extension ratio λ_{craze} versus the maximum extension ratio of an ideal entanglement network, λ_{max} (assuming no chain slippage or scission); and (b) extension ratio in a deformation zone, λ_{DZ} , versus λ_{max} (reproduced with permission from references 14,15,32,33)

Independent of the type of network structure (entanglements or crosslinks), a clear correlation can be observed between the value of λ_{max} on one hand, and the value of λ_{craze} and λ_{DZ} , on the other hand. For the shear deforming polymers roughly 60% of

the theoretical draw ratio is measured inside a deformation zone. In the situation of craze deforming polymers a one-to-one correlation seems plausible, however additional experiments revealed a large destruction of the original entanglement network during the craze formation³⁴. Hence, the one-to-one correlation is somewhat misleading for the crazing situation since the actual (local) network structure possessed a higher value of λ_{\max} after the craze formation ($\lambda_{\max, \text{after}}$). Consequently, roughly the same discrepancy between the natural draw ratio (after craze formation) and the value of λ_{craze} ($\lambda_{\text{craze}} / \lambda_{\max, \text{after}} = 0.6$) as found between the natural draw ratio and λ_{DZ} results.

1.6 Toughness Improvement in Practice

To improve the macroscopic toughness of amorphous glassy polymers several approaches have been proposed in the literature. In principle, two possibilities exist to increase the macroscopic toughness: (i) addition of a plasticizer and (ii) initiation of multiple deformation mechanisms in a large volume of the material induced by the presence of a low modulus dispersed phase. Both methods will be reviewed briefly.

1.6.1 Plasticization

The addition of a plasticizer is a relatively simple technique to improve the macroscopic toughness of the amorphous polymer¹⁹. The plasticizer lowers the yield stress of the polymer and can, consequently, increase the elongation at break of the polymer. The disadvantage of this approach is the (undesired) decrease in modulus, glass transition temperature and yield strength of the polymeric material. Recently, the concept of controlled local plasticization has been introduced by Argon et al.^{35,36}. This method is based on the principle of increased solubility under the influence of high negative pressures. Such high negative pressures are supposed to occur for instance in the active zone of a widening craze. Hence, only local plasticization occurs in the region of the deformation mechanism. Therefore, the disadvantages of the addition of a 'traditional' plasticizer would be minimized to only a minor decrease of Young's modulus and tensile strength. Recently, however, it has been shown for the model system polystyrene/polyisobutylene (PS/PIB)³⁷, where the solubility of the PIB can be increased in a controlled manner (by a decrease of the molecular weight as a consequence of electron beam irradiation), that a substantial change in solubility did not result in any change of the mechanical properties of the blend. Therefore, the

applicability and practical relevance of the mechanism proposed by Argon to impact toughening of polymeric systems must be questioned seriously.

1.6.2 Rubber Modification

The most frequently applied method to improve toughness of polymeric systems in general is the addition of dispersed rubbery particles. The function of these particles is to generate numerous stress concentrations throughout the polymeric matrix^{38,39}. As a result, multiple deformation mechanisms are initiated in the matrix and *multiple crazing* or *multiple shear deformation* is induced. The rubbery phase only marginally contributes to the toughness of the overall composite⁴⁰.

Multiple Crazing

The influence of various parameters (like rubber-phase volume fraction, rubber particle size and degree of adhesion between the rubbery particles and the matrix) have been given a lot of consideration since the introduction of the first commercial type of high impact polystyrene (HIPS) in 1948^{38,41-44}. The elongation to break of polystyrene can be increased by optimizing the variables mentioned above, up to a value of about 30%. Even if the testing conditions become more severe (i.e. high strain rates, notched impact testing at low temperatures) the toughening effect of the dispersed rubbery particles remains^{38,43}.

Although an enormous amount of papers can be found in literature dealing with rubber-toughening of *craze-deforming* polymers, only a few systematic studies reported on the influence of rubber-phase volume fraction and particle size on the rubber-toughening efficiency⁴⁴⁻⁴⁸. Bucknall et al. studied the influence of rubber-phase volume fraction on the notched Charpy impact strength of polystyrene by diluting a standard HIPS sample with pure PS⁴⁷. A sharp decrease in impact strength is observed below a certain rubber-phase volume fraction which was explained in terms of an altered local stress state of the matrix phase. The same authors investigated the influence of particle size on the notched Charpy impact strength of rubber-modified polystyrene, and the toughening efficiency of the rubbery particles is found to decrease below a diameter of 1 μm ⁴⁸. The explanation for this observation is given by Donald and Kramer^{49,50} in a separate paper where the detailed mechanisms of craze initiation, growth and breakdown around rubbery particles in thin films of HIPS

and acrylonitrile-butadiene-styrene copolymer (ABS) were studied using transmission electron microscopy. They demonstrated that crazes are rarely initiated in polystyrene by particles having a size below $1\ \mu\text{m}$ and it was suggested that the stress concentration induced by the rubbery particle must act over a certain critical distance in order to initiate crazes, since the distance over which the stress concentration of a rubbery particle acts is directly proportional its particle size. This critical size, below which the toughening efficiency decreases, depends on the type of polymeric matrix as clearly reported in a review paper of Wu^{11,12}. The observation of a minimum particle size to initiate crazes automatically explains the occurrence of an optimum particle size for a given concentration rubbery particles since this optimum particle size is equal to the minimum particle size below which crazes cannot be generated. So-called optimum particle sizes are reported in literature varying from $2.5\ \mu\text{m}$ for polystyrene down to $0.25\ \mu\text{m}$ for poly(methyl methacrylate)¹¹.

The influence of adhesion between the rubbery phase and the matrix on the Izod impact strength of rubber-toughened polystyrene has been reported by Van Gisbergen et al.⁵¹⁻⁵³. It was shown that the impact properties of polystyrene/Ethylene-Propylene-Diene Monomer (EPDM) blends can be improved significantly with electron beam irradiation when a suitable compatibilizer is used (in their experiments a styrene-butadiene diblock copolymer). Differences in morphology and crosslinking of the dispersed phase could be eliminated as explanations for the observed phenomenon due to the experimental setup used. Hence, a change in interfacial adhesion is the most plausible explanation.

Only recently, the precise function of the dispersed elastomer present in craze-deforming matrices has been clarified by Bubeck et al.⁵⁴ who performed real-time small-angle X-ray scattering measurements on rubber-modified craze-deforming thermoplastics. These experiments unambiguously demonstrate the occurrence of two distinct events during loading of rubber-modified craze-deforming thermoplastics. The first step of plastic deformation is the internal cavitation of the rubbery particles leading to microvoids within the dispersed spheres. Subsequently, crazes are initiated at the equator of the rubbery particles while the microvoids within the rubbery phase are prevented from coalescence to form larger voids (which could lead to premature crack initiation) as a result of a moderate degree of crosslinking of the rubbery phase.

Multiple Shear Deformation

The influence of dispersed rubbery particles on the macroscopic toughness of *shear-deforming* thermoplastic polymers has been studied extensively by Wu^{55,56} and Borggreve⁵⁷ for the semi-crystalline Nylon-6/EPDM-rubber model system. For shear-deforming polymers it has been demonstrated that, independent of the rubber-phase volume fraction and particle size, the maximum degree of toughness can be obtained on a macroscopic level if the polymeric material is made locally thin below the *critical matrix ligament thickness* (ID_c). The value of the critical matrix ligament thickness is related to the testing temperature⁵⁷. In *figure 1.8* the value of ID_c is shown as a function of testing temperature for Nylon-6.

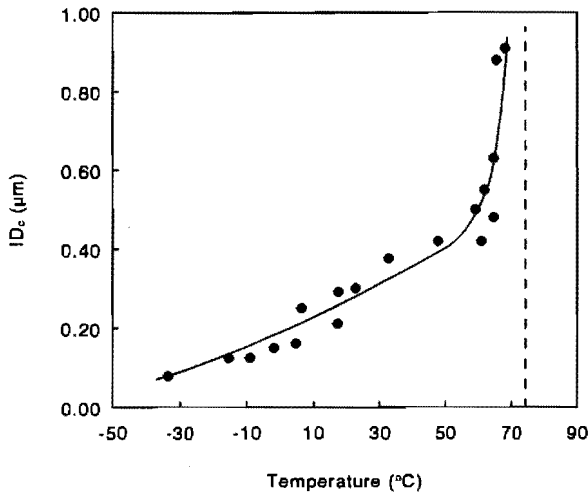


Figure 1.8 Critical matrix ligament thickness ID_c versus temperature for Nylon-6/rubber blends (reproduced with permission from reference 57)

Above a temperature of 50°C a steep increase in critical thickness is observed due to the approach of the glass transition temperature of Nylon-6 (60°C). Below this temperature the value of ID_c only moderately increases with increasing temperature, independent of the glass transition temperature of the Nylon-6 matrix or the dispersed EPDM rubber-phase⁵⁷. The physical explanation for this critical thickness, below which the polymer reveals this maximum degree of ductility, is not fully understood. Several explanations have been proposed by Margolina and Wu⁵⁸ and Sjoerdsma⁵⁹ based on percolation of yielding ligaments, however, no convincing

experimental verification was given for any of the explanations proposed.

An important feature of these rubber-modified shear-deforming thermoplastic polymers has been demonstrated by Borggreve et al.^{60,61} who have shown a pronounced influence of the mechanical properties of the dispersed elastomeric phase on the brittle-to-tough transition of Nylon-6 blends. Chou et al.^{62,63} have demonstrated for the system polypropylene (PP) blended with Ethylene-Propylene rubber (EPR; dispersed phase) that a brittle-to-ductile transition can not only be realized by a change in testing temperature, but also by a change in strain rate.

Thermosetting polymers also suffer from brittle fracture, especially under relatively severe testing conditions. Due to the high network density (i.e. crosslink density), thermosetting polymers deform by shear deformation, although very recently, Sue et al. reported the observation of crazes in a moderately crosslinked 1,2-dihydrobenzocyclobutene-Maleimide resin⁶⁴. The high network density of these materials, limits their intrinsic toughness through their low natural draw ratio (see equation (1.9)). Therefore, rubber-modification in these systems can only result in a marginal toughness improvement. An excellent review on toughening mechanisms occurring in (rubber-modified) epoxides has been published by Garg and Mai⁶⁵.

Several systematic studies on the influence of crosslink density on the toughen-ability of chemically crosslinked polymers are reported in literature where the influence of the dispersed toughening agent has been studied as well⁶⁶⁻⁶⁸. Compared to thermoplastic polymeric systems the toughening concepts do not differ much for the thermosetting polymers with respect to the addition of a dispersed phase of lower modulus. However, also alternative toughening concepts are applied comprising crack-tip bifurcation, crack-tip bridging, etc.⁶⁹ that furthermore only result in a marginal toughness improvement.

1.7 Scope of the Thesis

The original experiments performed by Kramer et al. in the 1980's⁴ resulted in a considerable progress in the understanding of toughness from a molecular point of view. However, the comparison of the local strain level within a deformation area with the theoretical strain to break of stretching the molecular network structure to its full extension was, up to now, of no relevance to the macroscopic toughness of

polymeric systems. Illustrative in this context is the paradox between the theoretical draw ratio of the entanglement network of polystyrene (300%) and the macroscopic elongation to break of only 3%: i.e. two orders of magnitude difference. Because, on a microscopic scale, the theoretical draw ratio can be approached (inside crazes or shear bands), it can be expected that a transition from brittle to ductile deformation occurs upon changing the sample dimensions (from 'macroscopic' to 'microscopic').

Experiments performed by Wu^{55,56} and Borggreve⁵⁷ with the Nylon-6/rubber system clearly revealed an influence of (local) dimension of the polymeric material (ligament thickness between rubbery particles) on the brittle-to-ductile transition of the blends. The physical explanation for this transition as well as the more general validity of this dimension-induced brittle-to-tough transition are not given.

Since toughness on a microscopic scale (i.e. in the localized deformation zones) can be well understood from a molecular point of view (see section 1.5), the critical dimension below which amorphous glassy polymers macroscopically deform up to the theoretical strain to break, is investigated. Basically, the concept of a critical thickness is introduced in chapters 2, 3, 4 and 5. In chapters 6 and 7 some refinements concerning the characteristics of the model systems are made, while in chapter 8 the concept is applied to some practical systems.

For thermoplastic polymers having different entanglement densities (polystyrene: chapter 2; polystyrene-poly(2,6-dimethyl-1,4-phenylene ether) (PS-PPE) blends: chapter 3) and thermosetting polymers with varying crosslink densities (epoxides based on diglycidyl ether of bisphenol-A: chapter 4) the local dimensions are decreased in one (films) or two directions (ligaments between non-adhering rubbery particles) by a control of the microstructure. Below a critical (local) size, the sample macroscopically demonstrates the maximum degree of ductility, comparable with the theoretical strain to break. The occurrence, and network density dependence, of the critical dimension is modelled in terms of an energy based criterion (chapter 3). The influence of temperature and strain rate on the value of the critical thickness of the thermoplastic PS-PPE model system is studied in chapter 5 and relatively easily interpreted based on the model introduced.

In chapter 6, the deformation behaviour of thin PS-PPE films is studied in more detail compared to chapters 2 and 3 and the existence of two, rather than one, critical

thicknesses in multilayered films is explained. The influence of the type of network structure on the critical matrix ligament thickness is studied for PS-PPE networks in chapter 7. High molecular weight PPE networks diluted with low and high molecular weight PS are compared at a constant value of the network density.

Since in practice often a considerable degree of adhesion is present between the dispersed rubbery phase and the matrix (in order to obtain a fine dispersion in the compatibilized melt-mixing process), in chapter 8 the influence of adhesion on the critical thickness is discussed. Polycarbonate blends containing rubbery particles that are adhering to the matrix and, consequently, can only generate a local thickness as a result of cavitation and/or detachment of the rubbery particles, are compared with blends containing non-adhering rubbery particles. The superiority of 'holes' is clearly demonstrated.

Finally, in chapter 9 some general conclusions are made with respect to the ultimate toughness of amorphous glassy polymers and directions are marked for a further development of the understanding of toughness of polymeric structures (controlled toughness combined with a manageable decrease in stiffness and strength). Unambiguous explanations can easily be given for (apparently) contradictory conclusions that arose in this introductory chapter 1, based on the general insights obtained in the ultimate toughness of amorphous glassy polymers. As an example the 'primus inter pares' of a tough amorphous glassy polymer is presented: a polystyrene foam-like structure. Preliminary results on the preparation of high-density ($\sim 0.7 \text{ g cm}^{-3}$) foams are presented containing sub-micron cell-wall dimensions.

The thesis is based on a collection of papers which have been published in, or have been submitted to, various journals ⁷⁰⁻⁷⁸. Furthermore the author has contributed to some papers on related subjects which are not presented in this thesis ⁷⁹⁻⁸⁵.

1.8 References

- 1 Smith, P., Lemstra, P.J. and Booij, H.C. *J. Polym. Sci., Polym. Phys. Ed.*, 1981, **19**, 877
- 2 Ferry, J.D. 'Viscoelastic Properties of Polymers', Wiley, New York, 1980
- 3 Wu, S. *J. Polym. Sci., Polym. Phys. Edn.* 1989, **27**, 723
- 4 Kramer, E.J. and Berger, L.L. *Adv. Polym. Sci.* 1990, **91/92**, 1
- 5 Kramer, E.J. *Adv. Polym. Sci.* 1983, **52/53**, 1
- 6 Kirste, R.G., Kruse, W.A. and Schelten, J. *Makromol. Chem.* 1973, **162**, 299
- 7 Porter, R.S. and Johnson, J.F. *Chem. Rev.* 1966, **66**, 1
- 8 Onogi, S., Masuda, T. and Kitagawa, K. *Macromolecules* 1970, **3**, 109
- 9 Vincent, P.I. *Polymer* 1960, **1**, 425
- 10 Gent, A.N. and Thomas, A.G. *J. Polym. Sci.(A-2)* 1972, **10**, 571
- 11 Wu, S. *Polym. Eng. Sci.* 1990, **30**, 753
- 12 Wu, S. *Polym. Int.* 1992, **29**, 229
- 13 Bastiaansen, C.W.M., Meijer, H.E.H. and Lemstra, P.J. *Polymer* 1990, **31**, 1435
- 14 Donald, A.M. and Kramer, E.J. *J. Polym. Sci., Polym. Phys. Edn.* 1982, **20**, 899
- 15 Henkee, C.S. and E.J. Kramer *J. Polym. Sci., Polym. Phys. Edn.* 1984, **22**, 721
- 16 Lauterwasser, B.D. and E.J. Kramer *Phil. Mag.* 1979, **A39**, 369
- 17 Bos, H., DSM Research, private communications
- 18 Miller, P., Buckley, D.J. and Kramer, E.J. *J. Mater. Sci.* 1991, **26**, 4445
- 19 Kinloch, A.J. and Young, R.J. 'Fracture Behaviour of Polymers' Elsevier Appl. Sci., London, 1985
- 20 Michler, G.H. *Makromol. Chem., Macromol. Symp.* 1990, **38**, 195
- 21 Michler, G.H. *J. Mater. Sci.* 1990, **25**, 2321
- 22 Michler, G.H. *Phys. Res.* 1990, **14**, 353
- 23 Brown, H.R. *Macromolecules* 1991, **24**, 2751
- 24 DeGennes, P.G. *Europhys. Lett.* 1991, **15** (2), 191
- 25 Haward, R.N. 'The Physics of Glassy Polymers', Appl. Sci., London, 1973
- 26 Nadai, A. 'Theory of Flow and Fracture of Solids', McGraw-Hill, New York, 1950
- 27 Vincent, P.I. *Polymer* 1960, **1**, 7
- 28 Govaert, L.E. and Tervoort, T.A. Proc. 'Polymer Science and Technology' Conf., Leeds, 1993
- 29 Bowden, P.B. *Phil. Mag.* 1970, **22**, 455
- 30 Termonia, Y. and Walsh, D.J. *J. Mater. Sci.* 1989, **24**, 247
- 31 Donald, A.M. *J. Mater. Sci.* 1985, **20**, 2630
- 32 Donald, A.M. and Kramer, E.J. *Polymer* 1982, **23**, 461
- 33 Donald, A.M. and Kramer, E.J. Proc. 5th Int. Conf. 'Deformation Yield and Fracture of Polymers', Cambridge, 1982, p.15.1
- 34 Henkee, C.S. and Kramer, E.J. *J. Mater. Sci.* 1986, **21**, 1398
- 35 Gebizlioglu, O.S., Beckham, H.W., Argon, A.S., Cohen, R.E. and Brown, H.R. *Macromolecules* 1990, **23**, 3968
- 36 Argon, A.S., Cohen, R.E., Gebizlioglu, O.S., Brown, H.R. and Kramer, E.J. *Macromolecules* 1990, **23**, 3975
- 37 Jansen, B.J.P., Masters Thesis, Eindhoven University of Technology, The Netherlands, 1993
- 38 Bucknall, C.B. 'Toughened Plastics', Appl. Sci., London, 1977
- 39 Coumans, W.J., Heikens, D. and Sjoerdsma, S.D. *Polymer* 1980, **21**, 103
- 40 Newman, S. and Strella, S. *J. Appl. Polym. Sci.* 1965, **9**, 2297
- 41 Hobbs, S.Y. *Polym. Eng. Sci.* 1986, **26**, 74
- 42 Keskkula, H., Schwarz, M. and Paul, D.R. *Polymer* 1986, **27**, 211
- 43 Bucknall, C.B. *Makromol. Chem., Macromol. Symp.* 1990, **38**, 1
- 44 Cigna, G., Maestrini, C., Castellani, L. and Lomellini, P. *J. Appl. Polym. Sci.* 1992, **44**, 505
- 45 Cigna, G., Matarrese, S. and Biglione, G.F. *J. Appl. Polym. Sci.* 1976, **20**, 2285

- 46 Cigna, G., Lomellini, P. and Merlotti, M. *J. Appl. Polym. Sci.* 37, 1527
- 47 Bucknall, C.B., Cote, F.F.P. and Partridge, I.K. *J. Mater. Sci.* 1986, 21, 301
- 48 Bucknall, C.B., Davies, P. and Partridge, I.K. *J. Mater. Sci.* 1987, 22, 1341
- 49 Donald, A.M. and Kramer, E.J. *J. Mater. Sci.* 1982, 17, 1765
- 50 Donald, A.M. and Kramer, E.J. *J. Mater. Sci.* 1982, 17, 2351
- 51 Van Gisbergen, J.G.M. Ph.D. Thesis, Eindhoven University of Technology, The Netherlands, 1991
- 52 Van Gisbergen, J.G.M., Borgmans, C.P.J.H., Van der Sanden, M.C.M. and Lemstra, P.J. *Polym. Commun.* 1990, 31, 162
- 53 Van Gisbergen, J.G.M., Van der Sanden, M.C.M., De Haan, J.W., Van de Ven, L.J.W. and Lemstra, P.J. *Makromol. Chem., Macromol. Symp.* 1991, 41, 153
- 54 Bubeck, R.A., Buckley Jr. D.J., Kramer, E.J. and Brown, H.R. *J. Mater. Sci.* 1991, 26, 6249
- 55 Wu, S. *Polymer* 1985, 26, 1855
- 56 Wu, S. *J. Appl. Polym. Sci.* 1988, 35, 549
- 57 Borggreve, R.J.M., Ph.D. Thesis, University of Twente, The Netherlands, 1988
- 58 Margolina, A. and Wu, S. *Polymer* 1988, 29, 2170
- 59 Sjoerdsma, S.D. *Polym. Commun.* 1989, 30, 106
- 60 Borggreve, R.J.M., Gaymans, R.J. and Schuijjer, J. *Polymer* 1989, 30, 71
- 61 Borggreve, R.J.M., Gaymans, R.J. and Eichenwald, H.M. *Polymer* 1989, 30, 78
- 62 Chou, C.J., Vijayan, K., Kirby, D., Hiltner, A. and Baer, E. *J. Mater. Sci.* 1988, 23, 2521
- 63 Chou, C.J., Vijayan, K., Kirby, D., Hiltner, A. and Baer, E. *J. Mater. Sci.* 1988, 23, 2533
- 64 Sue, H.-J., Yang, P.C. and Bishop, M.T. *J. Mater. Sci.*, in press
- 65 Garg, A.C. and Mai, Y.-W. *Compos. Sci. Technol.*, 1988, 31, 179
- 66 Yee, A.F. and Pearson, R.A. *J. Mater. Sci.* 1986, 21, 2462
- 67 Pearson, R.A. and Yee, A.F. *J. Mater. Sci.* 1986, 21, 2475
- 68 Pearson, R.A. and Yee, A.F. *J. Mater. Sci.* 1989, 24, 2571
- 69 Pearson, R.A. and Yee, A.F. *Polym. Mater. Sci. Eng.* 1990, 63, 311
- 70 Van der Sanden, M.C.M., Meijer, H.E.H. and Lemstra, P.J. *Polymer* 1993, 34, 2148
- 71 Van der Sanden, M.C.M., Meijer, H.E.H. and Tervoort, T.A. *Polymer* 1993, 34, 2961
- 72 Van der Sanden, M.C.M. and Meijer, H.E.H. *Polymer* 1993 in press
- 73 Van der Sanden, M.C.M. and Meijer, H.E.H. *Polymer* 1993, submitted for publication
- 74 Van der Sanden, M.C.M., Buijs, L.G.C., De Bie, F.O. and Meijer, H.E.H. *Polymer* 1993, submitted for publication
- 75 Van der Sanden, M.C.M. and Meijer, H.E.H. *Polymer* 1993, submitted for publication
- 76 Van der Sanden, M.C.M., de Kok, J.M.M. and Meijer, H.E.H., *Polymer* 1993, submitted for publication
- 77 Van der Sanden, M.C.M., Meijer, H.E.H. and Lemstra, P.J. *J. Coll. Polym. Sci.* 1993 in press
- 78 Van der Sanden, M.C.M. and Meijer, H.E.H. *Makromol. Chem., Macromol. Symp.* 1993 in press
- 79 Van der Sanden, M.C.M., Van Gisbergen, J.G.M., Tauber, I.D., Meijer, H.E.H. and Lemstra, P.J. in 'Integration of Fundamental Polymer Science and Technology-5', (Eds. P.J. Lemstra and L.A. Kleintjens), Elsevier, London, 1991, 66
- 80 Van der Sanden, M.C.M. and De Kok, J.M.M., Proc. 8th Int. Conf. 'Deformation Yield and Fracture of Polymers', Cambridge, 1991, p.122.1
- 81 Van der Sanden, M.C.M., Schulkes, R.G.M., Venderbosch, R.W., Meijer, H.E.H. and Lemstra, P.J., Proc. 8th Ann. Meeting 'Polymer Processing Society', New Dehli, 1992, p.257
- 82 Van der Sanden, M.C.M., Meijer, H.E.H. and Crevecoeur, J.J., Proc. Int. Conf. 'Advanced Composites 1993', Wollongong, Australia, 1993 in press
- 83 Van der Sanden, M.C.M. and Meijer, H.E.H., Proc. 2nd Nat. Mech. Conf., Kerkrade, 1992, 231
- 84 Van Gisbergen, J.G.M., Borgmans, C.P.J.H., Van der Sanden, M.C.M. and Lemstra, P.J. *Polym. Commun.* 1990, 31 (5), 162
- 85 Van Gisbergen, J.G.M., Van der Sanden, M.C.M., De Haan, J.W., Van de Ven, L.J.M. and Lemstra, P.J. *Makromol. Chem., Macromol. Symp.* 1991, 41, 153

Chapter 2*

The Concept of a Critical Thickness

2.1 Introduction

The toughness of polymeric systems has been studied extensively in the past. The paramount factors governing fracture, deformation and ultimate ductility, however, are still a matter of debate¹⁻⁶. Toughness is determined by *extrinsic* variables such as sample dimensions, notch geometries, testing speed and temperature, and *intrinsic* parameters such as the molecular structure and microstructure or morphology of the specimen under investigation.

Recently, important contributions have been made towards a better understanding of the relationship between (ultimate) toughness and molecular structure, or microstructure, of polymer blends⁷⁻¹¹. In the case of glassy, amorphous polymers, the basic approach is that the entanglement network is retained upon quenching in the glassy state. The characteristics of the entanglement network, like the molecular weight between entanglements, M_e , can be estimated in the melt from the apparent rubber plateau modulus. Based on this analysis, one could distinguish between loosely and highly entangled glassy, amorphous polymers. Applying the classical concept of rubber elasticity, the maximum draw ratio of a network, λ_{\max} , scales with $M_e^{1/2}$. Since the yield stress of glassy polymers only varies within the range of 50-80 MPa, the toughness, i.e. the work to break, is mainly determined by the strain at break of stretching the entanglement network to its maximum elongation. Following this simple analysis, which has been used before in drawing semi-crystalline polymers in the solid state¹², one easily derives that polystyrene (PS) possesses a λ_{\max} of 4.2 (320%) and polycarbonate (PC) a λ_{\max} of 2.5 (150%). In this perspective, PS is more ductile than

* This chapter is reproduced, in part, from:

1. Van der Sanden, M.C.M., Meijer, H.E.H. and Lemstra, P.J. *Polymer* 1993, **34**, 2148

PC.

In actual practice, however, one observes experimentally that PS is macroscopically brittle with a strain at break of less than 5%, whereas PC possesses a strain at break of approximately 100%, hence close to the theoretical limit. The premature fracture of PS is related to the uncontrolled crazing process. Upon deformation, crazing occurs random and locally, i.e. only the fibrils bridging the crazes are elongated. Kramer and Donald^{8,9} have shown that locally, inside a craze fibril or inside a plane-stress deformation zone (λ_{craze} , and λ_{DZ} , respectively), the extension ratio correlates very well with the theoretical value (λ_{max}).

A well known technique to control the local deformation mechanism is to add a second phase in the form of dispersed rubbery particles^{1,13}. An important parameter in these systems is the 'Interparticle Distance' (ID) as demonstrated by Wu^{10,11} and Borggreve¹⁴⁻¹⁶.

In this chapter, we wish to introduce the concept of a critical thickness below which brittle samples become ductile. PS is taken as the model system. Tapes consisting of alternating layers of polystyrene and polyethylene (PE) were prepared in order to investigate the influence of the PS layer thickness on the tensile deformation process. The concept of a minimum thickness is also transformed to a standard (3 mm thick) PS system in which the critical thickness is achieved locally by introducing non-adhering rubbery particles, i.e. the equivalence of holes.

2.2 Experimental

2.2.1 Sample preparation

PS and PE were coextruded using a Multiflux static mixer^{17,18}, into thin laminated tapes possessing a total thickness of appr. 0.3 mm, a width of 10 mm and infinite length, containing a varying number of layers (from 8 up to 1024). PS and PE were used in five different proportions: PS/PE: 100/0, 75/25, 50/50, 25/75 and 0/100. The principle of the static mixer is outlined in *figure 1.1*. Starting with parallel layers of both polymers (stage A, *figure 1.1*) the layers are split up and compressed vertically in opposite directions (stage B, *figure 1.1*). Subsequently, an extension in horizontal direction results in double the number of layers (stage C, *figure 1.1*). If the number of elements is increased, so too is the total number of layers (power of 2).

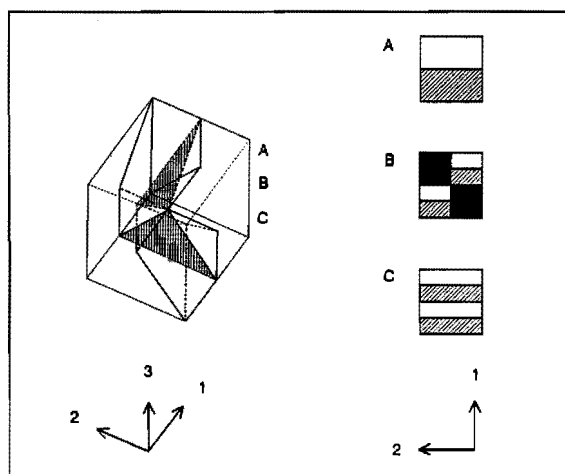


Figure 1.1 Principle of the Akzo Multiflux static mixer. One element is shown. In the text, 1 is referred to as the vertical direction, 2 the horizontal direction and 3 the direction of flow

The extrusion temperature was 200°C and the total film thickness was kept constant (0.3 mm). The PS was of commercial grade (DOW, Styron 638) with a molecular weight of 70 kg mol⁻¹ and a polydispersity index of 2.85. The polyethylene was a general-purpose type supplied by DSM (LDPE 1808 AN). Small dumb-bell shaped tensile specimens were machined parallel to the direction of extrusion according to ASTM D 1708. In order to exclude any influence of orientation on the mechanical properties, the tapes were annealed at 80°C during at least 24 hours.

Moulded PS samples, containing varying amounts of core-shell rubber (10-60 wt%) in order to obtain a small ligament thickness between the particles, were prepared in a co-rotating twin screw extruder (Werner and Pfleiderer ZSK 25) with a standard screw geometry, at an average barrel temperature of 125°C. In order to investigate the influence of adhesion between the rubbery particles and the matrix on the tensile properties of rubber-modified PS, two different types of core-shell rubber were used: a non-adhering type-I and an adhering type-II. Type-I core-shell rubber was a commercial grade supplied by Rohm and Haas Co. (Paraloid EXL 3647: styrene-butadiene core and a poly(methyl methacrylate) (PMMA) shell). The adhering rubbery particles (type-II) consisted of a styrene-butadiene core and a polystyrene shell, and were an experimental type of core-shell rubber kindly supplied by the General Electric Company. The size of the particles was in the range of 0.1-0.3 μm. Extruded strands were quenched, pelletized and subsequently injection-moulded (Arburg Allrounder 220-75-250) into dumb-bell shaped tensile bars (DIN 53 455) at a temperature of 200°C. In order to perform dilatometric measurements, a fraction of the pelletized materials was compression-moulded into sheets, possessing a thickness of 3 mm. These sheets were machined into rectangular shaped specimens with a length of 100 mm and cross-sectional dimensions of 3 mm x 10 mm.

2.2.2. Mechanical testing

Before mechanical testing, both the injection-moulded and the compression-moulded tensile bars were annealed at 80°C for 24 hours. Both the dumb-bell shaped layered samples of PS and PE and the dumb-bell shaped rubber-modified PS samples were strained at room temperature at a cross-head speed of 5 mm min⁻¹ on a Frank (type: 81565 IV) tensile machine. Extensometers were used in the latter case to obtain accurate data concerning the stress-strain curves of the samples. At least five specimens were fractured for each blend composition.

The dilatometric experiments were performed on a Instron (type: TTBM) tensile machine, equipped with a dilatometer filled with water. A detailed description of this method has been published elsewhere¹⁹, but some general aspects will be given here. Dilatometry allows measurement of the volume change ($\Delta V/V_0$) of the specimen during longitudinal straining. This is important with respect to the determination of the type of deformation mechanism occurring in the sample. Crazing will be accompanied by an increase in volume (void formation) of the specimen during longitudinal elongation¹³. In the case of shearing longitudinal straining will not result in an increase in volume-strain. For rubber-modified materials it is not always clear whether a volume increase during straining is the consequence of dilatation of the rubbery particles or the result of the crazing mechanism initiated at the rubbery particles. The strain rate applied in the dilatometer was 5 mm min⁻¹ and the span was 50 mm, resulting in a V_0 of 1500 mm³. The accuracy of the dilatometer was 1-2 mm³.

2.2.3 Scanning electron microscopy

Scanning electron microscopy (SEM; Cambridge Stereo Scan 200) was applied to investigate (i) the continuity and the thickness of the thin layers of PS and PE in the coextruded tapes, and (ii) the morphologies of the injection-moulded PS/rubber blends, to check the homogeneity of the distribution of the particles. In both cases, samples were cut parallel to the direction of extrusion at the centre of the specimen and subsequently sectioned at liquid-nitrogen temperature with a glass knife, etched in an oxygen plasma and finally covered with a gold layer.

2.3 Results and Discussion

2.3.1 The structure of multilayered tapes of PS/PE

Figure 2.2a is a SEM micrograph of an alternating PS/PE 50/50 w/w tape (3 mixing elements), possessing both PS and PE layers of 10 μm thickness. It is clear from this micrograph that the adhesion between the PS and PE layers is poor, due to the fact that PE crystallizes (causing shrinkage) during cooling from the melt to room temperature. Consequently, PE serves as a perfect laminator for the thin stratified PS structures.

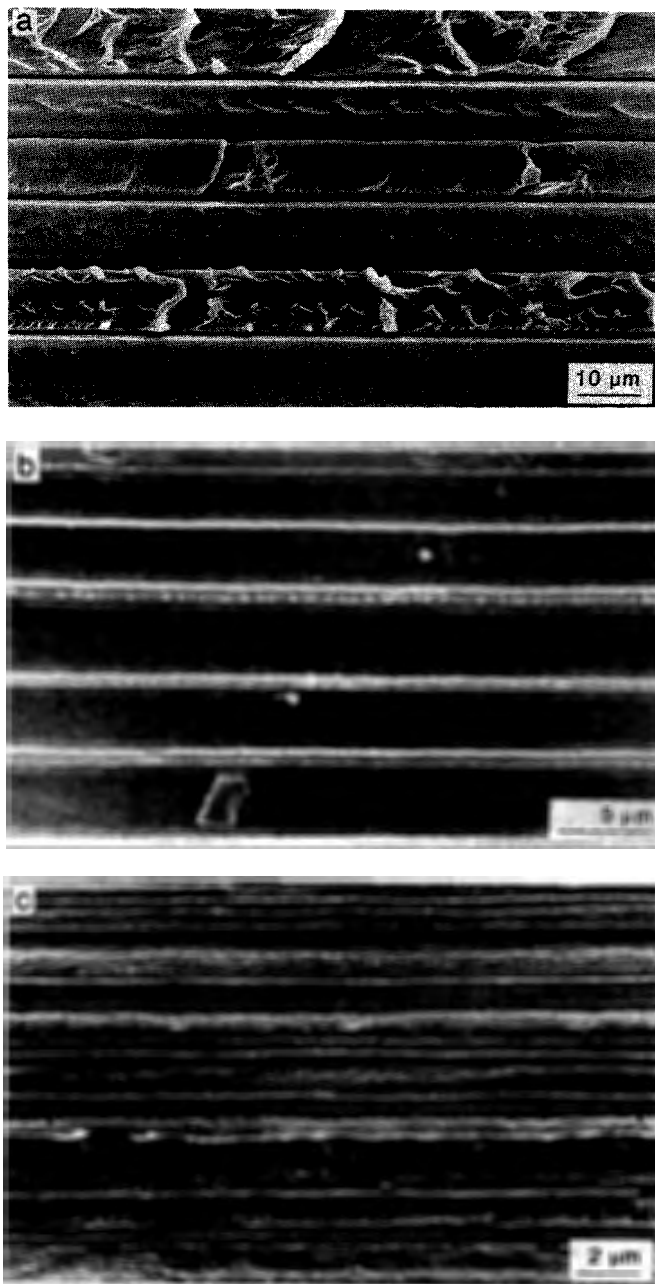


Figure 2.2 SEM micrographs of a PS/PE 50/50 w/w tape with three mixing elements (a); PS/PE 25/75 tapes with six mixing elements (b) and nine mixing elements (c)

Figure 2.2b represents the minimum PS layer thickness attainable with this static mixing equipment: $0.8 \mu\text{m}$ (PS/PE: 25/75 w/w; 6 mixing elements). Upon further increasing the number of elements, the tapes contain a lot of discontinuities due to rupture of the layers (figure 2.2c: PS/PE: 25/75 w/w; 9 mixing elements).

2.3.2 Mechanical properties of PS tapes

Figure 2.3 shows the stress-strain curves of pure PS and PE tapes with a total tape thickness of about 0.3 mm. Curve A represents the typical stress-strain curve of PS: a breaking stress of 40 MPa and a strain at break of 1.5%. PE, on the other hand (figure 2.3, curve B), is a very ductile polymer with a strain at break of about 225% under the same testing conditions.

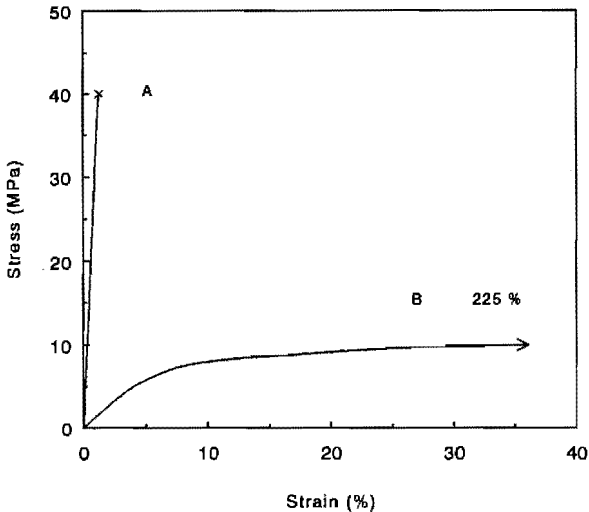


Figure 2.3 Stress-strain curves of the reference materials: A, PS; B, PE

In figure 2.4, a stress-strain curve of a multilayered tape (PS/PE 25/75 w/w, 6 mixing elements) is shown. The sharp decrease in stress at 33% strain is the result of rupture of the PS layers. After passing this strong decrease in stress the measurement is stopped, with the PE layers unbroken, as indicated by the constant level of stress after passing 33% strain. If we assume that the stress-strain behaviour of PE is not influenced by a change in absolute thickness²⁰ we can (corresponding to the volume fraction of PE present in the total composite) subtract the stress-strain curve of PE from the stress-strain curve of the multilayered composite. The stress-strain trace of

the thin PS component results. In *figure 2.5*, these traces are shown for four different tapes, with different PS/PE compositions and number of layers.

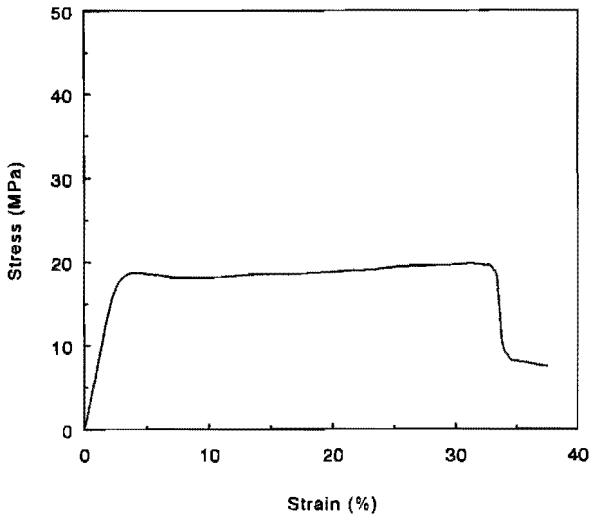


Figure 2.4 Stress-strain trace of a PS/PE 25/75 w/w multilayered tape (six mixing elements)

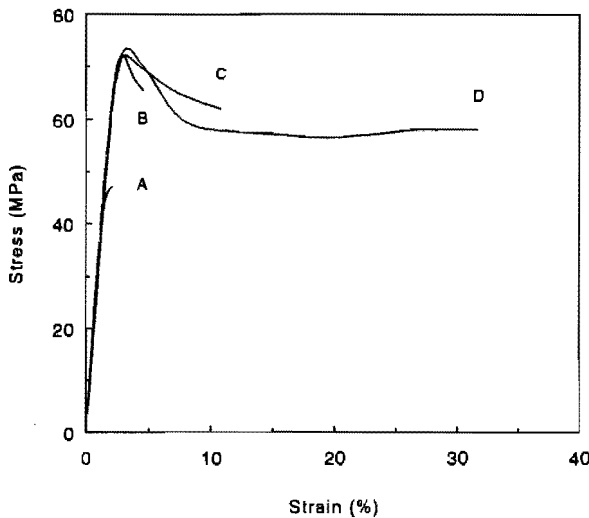


Figure 2.5 Stress-strain curves for pure PS tapes with varying PS layer thickness: A, 35 μm ; B, 4.5 μm ; C, 1.5 μm ; D, 0.8 μm

Curve A corresponds with a PS layer thickness of 35 μm (PS/PE: 50/50 w/w) and

resembles the ordinary stress-strain behaviour of PS as observed in *figure 2.3*, curve A. If the layer thickness of PS is decreased to $4.5 \mu\text{m}$ (PS/PE: 25/75 w/w) the maximum stress is raised to 70 MPa and the strain at break is increased to a value of 5% (*figure 2.5*, curve B). Further decreasing the PS layer thickness results in a shift of the strain at break to a value of more than 30% (*figure 2.5*, curve D, thickness of PS layers is $0.8 \mu\text{m}$; PS/PE: 25/75 w/w). In *figure 2.6* the strain at break of PS is plotted as a function of the absolute PS layer thickness as obtained from data of three different PS/PE ratios.

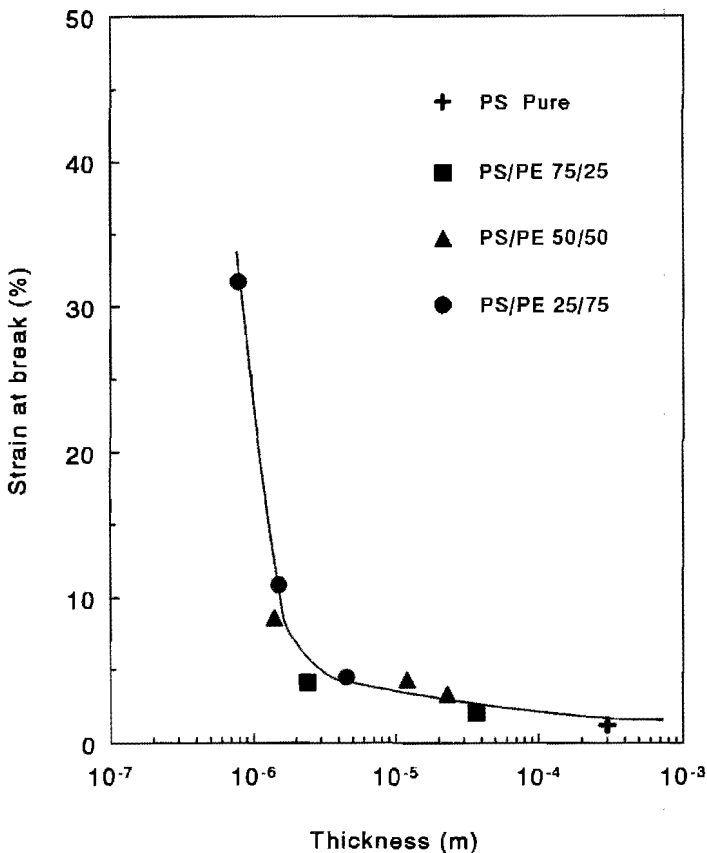


Figure 2.6 Strain at break of PS tapes as a function of PS layer thickness

As can be inferred from this figure, the 'critical thickness' for PS is below $1 \mu\text{m}$ for the given testing conditions. However, due to limitations in the minimum continuous PS layer thickness that could be achieved, the exact value of the critical PS layer

thickness cannot be determined. Kramer and co-workers^{21,22} have also noticed a change in craze structure if the thickness of a PS film (free surface, exposed to air) was below 0.15 μm . Clearly, there is a close correspondence with the critical thickness of PS reported here.

A similar size effect in multilayered structures has been observed by Ma et al.²³. Their explanation for the strong increase in strain at break of multilayered composites upon decreasing the layer thickness, based on polycarbonate (PC) and styrene-acrylonitrile copolymer (SAN), was related to the micromechanics of these multilayered structures. In the PC/SAN system, analyzed by Ma et al., a considerable level of adhesion is present between the two constituents of the composite, while in the case of the PS/PE system the level of adhesion is negligible²⁴. Hence, the size effects observed in the non-adhesive PS/PE multilayered structures are probably not induced by complex micromechanics that strongly depend on the precise level of adhesion.

In our PS/PE multilayered system, where adhesion is negligible, the explanation of an increase in drawability below a certain minimum thickness is straightforward. The process of deformation can only be sustained if the stress in the oriented parts is below the breaking stress, while the stress in the undeformed connected matrix surpasses the yield stress (analogous to the necking phenomenon in amorphous polymers²⁵). *This principle can be generally applied to polymer systems provided that initiation of deformation always starts locally.* By lowering the PS layer thickness ($< 1 \mu\text{m}$) these conditions are approximated, resulting in a continuation of the process of deformation.

2.3.3 Rubber-modified PS

The principle of a critical thickness, as approximated for thin layers of PS ($< 1 \mu\text{m}$), should also exist in a standard PS sample if the local thickness inside the sample is below the critical value. In order to test this hypothesis, 'holes' were introduced to create multiple thin PS ligaments inside the material. Holes were generated by the introduction of rubbery particles, which should not be attached to the PS matrix. For this purpose core-shell rubbers were used possessing a PMMA shell (type-I): the PMMA does not adhere to the PS matrix²⁴ and, as a consequence of thermal shrinkage, the rubbery domains easily become detached from the PS matrix upon, or

even before, mechanical deformation. In *figure 2.7* SEM micrographs of both types of core-shell rubber-modified PS samples are shown, containing different weight fractions rubber (40, 50 and 60 wt%). The samples are cut from injection-moulded tensile bars parallel to the direction of extrusion. In all cases, discrete rubbery particles are observed without any significant agglomeration.

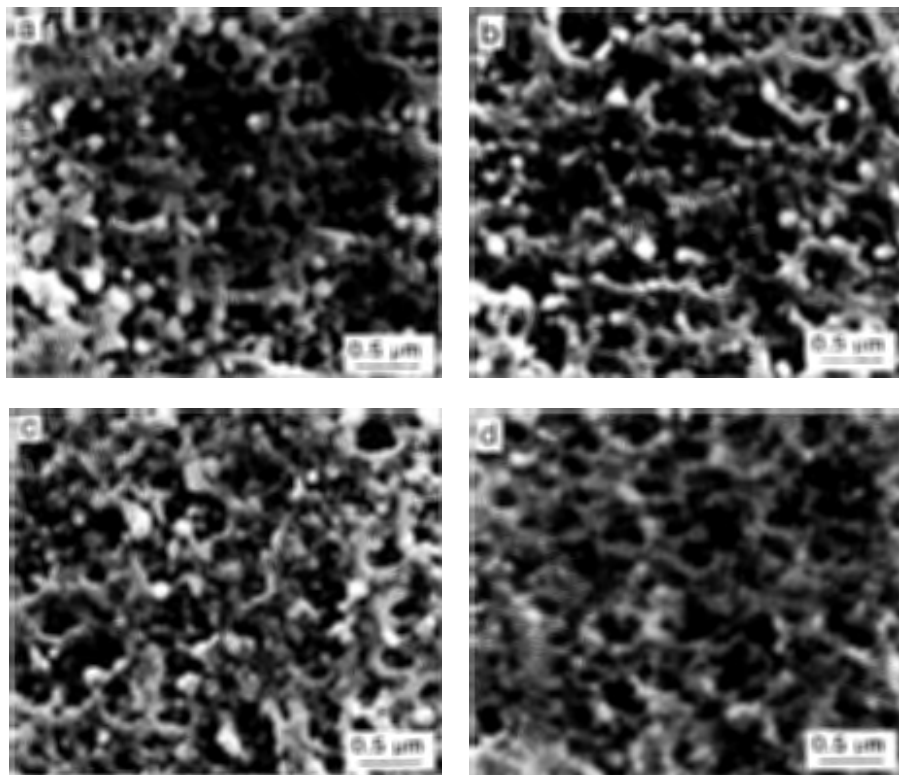


Figure 2.7 SEM micrographs of core-shell rubber-modified PS: (a) 40 wt% type-I; (b) 50 wt% type-I; (c) 60 wt% type-I; (d) 60 wt% type-II

In *figure 2.8* the stress-strain curves of PS containing various amounts of type-I core-shell rubber are shown (40, 50 and 60 wt%). Lower weight fractions rubber are omitted for the sake of simplicity (these samples are all brittle, possessing a strain at break not exceeding 10%). Curve A corresponds to a blend containing 40 wt% core-shell rubber. The strain to break is rather low taking the high weight fraction rubber into account. Increasing the rubber weight fraction to 50 wt% results in an increase in strain to break to 25%, comparable with the strain to break of commercially available high impact polystyrene, containing a rubber weight fraction of only about 25%, but

with a different microstructure. However, upon adding 60 wt% core-shell rubber a sharp increase in strain to break is observed clearly related to this critical ligament thickness below which a sharp increase in ductility is obtained.

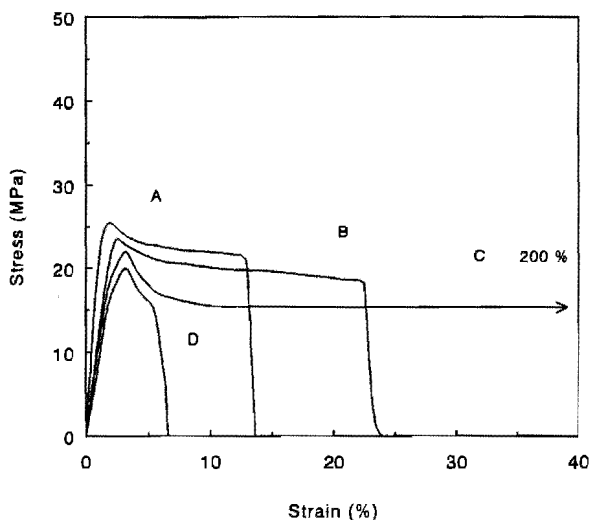


Figure 2.8 Stress-strain curves of type-I core-shell rubber-modified PS (A, 40 wt%; B, 50 wt%; C, 60 wt% rubber) and type-II core-shell rubber-modified PS (D, 60 wt% rubber)

Clearly, local deformation can be initiated at stress concentrations near defects ('holes') and more or less controlled by the introduction of a second, low modulus phase; however, deformation, i.e. stretching of the entanglement network, can only be sustained if the sample as a whole follows this deformation process. If the average distance between the rubber particles is calculated¹⁶ (ID) (due to the high rubber volume fraction a body-centred cubic lattice is assumed) it can be stated that the critical interparticle distance (ID_c) for PS is located at $0.05 \mu\text{m}$. The PS modified with 50 wt% rubber contains ligaments of a thickness of about $0.06 \mu\text{m}$, which is clearly above the critical thickness, while the 60 wt% rubber-modified sample contains matrix ligaments of a thickness of about $0.04 \mu\text{m}$, which is obviously just below the critical ligament thickness.

To check the importance of the absence of adhesion in obtaining locally thin PS ligaments which can easily be stretched to a macroscopic strain of 200%, also core-shell rubbers were also applied having a polystyrene shell (type-II; perfect adhesion to

the PS matrix). Even if 60 wt% of the adhering core-shell rubber is present in the PS matrix, only a strain at break of about 6% is measured (figure 2.8, curve D).

To gain more insight into the type of deformation mechanism of blends containing polystyrene and the non-adhering (type-I) core-shell rubber, tensile tests have been performed with simultaneous volume measurements. Figure 2.9 shows the results of these measurements for PS blends containing 40 wt% (curve A), 50 wt% (curve B) and 60 wt% (curve C) type-I core-shell rubber (the volume-strain curves for the blends containing 10, 20 and 30 wt% rubber are omitted for the sake of simplicity).

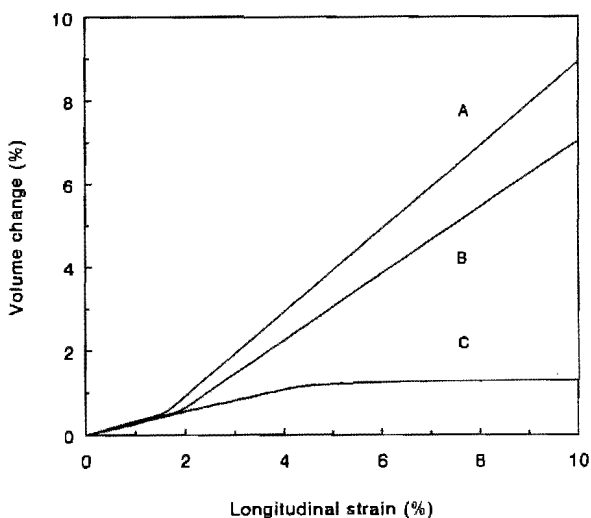


Figure 2.9 Volume-strain curves of type-I core-shell rubber-modified PS: A, 40 wt%; B, 50 wt%; C, 60 wt% rubber

For the blend containing 40 wt% core-shell rubber, the $(\Delta V/V_0)$ curve increases slightly in the region of elastic behaviour (0-1.5% longitudinal strain). At a longitudinal strain of about 2.5% the slope of the curve increases sharply. This may result from either of two processes: (1) the core-shell rubber becomes more detached from the PS matrix; or (2) the crazing mechanism is operative in this material¹³. The slope of the volume-strain curve goes asymptotically to unity, indicating an equilibrium between the increase in volume-strain (void content) and the increase in elongational strain. If the rubber concentration is increased to 50 wt%, almost the same behaviour is observed for the volume-strain curve, except that in this case the slope of the curve is less than unity, after passing the elastic region. This implies that

the increase in void content is lower than the increase in longitudinal elongation. This can only be explained by a contribution of shear deformation to the total deformation behaviour of the sample ¹³, since it is known that the mechanism of shear deformation occurs without an increase in sample volume. Finally, curve C clearly confirms this statement: in this case the slope of the ($\Delta V/V_0$) curve decreases to zero and remains at zero until the maximum strain of 200% is reached, indicating that under these conditions the sample deforms purely by shear deformation. Hence, a transition from crazing to shear deformation occurs if the interparticle distance is decreased from 0.06 μm (50 wt% rubber) to 0.04 μm (60 wt% rubber), which correlates well with the sharp increase in strain to break, shown in *figure 2.8*.

The value of ID_c obtained for type-I core-shell rubber-modified PS is more accurate than the value obtained from the multilayer composites. This is due to the limitations in PS layer thickness obtainable for the PS/PE system. At a layer thickness of 0.8 μm , only the onset of a sharp increase of the strain to break is measured and the critical layer thickness is obviously not yet reached. A further reduction of layer thickness should lead to a strain to break comparable with the value obtained with type-I core-shell rubber-modified PS (200%). Additional experiments with a newly designed multilayer mixer revealed that, if the viscosities of the two polymers are closely matched such as for the model system PS/PMMA, the minimum thickness of still continuous layers, can be reduced to 80 nm. However, for the system PS/PE these low values could not be reached.

2.4 Conclusions

2.4.1 Local thickness

It was shown that brittle polymers become ductile below a critical thickness, as demonstrated for isotropic tapes of polystyrene. The onset of a sharp increase in strain to break of polystyrene was found if the thickness was reduced below 1 μm . The exact value of the critical thickness could not be determined using layered structures, because the minimum continuous PS layer thickness that could be achieved was restricted to 0.8 μm . The true yield stress of PS was found to be about 70 MPa.

For rubber-modified polystyrene, the influence of the local ligament thickness on the mechanical response was investigated, and the exact value of the critical surface-to-

surface interparticle distance (i.e. ligament thickness) was determined to be $0.05 \mu\text{m}$. Below this critical value the material demonstrates a remarkable ductile behaviour.

2.4.2 Influence of network density

Our research is aimed at an overall investigation of the ultimate toughness of polymeric systems, by varying systematically the intrinsic network (entanglement and/or crosslink) density and the local thickness of the system (see *figure 2.10*).

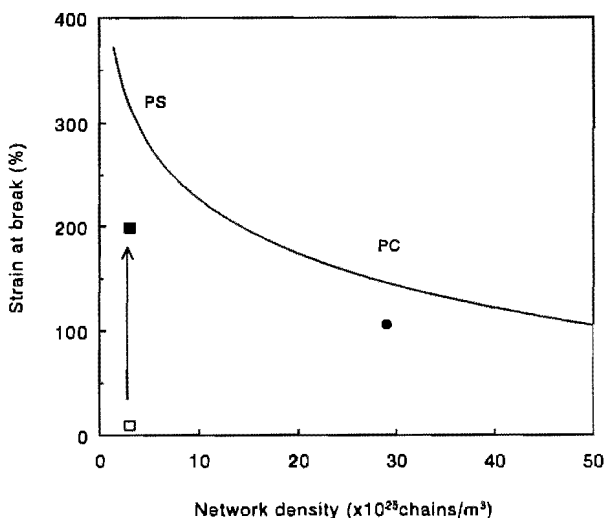


Figure 2.10 Strain at break versus network (entanglement and/or crosslink) density. The full curve represents the theoretical strain at break of the polymer network. See text for details

The full curve in *figure 2.10* corresponds to the theoretical strain at break based on the intrinsic network structure (λ_{max}). For polycarbonate the macroscopic strain at break is close to the theoretical value (*figure 2.10*, filled circle). For polystyrene however, the macroscopic strain at break of a standard sample (*figure 2.10*, open square), is far below the theoretical value. However, if the (local) thickness of PS is below its critical value, the macroscopic strain at break (*figure 2.10*, filled square) approximates the expected value rather well (as shown in this chapter).

In two subsequent chapters (chapter 3: Influence of entanglement density ²⁶, and chapter 4: Influence of crosslink density ²⁷) the critical (ligament) thickness between

non-adhering (or cavitated) rubbery particles will be investigated for other polymer systems, with different network density. In particular, the relationship between the absolute value of this critical thickness and the intrinsic molecular network structure will be emphasized. In chapter 3, entangled structures will be dealt with using the model system PS-poly(2,6-dimethyl-1,4-phenylene ether) in order to set the entanglement density. Chapter 4 will focus on different thermoset systems which can be considered as rather 'densely' crosslinked structures in terms of network density, compared with thermoplastic polymers.

2.5 References

- 1 Bucknall, C.B. 'Toughened Plastics', Appl. Sci. Publ., London, 1977
- 2 De Gennes, P.G. *Europhys. Lett.* 1991, **15** (2), 191
- 3 Parker, D.S., Sue, H.J., Huang, J. and Yee, A.F. *Polymer* 1990, **31**, 2267
- 4 Brown, H.R. *Macromolecules* 1991, **24**, 2752
- 5 Termonia, T. and Walsh, D.J. *J. Mater. Sci.* 1989, **24**, 247
- 6 Michler, G.H. *J. Mater. Sci.* 1990, **25**, 2321
- 7 Kramer, E.J. and Berger, L.L. *Adv. Polym. Sci.* 1990, **91/92**, 1
- 8 Donald, A.M. and Kramer, E.J. *Polymer* 1982, **23**, 461
- 9 Donald, A.M. and Kramer, E.J. *Polymer* 1982, **23**, 1183
- 10 Wu, S. *Polym. Eng. Sci.* 1990, **30** (13), 753
- 11 Wu, S. *Polymer* 1985, **26**, 1855
- 12 Smith, P., Lemstra, P.J., Kalb, B. and Pennings, A.J. *Polym. Bull.* 1979, **1**, 733
- 13 Kinloch, A.J. and Young, R.J. 'Fracture Behaviour of Polymers', Elsevier, London, 1985
- 14 Borggreve, R.J.M., Gaymans, R.J., Schuijjer, J. and Ingen Housz, J.F. *Polymer*, 1987, **28**, 1489
- 15 Borggreve, R.J.M. Ph.D. Thesis, University of Twente, The Netherlands, 1988
- 16 Wu, S. *J. Appl. Polym. Sci.* 1988, **35**, 549
- 17 Sluijters, R. *De Ingenieur* 1965, **77** (15), 33
- 18 Schilo, D. and Ostertag, K. *Verfahrenstechnik* 1972, **6** (2), 45
- 19 Coumans, W.J. and Heikens, D. *Polymer* 1980, **21**, 957
- 20 Pan, S.J., Hill, M.J., Keller, A., Hiltner, A. and Baer, E. *J. Polym. Sci., Polym. Phys. Edn* 1990, **28**, 1105
- 21 Donald, A.M., Chan, T. and Kramer, E.J. *J. Mater. Sci.* 1981, **16**, 669
- 22 Chan, T., Donald, A.M. and Kramer, E.J. *J. Mater. Sci.* 1981, **16**, 676
- 23 Ma, M., Vijayan, K., Hiltner, A., Baer, E. and Im, J. *J. Mater. Sci.* 1990, **25**, 2039
- 24 Wu, S. 'Polymer Interface and Adhesion', Dekker, Basel, 1982
- 25 Ward, I.M. 'Mechanical Properties of Solid Polymers', Wiley-Interscience, London, 1971, p.274
- 26 Van der Sanden, M.C.M., Meijer, H.E.H. and T.A. Tervoort *Polymer* 1993, **34**, 2961
- 27 Van der Sanden, M.C.M. and Meijer, H.E.H. *Polymer* in press

Chapter 3*

Influence of Entanglement Density

3.1 Introduction

In chapter 2¹ it was shown that the macroscopic deformation and toughness of amorphous polymers, which are prone to catastrophic strain localizations, can be controlled by changing the microstructure. The concept of a material-specific critical thickness, either in the form of thin sheets in stratified structures (with a non-adhering polymer acting as a spacer) or as ligaments separated by 'holes', was verified for polystyrene (PS). For PS, with ligaments of a (local) thickness of 0.05 μm , the maximum macroscopic strain at break was found to be 200%, about 60% of the theoretical maximum strain at break (320%). Kramer et al.^{2,3} observed the same deviation between the (maximum) natural draw ratio (λ_{max}) of a *shear deforming* polymer and the local strain level inside a plane-stress deformation zone (λ_{DZ}). They analyzed a large number of amorphous polymers (classified by entanglement molecular weight, M_e) and found in all cases a constant ratio $\lambda_{\text{DZ}}/\lambda_{\text{max}}$: 0.6. Their explanation for the discrepancy between the expected and the experimentally determined value is associated with the rather naive character of the model^{2,3}, which is based on the maximum extension of a *single* entanglement strand only.

In order to transfer the maximum strains from the distinct localizations in crazes and shear bands to the macroscopic level, the stress in the deformed regions should not surpass the breaking stress, while the stress in the connected undeformed material should be higher than the yield stress. From this qualitative explanation for the existence of a critical material thickness, a dependence of this thickness on the maximum extension ratio and thus on the network or entanglement density is to be

* This chapter is reproduced, in part, from:

1. Van der Sanden, M.C.M., Meijer, H.E.H. and Tervoort, T.A. *Polymer* 1993 **34**, 2961

expected. This aspect of the deformation behaviour of polymers was investigated in this chapter, combined with the influence of entanglement density on the final macroscopic strain to break.

The system polystyrene-poly(2,6-dimethyl-1,4-phenylene ether) (PS-PPE) was chosen as a model system because for this miscible pair of amorphous polymers^{4,5} the entanglement density can be varied by adjusting the relative volume fractions of both constituents⁶. Results of both multilayered tapes of PS-PPE/PE (thin films of PS-PPE alternating with polyethylene (PE)) as well as non-adhering core-shell rubber-modified materials (thin matrix ligaments) will be discussed, although the detailed analysis of multilayered PS-PPE/PE tapes is postponed to chapter 6⁷. Via dilatometry, the competition between crazing and shear deformation was investigated and, finally, a simple model will be proposed to explain the relationship between the critical thickness and the entanglement density.

3.2 Experimental

3.2.1 Materials

The materials used were polystyrene (DOW, Styron 638), poly(2,6-dimethyl-1,4-phenylene ether) (General Electric Co., PPE-803), low-density polyethylene (DSM, LDPE 1808 AN) and a core-shell rubber possessing a poly(methyl methacrylate) shell and a styrene-butadiene core (Rohm and Haas Co., Paraloid EXL 3647). The PS was a general-purpose extrusion grade: d.s.c., $T_g = 88^\circ\text{C}$; g.p.c. (CHCl_3), $M_n = 70 \text{ kg mol}^{-1}$ and $M_w = 200 \text{ kg mol}^{-1}$. The PPE was used as received: d.s.c., $T_g = 215^\circ\text{C}$; I.V. = 0.37 dl g^{-1} (CHCl_3 , 25°C); g.p.c. (CHCl_3), $M_n = 14.3 \text{ kg mol}^{-1}$ and $M_w = 31.5 \text{ kg mol}^{-1}$. The PE was an injection-moulding type possessing a melt flow index of 7.5 dg min^{-1} . The core-shell rubber was an extrusion grade and the size of the rubbery particles was in the range of $0.1\text{-}0.3 \mu\text{m}$.

3.2.2 Sample preparation

PS and PPE were compounded in various weight fractions (PS-PPE 80-20, 60-40, 40-60 and 20-80) in order to obtain blends with various entanglement densities. Extrusion was carried out on a co-rotating twin screw extruder (Werner and Pfleiderer ZSK 25) with a standard screw geometry. A master batch of PS-PPE 50-50 was prepared at 290°C . This master batch was used to prepare the PS-PPE 80-20 and 60-40 blends during a second extrusion cycle, at respectively 250°C and 270°C (the extrusion temperature was kept as low as possible in order to avoid (any) degradation of the PPE). The PS-PPE 40-60 and 20-80 blends were prepared during a double extrusion-cycle at 290°C .

Multilayered PS-PPE/PE samples were prepared using a Multiflux static mixer⁸⁹. The principle of this

mixer was described in chapter 2 ¹; however, in this study an improved version of the previously introduced Multiflux mixer was used. Thin laminated tapes consisting of alternating layers of PS-PPE and PE were prepared at respectively 220°C (PS-PPE: 80-20), 225°C (PS-PPE: 60-40) and 230°C (PS-PPE: 40-60) and contained a varying number of layers: from 128 (6 mixing elements) up to 4096 (11 mixing elements). PS-PPE and PE were applied in three different proportions: 75/25, 50/50 and 25/75 w/w. Small dumb-bell shaped tensile specimens were machined from these tapes parallel to the direction of extrusion according to ASTM D 1708 (the thickness was kept constant around 0.3 mm).

Core-shell rubber-modified PS-PPE blends containing 10, 20, 30, 40, 50 and 60 wt% rubber were prepared in a two-step compounding process, as described above. During the second extrusion step the core-shell rubber was added (processing temperatures are shown in table 3.1).

Table 3.1 Processing temperatures for the various neat and rubber-modified PS-PPE blends

Blend composition ^a	Processing temperature (°C)
80-20/X ^b	250
60-40/X	270
40-60/X	290
20-80/X	290

^a The blend composition is indicated with a three number code: 'weight fraction PS present in the matrix' - 'weight fraction PPE present in the matrix' / 'weight fraction core-shell rubber present in the total blend (=X)'.

^b The processing temperature was, independently of the rubber concentration, only determined by the matrix composition

Extruded strands were quenched and pelletized subsequently. Both the neat and the rubber-modified PS-PPE blends were injection-moulded (Arburg Allrounder 220-75-250) into dog-bone shaped tensile bars (DIN 53 455, sample thickness: 3 mm). The temperature at which the injection moulding was carried out depended on the blend composition and is listed in table 3.1 for the various PS-PPE blends.

3.2.3 Mechanical testing

Prior to mechanical testing, the layered samples as well as the injection-moulded tensile bars were annealed at a temperature 20°C below the glass transition temperature of the matrix for at least 24 hours.

The layered samples and the core-shell rubber-modified tensile specimens were uniaxially strained on a

Frank tensile machine (type: 81565 IV) at a cross-head speed of 5 mm min⁻¹ at room temperature. To obtain accurate data concerning the longitudinal strain level of the specimens, extensometers were used in the latter case. At least five specimens were fractured for each testing condition.

In order to obtain data on the relative volume change ($\Delta V/V_0$) of a (core-shell rubber-modified) PS-PPE blend during tensile loading, tensile dilatometry was used¹⁰. This technique not only allows determination of the mechanical characteristics of a material (e.g. Poisson's ratio), but can also be used to obtain information on the type of deformation mechanism. Tensile dilatometry, as applied in this investigation, is extensively described in ref. 1.

3.2.4 Dynamic mechanical thermal analysis

The storage shear modulus of neat PS-PPE blends was determined in the melt as a function of the angular frequency (10^{-2} - 10^2 rad s⁻¹) for at least five different temperatures over a range of 50°C, using a Rheometrics RDS II spectrometer. A plate-plate geometry was used (diameter 25 mm) at a maximum strain of 2%. The thickness of the samples was 1 mm. Shifting of the G' versus ω curves to a reference temperature, approximately 40°C above the glass transition temperature, resulted in a master curve. The rubber plateau modulus G_{No} is equal to the storage modulus G' at the frequency where $\tan\delta$ is at its minimum in the plateau zone of the master curve^{11,12}. Applying the classical concept of rubber elasticity theory, the molecular weight between entanglement nodes, M_e , could be calculated¹³:

$$M_e = \rho RT / G_{No} \quad (3.1)$$

where ρ is the density, R is the gas constant and T is the reference temperature.

3.2.5 Scanning electron microscopy

Scanning electron microscopy (SEM; Cambridge Stereo Scan 200) was applied to check the continuity of the layers in PS-PPE/PE tapes and the homogeneity of the rubber particle distribution in core-shell rubber-modified PS-PPE blends. Specimens were cut from respectively the centre of the layered specimen, parallel to the direction of extrusion and perpendicular to the layers, and from the centre of the injection-moulded tensile bar, again parallel to the direction of extrusion. The surface of the samples was microtomed using a glass knife at liquid-nitrogen temperature, in order to avoid any deformation during sample preparation. After microtoming, the sample was etched in an oxygen plasma to remove the polyethylene, respectively the rubbery particles, and to gain more contrast. Finally, the samples were covered with a conducting gold layer.

In order to investigate the deformation and fracture characteristics of the core-shell rubber-modified tensile specimens, post-mortem fracture surface analysis was carried out using SEM. For this purpose, the specimens were not etched in an oxygen plasma, but directly covered with a gold layer.

3.2.6 D.s.c. measurements

Glass transition temperatures of extruded neat PS-PPE blends were recorded using a Perkin-Elmer DSC-7 differential scanning calorimeter. The samples were first heated to 250°C, quenched from the melt to ambient temperature and then scanned at a standard heating rate of 20°C min⁻¹. Indium was used for temperature calibration ($T_{m, \text{onset}} = 156.6^\circ\text{C}$). The glass transition temperatures (T_g) were determined using the intercept of the tangent at the point of maximum slope and the extrapolated baseline on the low temperature side of the transition.

3.3 Results and Discussion

3.3.1 Characterization of layered PS-PPE/PE tapes and (rubber-modified) PS-PPE blends

Table 3.2 shows T_g values of PS-PPE blends after extrusion and injection moulding as revealed by d.s.c.. For all blend compositions only a single T_g value is observed, clearly confirming the miscibility of PS and PPE on a molecular scale ^{4,5}.

Table 3.2 Glass transition temperatures for neat PS-PPE blends

Blend composition	Glass transition temperature (°C)
80-20	105
60-40	123
40-60	144
20-80	174

The master curves of the PS-PPE 100-0, 80-20 and 60-40 blends as obtained from dynamic mechanical thermal analysis are shown in *figure 3.1*.

The master curves for the PS-PPE 40-60 and 20-80 blends are omitted because these samples showed void formation during measuring at the required high temperatures, indicating thermal degradation of the samples. The temperatures to which the master curves are shifted are respectively 130, 145 and 160°C ($T_g + 40^\circ\text{C}$) for the PS-PPE 100-0, 80-20 and 60-40 blends.

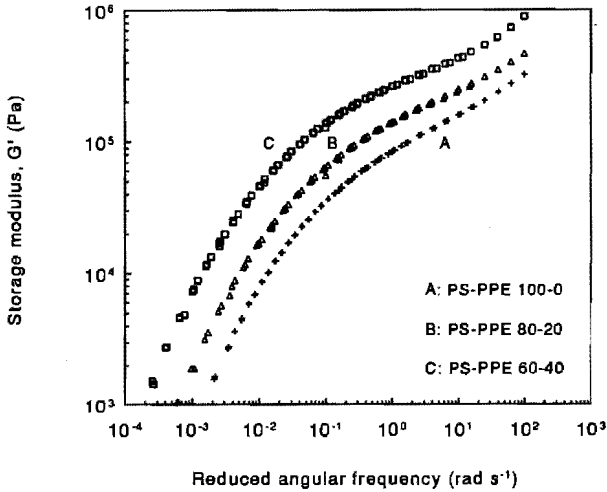


Figure 3.1 Master curves of PS-PPE blends ((A) 100-0, (B) 80-20 and (C) 60-40) as obtained from dynamic mechanical thermal analysis (reference temperatures are respectively 130, 145 and 160°C)

It is clear from figure 3.1 that an increase of the PPE content in the PS-PPE blends results in a shift of the G' curve to higher values. The rubber plateau modulus is determined at the minimum of $\tan\delta$ in the plateau region and is used to calculate the molecular weight between entanglement nodes using equation (3.1). The entanglement density (ν_e) can be calculated using ³:

$$\nu_e = \frac{\rho N_A}{M_e} \quad (3.2)$$

where N_A is Avogadro's number.

In figure 3.2 the value of the entanglement density is plotted versus the PS-PPE composition (filled squares). Prest and Porter ⁶ have determined the entanglement density for several PS-PPE blends as well. They experimentally derived an equation to describe the entanglement molecular weight as a function of the blend composition:

$$M_e(\chi) = \frac{M_e(PS)}{(1 + 3.2\chi)} \quad (3.3)$$

where χ is the weight fraction of PPE in the blend and $M_e(PS)$ is the entanglement molecular weight of polystyrene ¹⁴, $M_e(PS) = 19.1 \text{ kg} \cdot \text{mol}^{-1}$. Although Prest and Porter

derived this equation for a limited range of blend compositions ($0 < \chi < 0.4$) the equation is assumed to be valid up to $\chi = 0.8$.

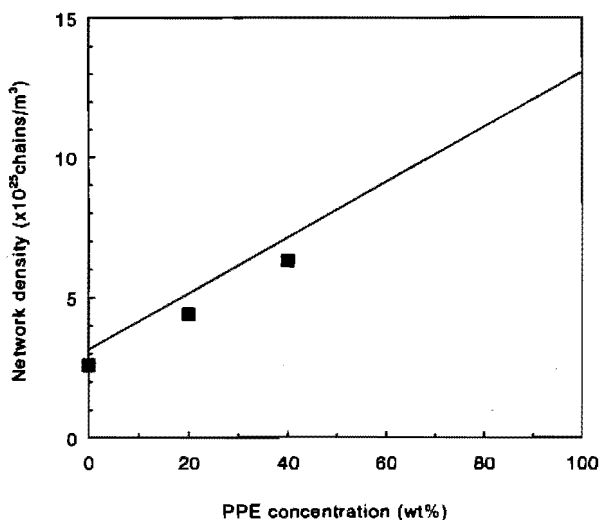


Figure 3.2 Entanglement density versus PPE content in PS-PPE blends. The full curve is according to Prest and Porter⁶

Values of ν_e for the various PS-PPE compositions are calculated by combining equations (3.2) and (3.3). The results of these calculations are also shown in figure 3.1 (full curve). As can be inferred from this figure the entanglement density as obtained from our rheological measurements corresponds well with the values as obtained from data of Prest and Porter. The entanglement density varies linearly between the values of pure PS (3.2×10^{25} chains m⁻³) and of pure PPE (13.2×10^{25} chains m⁻³).

In figure 3.3 SEM micrographs are shown of various microtomed multilayered PS-PPE/PE tapes. The continuity of the layers is clear for figures 3.3a and 3.3c and only a small variation in layer thickness can be observed. For the PS-PPE/PE 25/75 w/w tape (PS-PPE 80-20; 11 mixing elements; figure 3.3b) however, the layer continuity is clearly absent. Obviously, the PS-PPE composition (read: viscosity ratio of PS-PPE/PE) has a large influence on the maximum number of mixing elements possible to apply in the Multiflux mixer before layer discontinuity occurs (compare figures 3.3b and 3.3c). (For pure PS¹, tapes consisting of continuous layers could only be obtained if the number of mixing elements in the previously used Multiflux static mixer did not exceed 6.)



Figure 3.3 SEM micrographs of multilayered PS-PPE/PE tapes: (a) PS-PPE/PE 75/25 (PS-PPE 80-20), 6 mixing elements, (b) PS-PPE/PE 25/75 (PS-PPE 80-20), 11 mixing elements and (c) PS-PPE/PE 25/75 (PS-PPE 60-40), 11 mixing elements

A selection of various microtomed injection-moulded rubber-modified PS-PPE blends is shown in figure 3.4.

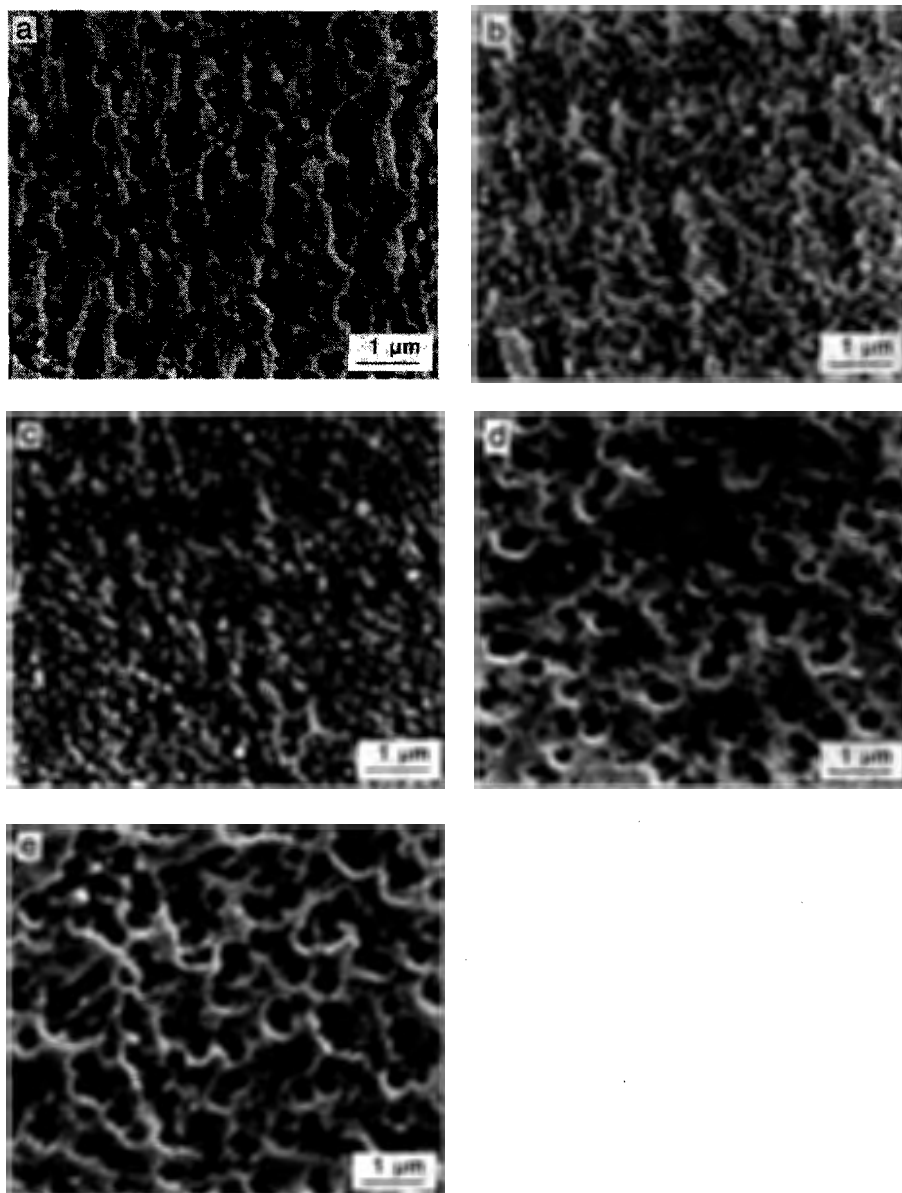


Figure 3.4 SEM micrographs of microtomed core-shell rubber-modified PS-PPE blends: (a) 80-20/20, (b) 80-20/40, (c) 80-20/60, (d) 20-80/10 and (e) 20-80/20

For the lower rubber concentrations (*figure 3.4a*, PS-PPE/rubber 80-20/20 blend) the particle distribution shows a moderate degree of orientation of the particles parallel to the direction of mould flow during the injection moulding step. However, for the higher-weight-fraction core-shell rubber the particle distribution is fairly homogeneous (*figures 3.4b and 3.4c*). If the matrix consists of PS-PPE 20-80 however, a homogeneous particle distribution is already obtained for the lower rubber concentrations (see *figures 3.4d and 3.4e*). However, the particles seem to be coagulated to a small extent for the PS-PPE 20-80 blends.

3.3.2 Mechanical properties of multilayered PS-PPE/PE tapes

In chapter 6 a more extended discussion of the deformation behaviour and mechanical properties of PS-PPE/PE tapes will be given ⁷. Here, only a few results of the multilayered systems will be presented in order to compare these with data obtained from core-shell rubber-modified PS-PPE blends.

In *figure 3.5* the strain to break of stratified tapes is plotted versus the PS-PPE layer thickness for PS-PPE 60-40 and 40-60 blends.

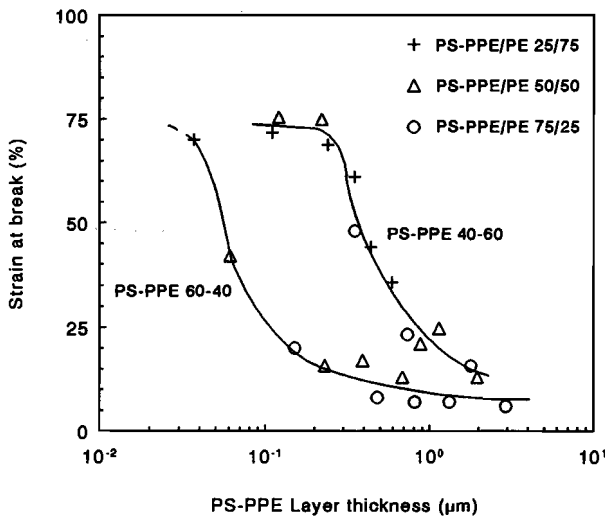


Figure 3.5 Strain at break of PS-PPE/PE tapes as a function of PS-PPE layer thickness

As can be inferred from *figure 3.5* (PS-PPE 60-40), the strain to break increases with

decreasing layer thickness. The experimentally achievable maximum strain at break (about 70%) is observed for the thinnest PS-PPE layers (PS-PPE/PE 25/75, 11 mixing elements). A further decrease in layer thickness, by an increase in number of mixing elements, results in a discontinuous layer structure.

For PS-PPE 40-60 (*figure 3.5*) the thickness below which an increase in strain at break is observed is located at a higher level ($\approx 0.25 \mu\text{m}$) compared to PS-PPE 60-40 ($\approx 0.06 \mu\text{m}$). Thus, a pronounced influence of the entanglement density is found. For the PS-PPE 40-60 blend, the maximum level of strain at break attainable in the ductile region can be estimated to be 70%.

In contrast to pure PS¹, which only showed the onset of an increase in strain at break with stratified structures, the PS-PPE 40-60 blend seems to reach its maximum macroscopic strain, and thus the true critical thickness is found. It is, therefore, even more interesting to compare these data with the more practical 'holey' structures obtained by adding non-adhering core-shell rubbers.

3.3.3 Mechanical properties of rubber-modified PS-PPE blends

1) Strain to break

Strain-to-break data, obtained from slow-speed (5 mm min^{-1}) tensile tests of various rubber-modified PS-PPE blends, are shown in *figure 3.6*. The data for PS¹ (*figure 3.6*, curve A) are taken as a reference. If 20 wt% PPE is added to PS, the strain to break as a function of the rubber concentration (*figure 3.6*, curve B) shows, analogous to PS, a steep increase with increasing rubber weight fraction. However, in this case the transition already occurs at a lower rubber concentration (50 wt%), i.e. a higher ligament thickness compared to PS. The maximum value of the strain to break in the 'tough region' is about 100% and considerably lower than the value for core-shell rubber-modified blends having a pure PS matrix (strain at break of approximately 200%).

Curves C and D in *figure 3.6* clearly confirm this trend. With an increasing PPE content in the matrix, two phenomena are observed: (i) the critical ligament thickness is positioned at a lower rubber concentration and (ii) the maximum value of the strain to break in the ductile region decreases (for curves C and D the levels of strain

to break in the tough region are equal).

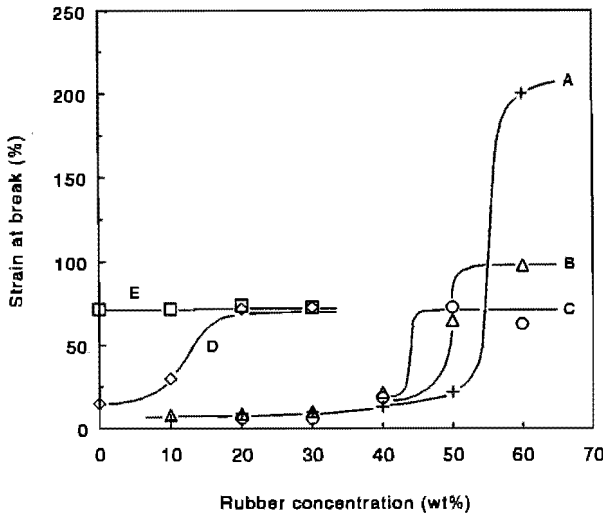


Figure 3.6 Strain at break of rubber-modified PS-PPE blends versus rubber concentration with parameter the matrix composition (PS-PPE): (A) 100-0, (B) 80-20, (C) 60-40, (D) 40-60 and (E) 20-80

Notice that the strain to break in the ductile region of the core-shell rubber-modified PS-PPE 60-40 and 40-60 blends coincides with the maximum strain to break observed for the corresponding PS-PPE/PE tapes. For the PS-PPE 20-80 blend all samples show a macroscopic strain to break of about 65%, independently of the rubber weight fraction (figure 3.6, curve E). Clearly, no brittle-to-ductile transition is found in the given test range. As will be shown in chapter 5, PS-PPE 20-80 blends can demonstrate a brittle-to-ductile transition under more extreme testing conditions (tensile speed: 1 m s^{-1} ; notched)¹⁵.

2) Tensile dilatometry

To analyze the type of deformation mechanism operative in the various core-shell rubber-modified PS-PPE blends, slow-speed tensile dilatometry is carried out (figures 3.7, 3.8 and 3.9). If PS-PPE 80-20 forms the matrix phase the slope of the $\Delta V/V_0$ curve goes to unity if the rubber concentration is 20 wt% or less (figure 3.7), indicating a process of void formation during elongation.

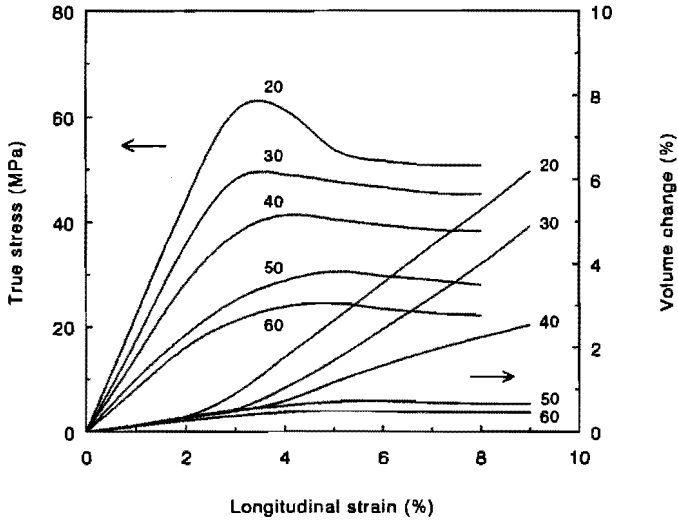


Figure 3.7 Stress-strain and volume-strain curves of rubber-modified PS-PPE 80-20 blends, with parameter the rubber content

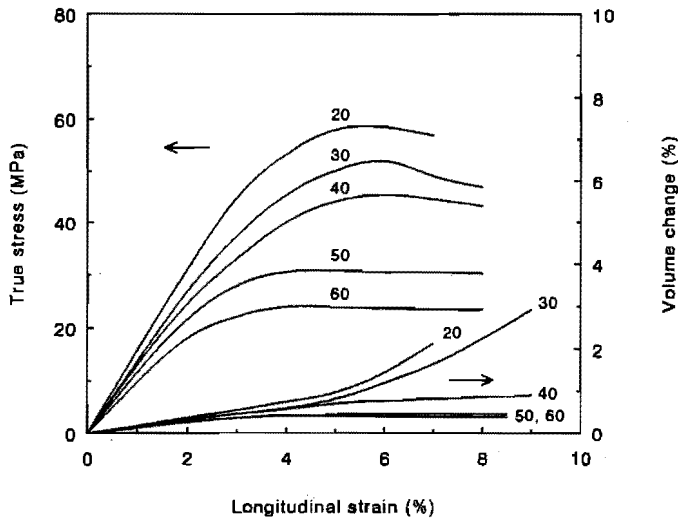


Figure 3.8 As figure 3.7, for PS-PPE 60-40 blends

Void formation can be either the result of the continuation of further detachment of the rubbery particles from the matrix phase or the result of the crazing mechanism normally operative in this blend¹⁶. However, if the rubber weight fraction is increased to 50 wt% (see figure 3.7) the slope decreases to zero after passing the elastic region (0-1.5% strain). This clearly indicates a shear deforming mechanism to be operative

in the blend during longitudinal elongation. The transition from a deformation mechanism accompanied by void formation to a shear deforming mechanism occurs at the same rubber concentration (50 wt%) as the sudden increase in strain to break as shown in *figure 3.6*, curve B.

The results of the dilatometry experiments for PS-PPE 60-40 core-shell rubber-modified blends are shown in *figure 3.8*. If the rubber concentration is below the critical level (see *figure 3.6*, curve C: 20, 30 and 40 wt% rubber) deformation is always accompanied by an increase in volume-strain, while in the ductile region pure shear deformation is observed. Analogous to the PS-PPE 80-20 blend the transition from brittle to ductile deformation behaviour occurs simultaneously with the transition from a deformation mechanism accompanied by void formation to a shearing type of deformation.

For the neat PS-PPE 20-80 blend the slope of the $\Delta V/V_0$ curve (*figure 3.9*, 0 wt% core-shell rubber) decreases to zero after passing the elastic region, confirming that shear deformation occurs in this blend during longitudinal elongation, as also reported in literature^{17,18}.

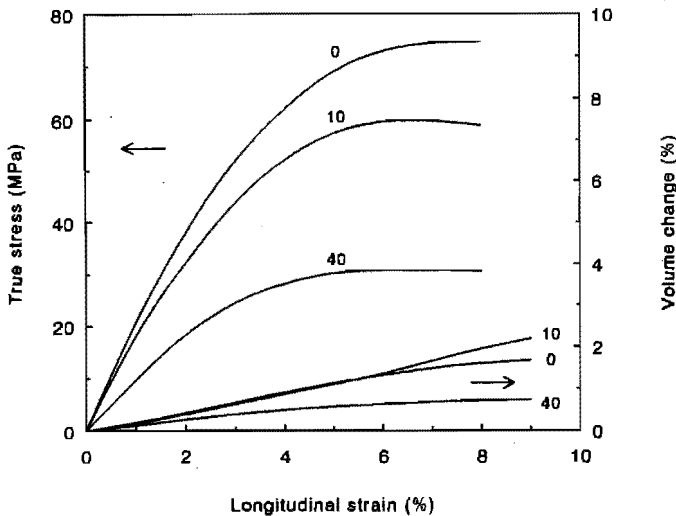


Figure 3.9 As *figure 3.7*, for PS-PPE 20-80 blends

If 10 wt% core-shell rubber is present, the $\Delta V/V_0$ curve shows a moderate increase in slope after exceeding 4% longitudinal strain. This is probably the consequence of

detachment of the rubbery particles upon an increase in strain level since even in the neat blend shear deformation was demonstrated to occur. The slope of the $\Delta V/V_0$ curve corresponding to 40 wt% rubber (*figure 3.9*) decreases to zero after passing the elastic region, again demonstrating the shear deformation mechanism to be operative.

3.3.4 Fracture surfaces

Figure 3.10 shows SEM micrographs of fracture surfaces of various PS-PPE 80-20 and 20-80 blends, uniaxially strained at 5 mm min^{-1} . For the 80-20/20 mixture a brittle fracture surface is observed (*figure 3.10a*). Clearly, the fracture surface is influenced by the presence of the non-adhering rubbery particles, which act as potential crack initiators.

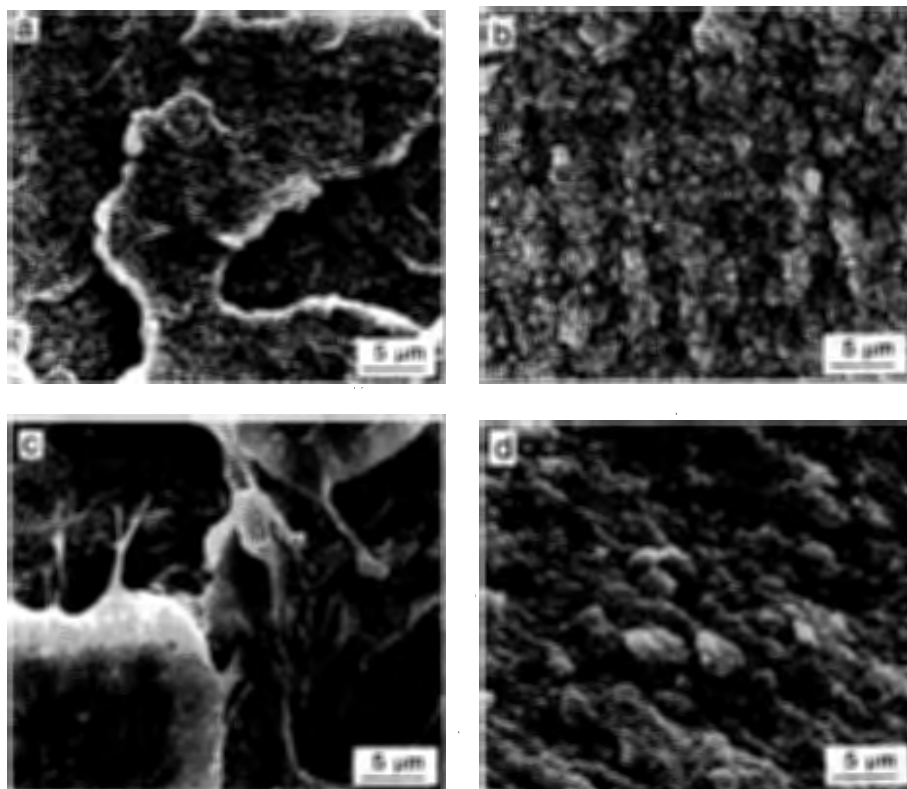


Figure 3.10 SEM micrographs of fracture surfaces of rubber-modified PS-PPE blends: (a) 80-20/20, (b) 80-20/60, (c) 20-80/0 and (d) 20-80/20

If 60 wt% core-shell rubber is added to the PS-PPE 80-20 matrix, extensive ductility can be observed on the fracture surface (*figure 3.10b*). The PS-PPE 20-80 blend, on the other hand, shows even ductility on the fracture surface without rubber toughening (*figure 3.10c*). Addition of 20 wt% rubbery particles does not change the fracture surface considerably: the level of ductility remains about the same (*figure 3.10d*).

3.4 Theoretical Considerations

3.4.1 Macroscopic strain

The maximum extension ratio of an entanglement network can be calculated using the classical theory of rubber elasticity¹⁹. In *figure 3.11* the experimentally determined maximum macroscopic strain to break (λ_{macr}) of the various multilayered and rubber-modified PS-PPE blends is shown as a function of the theoretical maximum extension ratio (λ_{max}) of the entanglement network of the PS-PPE phase.

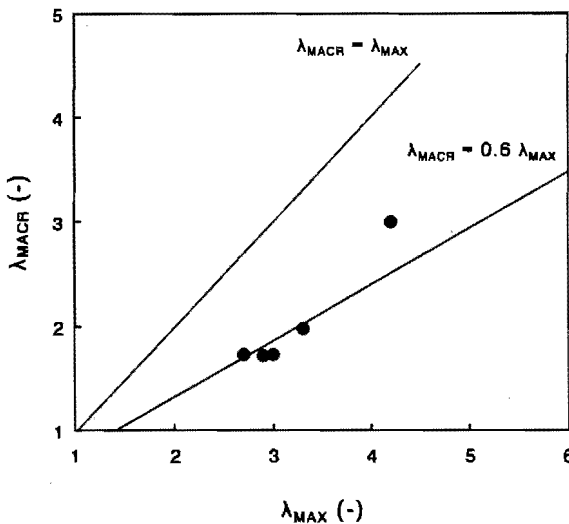


Figure 3.11 Maximum macroscopic draw ratio (λ_{macr}) versus the natural draw ratio (λ_{max}) for stratified and core-shell rubber-modified PS-PPE blends

As can be inferred from *figure 3.11*, the experimentally determined values correlate well with results of Kramer et al. on strain levels determined *locally* inside a deformation zone^{2,3} ($\lambda_{\text{DZ}} = 0.6 * \lambda_{\text{max}}$). The reason for the discrepancy between the

theoretical value, λ_{\max} , and λ_{DZ} (or λ_{macr}) must be related to the non-ideal character of the entanglement network and the assumption of taking one single entanglement strand in order to estimate the theoretical extension ratio of a three-dimensional entanglement network, as already discussed in the 'Introduction' of this chapter.

The macroscopic strain-to-break data of *figure 3.11* can be presented as a function of the entanglement density (see *figure 3.12*) to yield the overall picture of deformation and toughness of amorphous polymers. The filled squares correspond to data obtained from multilayered and rubber-modified PS-PPE blends, and the open square corresponds to PS¹. In chapter 4²⁰ the right hand side of this figure will be investigated, using thermosets of varying crosslink density.

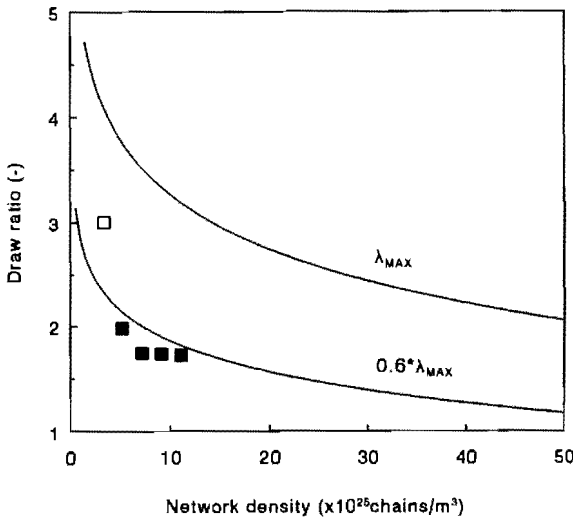


Figure 3.12 Draw ratio versus network density (entanglement and/or crosslink density). For details, see text

3.4.2 Critical microscopic thickness

The rubber weight fraction at which a sharp increase in strain to break is observed for rubber-modified PS-PPE blends (*figure 3.6*) corresponds to a certain average surface-to-surface interparticle distance, ID (read: ligament thickness), which can be calculated from the rubber particle size and volume fraction (assuming a body-centred-cubic lattice)²¹⁻²³. It can be inferred from *figure 3.6* that the critical ligament thickness increases with increasing PPE content present in the matrix (analogous to

multilayered PS-PPE/PE tapes; see *figure 3.5*). In order to derive a simple first-order model describing the phenomenon of the thickness-dependent brittle-to-ductile transition, the conditions have to be investigated that allow for a continuation of local deformation without fatal fracture. A lattice of holes, which is a schematic representation of non-adhering rubbery particles in a PS-PPE matrix, creates thin ligaments of polymeric material, i.e. potential initiation places of deformation. The smallest size of a fracture surface is the stretched fibril originating from the matrix ligament between two neighbouring particles. Brittle fracture can only occur if the stored elastic energy per matrix ligament is larger than the energy required to create a brittle fracture of this fibril. The stored elastic energy per ligament can be considered to be correlated with the volume of matrix material that is relieved from elastic stress if a brittle fracture were to occur in the connecting fibril. Although only detailed micromechanical analysis in a substantial volume around a matrix filament could give conclusive answers on the elastic energy stored in the volume that is released after the rupture of the fibril, a rough first approximation could be the matrix volume between two holes: see the shaded area in *figure 3.13a* (direction 1 is the direction of the applied stress). This volume can be estimated to be a sphere, having a diameter of d_1 ($=h$). The maximum average stress in this volume is estimated to be the yield stress, σ_y , since higher stresses would result in ductile plastic deformation of the ligament. The *available* elastic energy, U_{av} , per ligament is therefore:

$$U_{av} = \frac{\pi}{6} (d_1)^3 \frac{\sigma_y^2}{2 E_1} \quad (3.4)$$

where E_1 is the Young's modulus of the PS-PPE blend.

The energy *required* to create a brittle fracture, U_{re} , can be estimated to be:

$$U_{re} = 2 \frac{\pi}{4} (d_2)^2 \Gamma \quad (3.5)$$

where Γ is the surface energy of the polymeric matrix material. The size of a possible fracture surface (diameter d_2 ; *figure 3.13b*) is proportional to original cross-sectional area of the matrix ligament divided by λ_{max} , since this is the most critical condition, analogous to the use of the yield stress in equation (3.4).

The surface energy is given by ³:

$$\Gamma = \gamma + \frac{1}{4} v_e d U \quad (3.6)$$

where γ is the Van der Waals surface energy, d is the root-mean-square end-to-end distance between junction points in the network and U is the polymer backbone bond energy (the influence of the moderate degree of molecular orientation on the value of the surface energy is neglected).

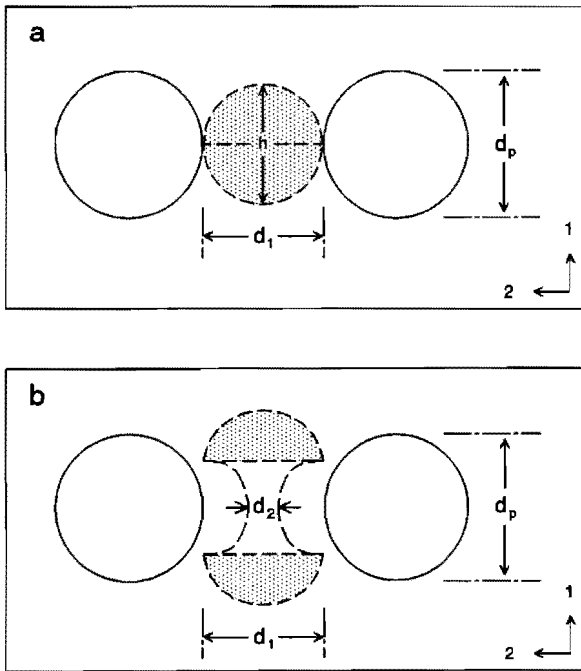


Figure 3.13 Schematic view of a matrix ligament between two holes, representing non-adhering rubbery particles: (a) before plastic deformation and (b) during plastic deformation. The shaded area represents the elastically deformed volume that is relieved from elastic stress once the fibril breaks

According to Kramer et al. ³, $v_e d$ scales roughly as $v_e^{1/2}$ (the polymer backbone bond energy is roughly equal for all amorphous polymers).

Combining equations (3.4), (3.5) and (3.6) results in an energy criterion for the

brittle-to-ductile transition:

$$d_1 = ID_c = \frac{6 (\gamma + k_1 v_e^{1/2}) E_1}{\lambda_{\max} \sigma_y^2} \quad (3.7)$$

If the value of ID is larger than ID_c ('critical interparticle distance'), brittle fracture of the ligament is possible ($U_{av} > U_{re}$) and therefore will occur. If, on the other hand, $ID < ID_c$, brittle fracture cannot occur ($U_{av} < U_{re}$) and complete deformation of the ligament will take place, eventually leading to a fully ductile macroscopic fracture behaviour.

Taking for PS, $\gamma = 40 \text{ mJ m}^{-2}$, $k_1 = 7.13 \times 10^{-15} \text{ J chain}^{-1/2} \text{ m}^{-1/2}$ (ref. 3), $E_1 = 3.28 \times 10^9 \text{ Pa}$ (ref. 24), $\lambda_{\max} = 4.2$ and $\sigma_y = 82.8 \text{ MPa}$ (ref. 24), results in $ID_c = 0.055 \text{ }\mu\text{m}$ (equation (3.7)), which is surprisingly close to the experimentally determined value ¹ ($0.05 \text{ }\mu\text{m}$) given the simplicity of the model and the assumptions made of the volume of matrix material released after rupture of the fibril.

Extending the model by introducing the v_e dependence of λ_{\max} ($\lambda_{\max} = k_2 v_e^{-1/2}$; constant $k_2 = 2.36 \times 10^{13} \text{ chains}^{1/2} \text{ m}^{-3/2}$ (ref. 3)) results in:

$$d_1 = ID_c = \frac{6 (\gamma + k_1 v_e^{1/2}) E_1}{k_2 v_e^{-1/2} \sigma_y^2} \quad (3.8)$$

In *figure 3.14* the calculated value of ID_c is plotted as a function of the entanglement density for several PS-PPE blends. The full curve is drawn according to equation (3.8) taking for the yield stress a constant value of 70 MPa; the broken curve is also drawn according to equation (3.8), but taking for the yield stress data published by Kambour ²⁴. The Young's modulus of the PS-PPE phase is assumed to be independently of the entanglement density ($E_1 = 3.28 \times 10^9 \text{ Pa}$). In *figure 3.14* the experimentally determined values of ID_c for various core-shell rubber-modified PS-PPE blends are given as well (filled squares). The value of ID_c for the PS-PPE 20-80 blend is taken from ref. 15 (high-speed tensile tests). Not only is the slope representing the entanglement density dependence of the critical thickness predicted well by both curves, but also the absolute values of the critical thickness are surprisingly correct taking into account the simplicity of the model and the serious assumptions that have been made.

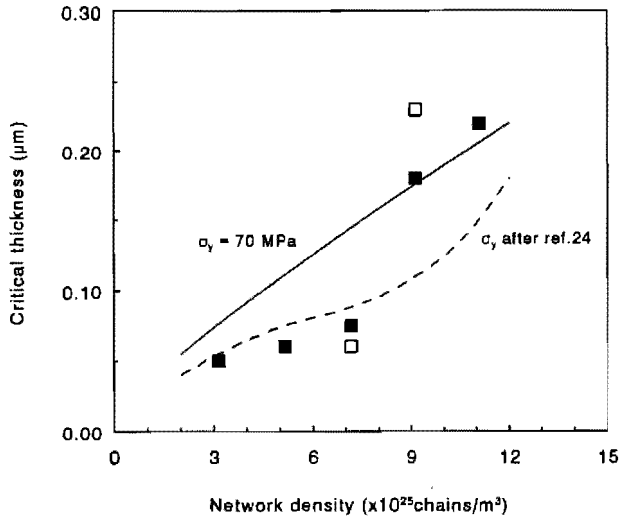


Figure 3.14 Critical material thickness (ID_c) versus the matrix entanglement density (v_e) for the various PS-PPE blends. The curves are according to the model. For details, see text

In figure 3.14 also two data points are shown obtained from multilayered PS-PPE blends (open squares). As already discussed, these data compare well to those obtained from core-shell rubber-modified PS-PPE blends but, surprisingly, they are also close to the predicted values. In the stratified structures the estimation of the volume of matrix material containing elastic energy to create a brittle fracture is much more complicated and, moreover, requires a number of assumptions to be made on the development of the deforming parts.

Although the model presented needs refinements in, for instance, the estimation of the released volume containing stored elastic energy, the results are promising towards an understanding of the phenomenon of a brittle-to-ductile transition. Moreover, the influence of testing temperature and testing speed can be incorporated relatively easily via the temperature and strain rate dependence of the yield stress and Young's modulus of the matrix.

3.5 Conclusions

The critical thickness below which brittle amorphous glassy polymers become ductile is determined for thin films of PS-PPE (alternating with PE) and for non-adhering core-shell rubber-modified PS-PPE blends in the composition range of 80-20 to 20-80. For the multilayered PS-PPE/PE tapes brittle-to-ductile transitions occurred at 0.06 μm and 0.3 μm for PS-PPE 60-40 and 40-60 blends respectively. The value of the critical ligament thickness as obtained from core-shell rubber-modified PS-PPE blends varies between 0.06 μm (PS-PPE 80-20) and 0.18 μm (PS-PPE 40-60) for slow-speed tensile testing (5 mm min^{-1}). Under these relatively mild testing conditions the PS-PPE 20-80 blend did not show a brittle-to-ductile transition: the strain to break of this blend was independent of the rubber concentration ($\approx 65\%$). The strain to break and the critical material thickness as obtained from the multilayered PS-PPE/PE tapes and core-shell rubber-modified PS-PPE blends coincide (at least for the PS-PPE 40-60 blend).

The maximum macroscopic strain to break (λ_{macr}) in the ductile region correlates well with the natural draw ratio (λ_{max}) of the amorphous glass based on its intrinsic entanglement network structure: $\lambda_{\text{macr}} = 0.6 \lambda_{\text{max}}$.

The transition from a brittle to a ductile fracture type of core-shell rubber-modified PS-PPE blends coincides with a transition from a deformation mechanism accompanied by void formation to a shearing type of deformation mechanism for the PS-PPE 80-20 and 60-40 blends, as revealed by tensile dilatometry.

An explanation for the existence of a critical material thickness for 'holey' modified PS-PPE blends is given, based on an energy criterion. This first-order model is verified by the experimental results. Given the simplicity of the model, not only is the qualitative dependence of the critical thickness on network density satisfying, but even the quantitative agreement is surprisingly good. Only a more extended micromechanical stress state analysis around a localized deformed ligament will provide a more solid basis especially for the estimation of the volume that is released upon break-up of the extended fibril. This aspect is still under investigation in our laboratory.

3.6 References

- 1 Van der Sanden, M.C.M., Meijer, H.E.H. and Lemstra P.J. *Polymer* 1993, **34**, 2148
- 2 Donald, A.M. and Kramer, E.J. *Polymer* 1982, **23**, 1183
- 3 Kramer, E.J. and Berger L.L. *Adv. Polym. Sci.* 1990, **91/92**, 1
- 4 Fried, J.R., Hanna, G.A. and Kalkanoglu, H. 'Polymer Compatibility and Incompatibility', Harwood Academic, New York, 1982, Vol.2, 237
- 5 MacKnight, W.J., Karasz, F.E. and Fried, J.R. 'Polymer Blends 1', (Eds. D.R. Paul and S. Newman), Academic Press, San Diego, 1978, 186
- 6 Prest, W.M. and Porter, R.S. *J. Polym. Sci.(A-2)* 1972, **10**, 1639
- 7 Van der Sanden, M.C.M., De Bie, F.O., Buijs, L.G.C. and Meijer, H.E.H. *Polymer*, submitted for publication
- 8 Sluijters, R. *De Ingenieur* 1965, **77** (15), 33
- 9 Schilo, D. and Ostertag, K. *Verfahrenstechnik* 1972, **6** (2), 45
- 10 Coumans, W.J. and Heikens D. *Polymer* 1980, **21**, 957
- 11 Wu, S. *J. Polym. Sci., Polym. Phys. Edn.* 1987, **25**, 557
- 12 Wu, S. *J. Polym. Sci., Polym. Phys. Edn.* 1987, **25**, 2511
- 13 Ferry, J.D. 'Viscoelastic Properties of Polymers', Wiley, New York, 1980
- 14 Onogi, S., Masuda, T. and Kitagawa, K. *Macromolecules* 1970, **3**, 109
- 15 Van der Sanden, M.C.M. and Meijer, H.E.H., *Polymer*, submitted for publication
- 16 Kinloch, A.J. and Young, R.J. 'Fracture Behaviour of Polymers', Elsevier Appl. Sci., London, 1985
- 17 Maxwell, M.A. and Yee, A.F. *Polym. Eng. Sci.* 1981, **21** (4), 205
- 18 Bucknall, C.B. 'Toughened Plastics', Appl. Sci., London, 1977
- 19 Kramer, E.J. *Adv. Polym. Sci.* 1983, **51/52**, 1
- 20 Van der Sanden, M.C.M. and Meijer, H.E.H., *Polymer* in press
- 21 Borggreve, R.J.M., Gaymans, R.J., Schuijjer, J. and Ingen Housz, J.F. *Polymer* 1987, **28**, 1489
- 22 Wu, S. *Polymer* 1985, **26**, 1855
- 23 Wu, S. *J. Appl. Polym. Sci.* 1988, **35**, 549
- 24 Kambour, R.P. *Polym. Commun.* 1983, **24**, 292

Chapter 4*

Influence of Crosslink Density

4.1 Introduction

In our previous studies ^{1,2} we have investigated the macroscopic toughness (read: strain to break) of neat and core-shell rubber-modified polystyrene and polystyrene-poly(2,6-dimethyl-1,4-phenylene ether) (PS-PPE) blends. Core-shell rubber-modified PS demonstrated the highest macroscopic draw ratio (λ_{macr}) within the investigated composition range: 3 (200%). Increasing the entanglement density (PPE content) of the matrix material resulted in a continuous decrease of λ_{macr} to a final value of 1.7 (70%). According to classical rubber elasticity theory ³, the maximum draw ratio of a network (λ_{max}) is proportional to the molecular weight between entanglements (M_e):

$$\lambda_{\text{max}} \sim M_e^{1/2} \quad (4.1)$$

Comparing the experimentally determined values of λ_{macr} with the theoretical natural draw ratio of a network resulted in the following correlation:

$$\lambda_{\text{macr}} / \lambda_{\text{max}} = 0.6 \quad (4.2)$$

In order to obtain these high strain values on a macroscopic level, the polymeric material had to be made very thin locally by the introduction of non-adhering rubbery particles ('holes'). The critical thickness below which the polymeric material demonstrates the maximum ductility is called the critical ligament thickness (ID_c) and depends strongly on the network density ². In chapter 3 a simple model was presented that quantitatively describes the existence of the critical ligament thickness based on an energy criterion ². The available elastic energy (U_{el}) stored in a matrix ligament between two non-adhering rubbery particles is compared with the required surface

* This chapter is reproduced, in part, from:

1. Van der Sanden, M.C.M. and Meijer, H.E.H. *Polymer* 1993, accepted for publication

energy (U_{re}) of a potential brittle fracture of the matrix ligament. Equating U_{av} with U_{re} resulted in an expression of the critical ligament thickness, ID_c , in dependence on several material parameters, i.e. network density (ν ; entanglement and/or crosslink density), Young's modulus (E_1) and yield stress (σ_y) of the matrix material:

$$ID_c = \frac{6 (\gamma + k_1 \nu^{1/2}) E_1}{k_2 \nu^{-1/2} \sigma_y^2} \quad (4.3)$$

where γ is the Van der Waals surface energy and k_1 and k_2 are constants ($k_1 = 7.13 \times 10^{-15} \text{ J chain}^{-1/2} \text{ m}^{-1/2}$ and $k_2 = 2.36 \times 10^{13} \text{ chains}^{1/2} \text{ m}^{-3/2}$)⁴.

In this study, the concept of a material-specific critical ligament thickness is extended to thermosetting polymers. Compared with thermoplastic polymers, the class of thermosets comprises values of network density (crosslink density, ν_c) comparable with, up to values much higher than, the entanglement density of most thermoplastic polymers: $9 \times 10^{25} \leq \nu_c \leq 250 \times 10^{25} \text{ chains m}^{-3}$. Hence, the theoretical maximum strain to break for this class of amorphous polymers is rather low compared with the thermoplastic polymers, since the natural draw ratio is inversely proportional to the square root of the network density (see equation (4.1))³.

The thermosetting model system consists of epoxides based on diglycidyl ether of bisphenol A (DGEBA), stoichiometrically cured with 4,4'-diamino diphenyl sulfone (DDS). The macroscopic toughness was investigated not only by slow-speed uniaxial tensile testing (λ_{macro}) but also by measuring the resistance to crack growth. For low testing rates (10 mm min^{-1}), the G_{Ic} fracture toughness was determined at room temperature. In order to investigate the toughness of the epoxides under very extreme testing conditions, notched high-speed (1 m s^{-1}) tensile tests were performed at various temperatures. The local thickness was set by changing the volume fraction of the previously introduced type of non-adhering core-shell rubbery particles¹. The critical ligament thickness data obtained from this study will be verified with predictions based on the simple first-order model introduced in the previous chapter².

4.2 Experimental

4.2.1 Materials

Various epoxides were used, all based on diglycidyl ether of bisphenol A (DGEBA), produced by the Shell Chemical Co. (trade name Epikote). Curing was performed using stoichiometric amounts of 4,4'-diamino diphenyl sulfone (DDS; Aldrich Chemical Co.). A non-adhering core-shell rubber with a poly(methyl methacrylate) shell and a styrene-butadiene core was used as impact modifier in concentrations of 5, 10, 15 and 20 wt% (Paraloid EXL 2600; powder form, produced by Rohm & Haas Co.). The size of the rubbery particles was in the range 0.1-0.3 μm . Table 4.1 lists the properties of the epoxides.

Table 4.1 Properties of Epikote as supplied by the Shell Chemical Co.

DGEBA type	Code	Epoxide equivalent weight (kg eq. ⁻¹)	Physical appearance at room temperature
Epikote 1009	A	2.400-4.000 (3.200) ^a	solid
Epikote 1007	B	1.550-2.000 (1.775) ^a	solid
Epikote 1004	C	0.850-0.940 (0.895) ^a	solid
Epikote 1001	D	0.450-0.500 (0.475) ^a	solid
Epikote 828	E	0.182-0.194 (0.188) ^a	liquid

^a Average value of the epoxide equivalent weight (kg eq.⁻¹), used to calculate the stoichiometric amount of DDS. The number-average molecular weight between crosslinks equals two times the epoxide equivalent weight in kg mol⁻¹.

4.2.2 Sample preparation

Neat epoxide resins were stirred mechanically with the DDS curing agent at different temperatures (see table 4.2). For the rubber-modified materials the epoxide resins were premixed with the core-shell rubber in a Brabender mixer (Model GNF 106/2), with the exception of the Epikote 828, which could be stirred mechanically because of its low viscosity at room temperature. After premixing, the DDS was added and the mixing was continued for at least 30 minutes (see table 4.2: mixing step).

The blended materials were compression-moulded at a pressure of 40 MPa. Curing and post-curing were carried out according to table 4.2.

Table 4.2 Preparation of neat and rubber-modified epoxide plaques

DGEBA type	Kneading step ^a		Mixing step		Curing step		Post-curing step	
	(°C)	(min)	(°C)	(min)	(°C)	(h)	(°C)	(h)
Epikote 1009	160	30	160	30	180	16	200	2
Epikote 1007	140	30	140	60	160	16	200	2
Epikote 1004	140	30	140	60	160	16	200	2
Epikote 1001	120	30	120	90	140	16	200	2
Epikote 828	120	30	120	45	120	16	220	2

^a Only in the presence of core-shell rubber.

4.2.3 Crosslink density

Two methods were used to determine the crosslink density (ν_c) of the cured samples. The first method is based on the theory of rubber elasticity⁵. The number-average molecular weight between crosslinks (M_c) is correlated with the rubber plateau modulus (G_{No}):

$$M_c = \rho RT / G_{No} \quad (4.4)$$

where ρ is the density at temperature T and R is the universal gas constant⁵.

The crosslink density (ν_c) can be calculated using equation (4.4)⁴ since

$$\nu_c = \frac{\rho N_A}{M_c} \quad (4.5)$$

where N_A is Avogadro's number.

The rubber plateau modulus was measured using a Rheometrics RDSII dynamic mechanical spectrometer operated at an oscillating torsion frequency of 1 Hz. The rubber plateau modulus is defined as the value of the storage shear modulus measured at 40°C above the glass transition temperature. Storage shear moduli were measured with a maximum strain amplitude ranging from 0.4% to 5% (0.4% in the glassy state and 5% in the rubbery region). The sample heating rate was 2°C min⁻¹ with a stabilization time of 1 minute before measurement. All measurements were performed within the range of 25°C to 250°C using rectangular-shaped samples (size: 50 mm x 12.5 mm x 2.9 mm).

A second method used to determine the number-average molecular weight between crosslinks (M_c) of a crosslinked epoxide resin was based on an empirical relationship described by Nielsen ⁶:

$$T_g - T_{g0} = \frac{3.9 \cdot 10^4}{M_c} \quad (4.6)$$

where T_g is the glass transition temperature of the crosslinked epoxide resin and T_{g0} is the glass transition temperature of the corresponding linear polymer. According to Bellenger et al. ⁷, the value of T_{g0} is 91°C for the DGEBA/DDS system. Glass transition temperatures were determined as being the maximum in $\tan \delta$, as obtained from dynamic mechanical data.

4.2.4 Mechanical properties

1) Strain to break

The post-cured samples were machined into dog-bone shaped tensile bars (DIN 53 455, sample thickness 7.5 mm) and then carefully polished using fine sand-paper to remove any irregularities introduced by the machining step. The polished samples were uniaxially strained on a Frank tensile machine (type: 81565 IV) at a crosshead speed of 5 mm min⁻¹ at room temperature. To ensure accurate data concerning the longitudinal strain level of the samples, extensometers were used. At least five specimens were fractured for each testing condition.

2) Fracture toughness

Fracture toughness (critical strain energy release rate; G_{Ic}) was measured according to the protocol of the European Group on Fracture of Polymers ⁸. All measurements were performed on a single-edge notched (razor-blade tapped) three-point bending specimen. The specimens were machined to 50 mm x 10.35 mm x 7.5 mm (length x width x thickness). The span was approximately 42 mm. A crosshead rate of 10 mm min⁻¹ was used. All fracture toughness measurements were performed at room temperature using a Zwick hydraulic tensile machine (type Rel SB 3122). At least 5 specimens were fractured to obtain an average value of G_{Ic} .

3) Impact toughness

The high-speed notched impact toughness (G_h ; 1 m s⁻¹) is defined as the energy absorption during fracture of a single-edge notched (razor-blade tapped) tensile specimen divided by the original area behind the crack-tip of the specimen:

$$G_h = \frac{U}{t(w-a)} \quad (4.7)$$

where U is the absorbed energy during fracture (integrated area under the recorded stress-strain curve),

t is the specimen thickness, w is the specimen width and a is the initial crack-length. The sample geometry was according to the Izod impact test protocol (ASTM D256). The specimen dimensions were: 55 mm x 12.5 mm x 2.9 mm. The free sample length between the clamps was 20 mm. All impact measurements were performed within the range -50°C to $+150^{\circ}\text{C}$ on a Zwick Rel SB 3122 tensile machine equipped with a climate chamber. At least 5 specimens were fractured for each testing condition.

4.2.5 Microscopy

Scanning electron microscopy (SEM) was applied to investigate the morphology (i.e. homogeneity of the particle distribution) of the rubber-modified epoxides. Samples were fractured in liquid nitrogen and subsequently coated with a Au/Pd film. A Cambridge Stereo Scan 200 apparatus was used.

Visualization of the size of the whitened area (deformed region) of the fractured samples was carried out using reflection optical microscopy (ROM). After fracture, the specimen were embedded in a polyester matrix and polished to a thin sheet, perpendicular to the growth direction of the crack tip. Thin sections were then examined by applying reflected light.

4.3 Results and Discussion

4.3.1 Crosslink density

In *figure 4.1* the storage shear modulus (G') and $\tan \delta$ of the stoichiometrically cured neat epoxide resins are plotted as a function of temperature. M_c is calculated from the rubber plateau modulus via equation (4.4) (see *table 4.3*; a density of 1 g cm^{-3} is assumed). For comparison also the M_c values determined from the glass transition temperature (equation (4.6)) are also listed in *table 4.3*. The values of M_c obtained via the rubber elasticity theory agree well with the data of the epoxide monomer molecular weight supplied by the manufacturer (see *table 4.3*). The values of M_c deduced from the empirical relationship described by Nielsen (equation (4.6)), on the other hand, demonstrate a deviation especially at high values of the epoxide monomer molecular weight. Clearly, the value of M_c increases with an increasing value of the epoxide monomer molecular weight. In the region of high values of the epoxide monomer molecular weight, the value of M_c cannot be set very accurately because of the small number of reactive epoxide groups per volume. In addition, the polydispersity of the epoxide system increases strongly at high values of the epoxide monomer molecular weight. Nevertheless, these materials are still suitable for the present investigation: M_c can be varied over a wide range; $0.26 \leq M_c \leq 6.79 \text{ kg mol}^{-1}$.

Further in the discussion, only the M_c values obtained from the rubber plateau modulus will be referred to.

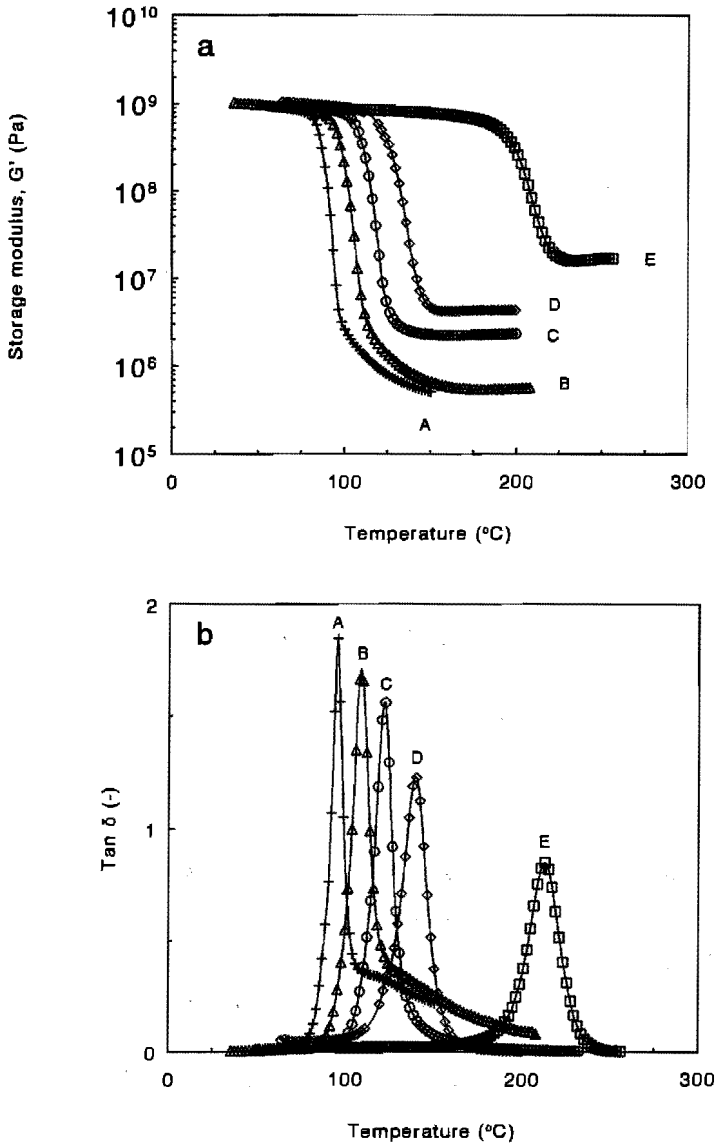


Figure 4.1 Dynamic mechanical data for neat epoxides: (a) Storage modulus (G') versus temperature; (b) $\tan \delta$ versus temperature. The epoxide molecular weight between crosslinks: $M_c =$ (A) 6.79; (B) 4.38; (C) 1.64; (D) 0.88; (E) 0.26 kg mol^{-1}

Table 4.3 Epoxide molecular weight between crosslinks

Code	Epoxide molecular weight (kg mol ⁻¹) ^a	M _c from G _{No} (kg mol ⁻¹)	T _g (°C)	M _c from T _g (kg mol ⁻¹)
A	4.80-8.00	6.79	95	9.30
B	3.10-4.00	4.38	109	2.23
C	1.70-1.88	1.64	122	1.25
D	0.90-1.00	0.88	140	0.80
E	0.36-0.39	0.26	213	0.32

^a Data supplied by the manufacturer.

Table 4.4 lists the values for the epoxide molecular weight between crosslinks (M_c) and the crosslink density (ν_c; see equation (4.5)) determined from G_{No}.

Table 4.4 M_c and ν_c as determined from the rubber plateau modulus

DGEBA type	Code	M _c (kg mol ⁻¹)	ν _c (chains m ⁻³)
Epikote 1009	A	6.79	9x10 ²⁵
Epikote 1007	B	4.38	14x10 ²⁵
Epikote 1004	C	1.64	37x10 ²⁵
Epikote 1001	D	0.88	68x10 ²⁵
Epikote 828	E	0.26	230x10 ²⁵

The epoxide having an M_c value of 6.79 kg mol⁻¹ behaves like a real thermoplastic polymer as can be seen in *figure 4.1*. The storage shear modulus versus temperature curve does not clearly show a rubber plateau; instead only a small change in slope is observed analogous to thermoplastics possessing a low molecular weight (see *figure 4.1*, curve A). Also the tan δ curve does not reach the value of zero after passing

through the glass transition. The other epoxides clearly demonstrate a rubbery plateau after passing the glass transition temperature.

4.3.2 Morphology

As described in the experimental section, different volume fractions of non-adhering core-shell rubbers are added to the neat epoxide system. Scanning electron microscopy (SEM) is used to study the surfaces of liquid-nitrogen fractured samples in order to check the homogeneity of the particle distribution. *Figure 4.2* shows two SEM micrographs of fracture surfaces of rubber-modified epoxides fractured in liquid nitrogen. It is clear that the rubber particle distribution is fairly homogeneous for both epoxides used despite the large differences in matrix viscosity.

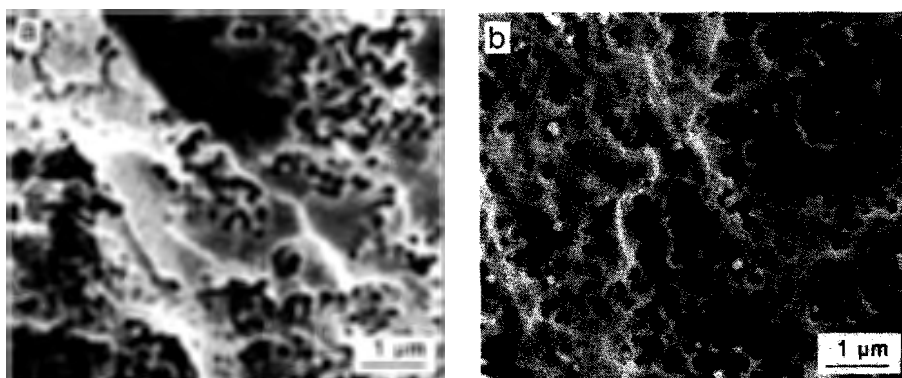


Figure 4.2 SEM micrographs of liquid-nitrogen fractured core-shell rubber-modified epoxides (10 wt%): (a) 0.26 kg mol^{-1} ; (b) 6.79 kg mol^{-1}

4.3.3 Strain to break

The strain to break of the core-shell rubber-modified epoxides determined by uniaxial slow-speed tensile testing, is shown in *figure 4.3*. The strain to break data of the neat epoxides are omitted because of the large scattering in these data caused by the high defect sensitivity of these samples. The epoxide with an M_c of 0.26 kg mol^{-1} is not analyzed with respect to its slow-speed uniaxial tensile properties. In contrast with most of the core-shell rubber-modified PS-PPE blends ^{1,2}, the strain to break of all of the rubber-modified epoxides is constant, independent of the amount of core-shell rubber present. Clearly, no brittle-to-ductile transitions are detectable within the

investigated range of testing speed and temperature. With an increasing molecular weight between crosslinks, the strain to break increases. Increasing the M_c of the epoxy matrix from 0.88 kg mol^{-1} (curve D) to 6.79 kg mol^{-1} (curve A) leads to an increase in maximum strain to break from 12% to 70%.

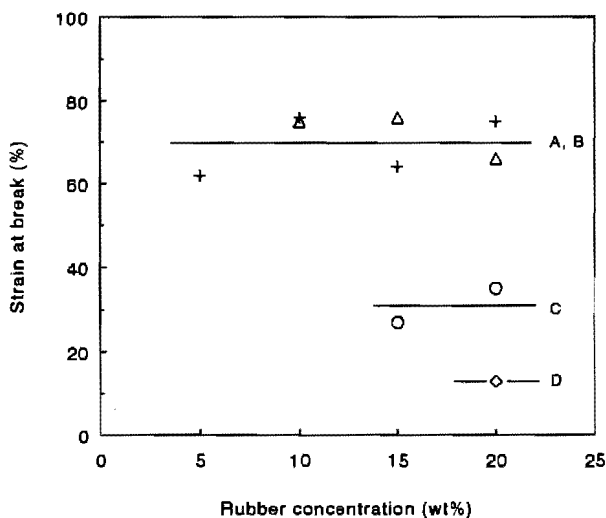


Figure 4.3 Strain at break of core-shell rubber-modified epoxides versus rubber concentration as a function of the epoxide molecular weight between crosslinks: $M_c =$ (A) 6.79; (B) 4.38; (C) 1.64; (D) 0.88 kg mol^{-1}

The maximum strain to break level of the epoxide with an M_c of 6.79 kg mol^{-1} agrees well with that of a core-shell rubber-modified PS-PPE 20-80 blend ($M_c = 5.5 \text{ kg mol}^{-1}$, see ref. 2). In accordance with the findings here, this PS-PPE 20-80 w-w composition also did not show a brittle-to-ductile transition in uniaxial slow-speed tensile testing.

In figure 4.4 the macroscopic draw ratio of core-shell rubber-modified epoxides is plotted versus the network density (filled circles). For comparison, the strain to break data of core-shell rubber-modified PS-PPE blends are incorporated in the same figure (open circles)^{1,2}. The full curve in figure 4.4 (indicated by ' λ_{max} ') is according to the maximum draw ratio of a single network strand (see equation (4.1)). As can be seen in figure 4.4, the experimental data are all situated systematically below the full curve. The broken curve, on the other hand, shows a close agreement with the experimentally determined (maximum) macroscopic draw ratios.

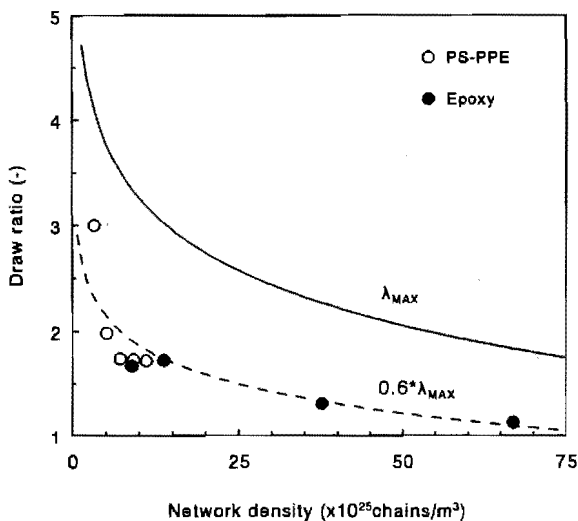


Figure 4.4 Draw ratio versus network density (entanglement and/or crosslink density). For details, see text

The broken curve is according to equation (4.2), a relationship shown to be valid for the maximum macroscopic draw ratio of core-shell rubber-modified thermoplastic PS-PPE blends². Clearly, the experimental data obtained from the crosslinked epoxides coincide with the broken curve.

The physical origin of the lower value found for the maximum attainable macroscopic strain to break is related to the difference between the idealization of a representative single network strand and a fully three-dimensional structure of strands with a distribution in molecular weight between network nodes^{1,2,4,9}.

Figure 4.5 confirms the statements made above; the maximum macroscopic draw ratio is plotted versus the theoretical natural draw ratio, λ_{max} . The data obtained from the core-shell rubber-modified epoxides show some overlap with the data extracted from the thermoplastic PS-PPE system^{1,2}, clearly demonstrating the principle similarity of the influence of a chemical crosslink- and a physical entanglement-network on the deformation behaviour of polymer systems.

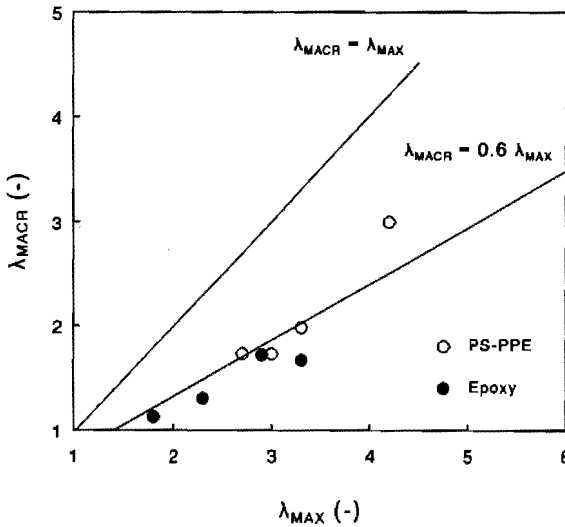


Figure 4.5 Maximum macroscopic draw ratio (λ_{macr}) versus the natural draw ratio (λ_{max}) for core-shell rubber-modified epoxides and thermoplastic PS-PPE blends

4.3.4 Fracture toughness

As mentioned, the low entangled thermoplastic PS-PPE blends already show a brittle-to-ductile transition with increasing core-shell rubber content in slow-speed tensile testing at room temperature. For the PS-PPE 20-80 w-w composition, more extreme testing conditions are required, e.g. notched tensile testing at high speed and/or low temperature¹⁰. (For a more detailed analysis of the influence of testing speed and temperature on the value of the critical ligament thickness of thermoplastic PS-PPE systems the reader is referred to chapter 5¹⁰.) By definition, the critical ligament thickness is the material-specific thickness below which the polymer network can be stretched to its theoretical extension ratio. Hence, in order to obtain more information on thermosets concerning the phenomenon of a brittle-to-ductile transition in relation with a critical ligament thickness between rubbery particles, the mode-I fracture toughness and high-speed tensile toughness of neat and core-shell rubber-modified epoxides was investigated. Due to the introduction of a crack in the samples (G_{Ic} fracture toughness; notched high-speed tensile toughness) stable versus instable crack growth has to be considered. However, in the case of rubber-toughened polymers, where the rubbery particles are non-adhering to the matrix ('holes'), the

introduction of a crack only results in an increase of the *local* strain rate in the matrix ligaments. The stress-state in the ligaments will always be one- or two-dimensional. Hence, a macroscopic ductile fracture behaviour can be directly correlated with a local ductile deformation behaviour ($ID \leq ID_c$). In *figure 4.6*, the G_{Ic} fracture toughness data for the neat and rubber-toughened epoxides are shown as a function of the epoxide monomer molecular weight (M_c).

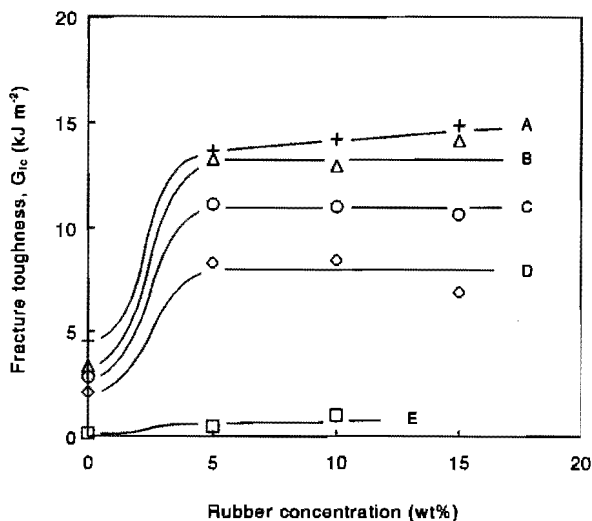


Figure 4.6 G_{Ic} fracture toughness versus rubber concentration for neat and rubber-modified epoxides as a function of the epoxide molecular weight between crosslinks: $M_c =$ (A) 6.79; (B) 4.38; (C) 1.64; (D) 0.88; (E) 0.26 kg mol⁻¹

The G_{Ic} fracture toughness of the neat epoxides (0 wt% rubber) is rather sensitive towards changes in the epoxide monomer molecular weight. G_{Ic} increases from 0.15 kJ m⁻² ($M_c = 0.26$ kg mol⁻¹) to approximately 4.5 kJ m⁻² ($M_c = 6.79$ kg mol⁻¹). The latter G_{Ic} value is still within the validity limits of the G_{Ic} test. Comparing the G_{Ic} data of the neat epoxides with data published by Pearson and Yee¹¹, it can be concluded that our G_{Ic} values are considerably higher than those listed in ref. 11. This may be due to differences in epoxide monomer molecular weight used; Pearson et al. used molecular weights in the range of 0.34–3.6 kg mol⁻¹ while in this investigation up to 6.8 kg mol⁻¹ was used. The rather high G_{Ic} values of the neat epoxides could also partly originate from plastic deformation occurring at the crack tip. It would be more convenient to compare the G_{Ic} value of the epoxide possessing a M_c value of 6.79

kg mol⁻¹ with toughness data of neat thermoplastics having a molecular weight between entanglements of approximately 6.5 kg mol⁻¹. This topic will be discussed in more detail in chapter 5¹⁰.

Adding 5 wt% core-shell rubbery particles to the epoxides results in a strong increase in fracture toughness, except for the epoxide having the lowest M_c (0.26 kg mol⁻¹). Further increasing the rubber concentration does not result in a further increase in G_{Ic} . Although the G_{Ic} values of the core-shell rubber-modified epoxides do not meet the requirements imposed by the validity criteria of the protocol of the European Group on Fracture of Polymers⁸, a quantitative comparison can still be made between the various rubber-modified epoxides. Clearly, the fracture toughness value of the rubber-modified epoxides depends on the epoxide monomer molecular weight: G_{Ic} increases from 0.4 kJ m⁻² ($M_c = 0.26$ kg mol⁻¹; 5 wt% rubber) to 14 kJ m⁻² ($M_c = 6.79$ kg mol⁻¹; 5 wt% rubber). Hence, the fracture toughness values of the core-shell rubber-modified epoxides display the same trend as already observed for the maximum strain to break of these materials (compare *figure 4.3*), confirming the statement that toughness is mainly dictated by the strain to break and to a lesser extent by the yield stress¹.

Clearly, a brittle-to-ductile transition is observed between 0 and 5 wt% core-shell rubber for all epoxides shown in *figure 4.6* (excluding the epoxide with an M_c value of 0.26 kg mol⁻¹). However, the exact determination of the critical ligament thickness (ID_c) cannot be done. The calculated ID_c is located between 0.35 μ m (based on 5 vol% rubbery particles having a diameter of 0.2 μ m and assuming a body-centred lattice^{12,13}) and infinity. Moreover, no distinction can be made between the ID_c values for the various epoxides, so no M_c dependence can be extracted from these experiments. In order to determine the values of the critical ligament thickness more accurately, small weight fractions (≈ 0.5 -5 wt%) of larger (non-adhering to the matrix) rubbery particles should be used or more extreme testing conditions should be chosen (e.g. notched high-speed impact testing at low temperatures).

4.3.5 Impact toughness

For the semi-crystalline thermoplastic system polyamide-6 / (easy cavitating) rubber, Borggreve et al.^{13,14} have shown that a brittle-to-ductile transition can be observed not only as a consequence of a change in matrix ligament thickness but also by

increasing the testing temperature at a constant value of the matrix ligament thickness. The authors^{13,14} have also shown that the temperature at which the brittle-to-ductile transition occurred was independent of the glass transition temperature of the matrix and of the dispersed rubbery phase^{13,14}. Because brittle-to-ductile transitions for the epoxides studied in this investigation are not observed during slow-speed uniaxial tensile testing and cannot be very accurately analyzed with respect to their M_c dependence using (slow-speed) fracture toughness measurements, notched high-speed tensile measurements (G_h) were performed within the temperature range -50°C to 150°C . In figure 4.7 the G_h values of the neat and rubber-modified epoxides are displayed as a function of testing temperature.

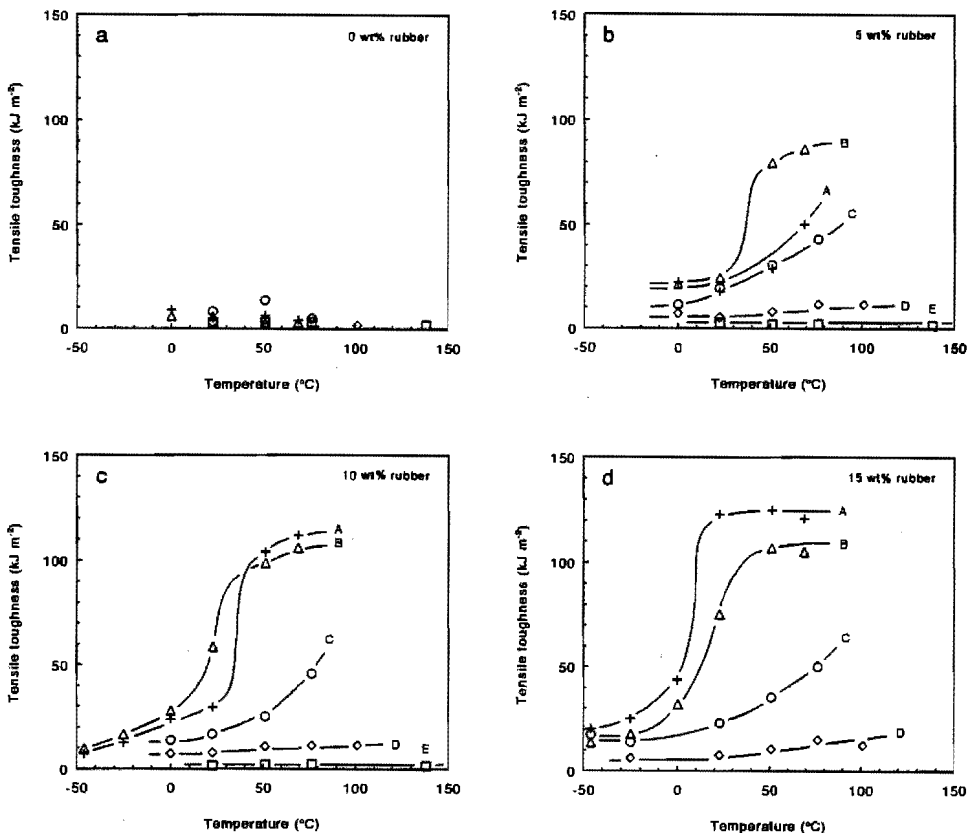


Figure 4.7 Notched tensile toughness (G_h) of neat and rubber-modified epoxides versus temperature as a function of the epoxide molecular weight between crosslinks: $M_c =$ (A) 6.79; (B) 4.38; (C) 1.64; (D) 0.88; (E) 0.26 kg mol^{-1} : (a) 0 wt%; (b) 5 wt%; (c) 10 wt%; (d) 15 wt% rubber

Figure 4.7a shows that the neat epoxides demonstrate brittle fracture behaviour over the entire temperature range investigated. Although there is some scattering in the data, there seems to be no correlation between the epoxide monomer molecular weight and the energy absorption.

If 5 wt% core-shell rubber is added, the energy absorption during fast tensile fracture depends strongly on both the testing temperature and the epoxide monomer molecular weight (see figure 4.7b). The highly crosslinked epoxides (curves D and E, $M_c = 0.88 \text{ kg mol}^{-1}$ and $M_c = 0.26 \text{ kg mol}^{-1}$, respectively) still behave 'brittle' at temperatures up to 150°C. The epoxides corresponding to curves A, B and C ($M_c = 6.79 \text{ kg mol}^{-1}$, $M_c = 4.38 \text{ kg mol}^{-1}$ and $M_c = 1.64 \text{ kg mol}^{-1}$, respectively) already demonstrate the characteristics of a brittle-to-ductile transition with increasing temperature. The epoxide with an M_c of 4.38 kg mol⁻¹ (curve B) possesses the most pronounced transition with increasing temperature. Clearly, the brittle-to-tough transition temperature (T_{BT}) is located at 35°C for this epoxide with a ligament thickness of 0.35 μm (corresponding to 5 wt% core-shell rubber). Surprisingly, the epoxide having the highest molecular weight between crosslinks (curve A) does not possess the highest degree of ductility. Apparently, for this epoxide the critical ligament thickness is not yet reached under the given testing conditions, within the temperature range investigated, with the addition of 5 wt% rubber.

If the concentration of the core-shell rubber is raised to 10 wt%, stronger dependencies of G_h on M_c are observed, as shown in figure 4.7c. The epoxides having a rather densely crosslinked network structure (curves C, D and E) still respond in a rather brittle manner over the entire temperature range investigated analogous to the 5 wt% core-shell rubber-modified epoxides (compare figures 4.7b and 4.7c). The epoxide having an M_c of 4.38 kg mol⁻¹ (curve B), on the other hand, shows a pronounced increase in ductility compared to the 5 wt% rubber-modified epoxide; the maximum level of toughness, G_h , is increased and the brittle-to-ductile transition temperature is lowered by 15°C. Hence, the critical ligament thickness of this epoxide is located at 0.24 μm (corresponding to 10 wt% rubber) at 15°C under the given circumstances. The epoxide corresponding to curve A demonstrates a strong increase in ductility due to the increased rubber concentration (compare curve A in figures 4.7b and 4.7c) and a sharp transition is observed at 30°C.

Further increasing the rubber concentration to 15 wt% confirms the trends as

described above; see *figure 4.7d*. The tensile toughness of epoxides corresponding to curves C and D (epoxide E is omitted for the sake of simplicity) is not influenced by an increase in rubber concentration. Also the maximum level of tensile toughness of the epoxide with an M_c of 4.38 kg mol^{-1} (curve B) remains unchanged, only the value of T_{BT} is decreased by an extra 5°C compared to the 10 wt% rubber-modified epoxide. Obviously, the maximum degree of ductility is obtained for this epoxide in the tough region. The shift of T_{BT} to lower temperatures because of the increased rubber concentration, confirms that the brittle-to-ductile transition is independent of the glass transition of the matrix^{13,14}. The level of tensile toughness of the epoxide corresponding to curve A is increased considerably ($\approx 20 \text{ kJ m}^{-2}$) due to the decrease in ligament thickness (compare curve A in *figures 4.7c* and *4.7d*). Hence, this epoxide with the highest molecular weight between crosslinks also possesses the highest degree of ductility confirming the conclusions made during the discussion of the slow-speed uniaxial tensile testing and the (slow-speed) fracture toughness measurements. In the literature¹⁵⁻¹⁷ several studies reported a maximum toughness value at a certain crosslink density for neat and rubber-modified epoxides; however, the authors did not realize the importance of the critical ligament thickness. Conclusions with respect to the M_c dependency of toughness can only be made if the polymer under investigation is toughened to its maximum extent.

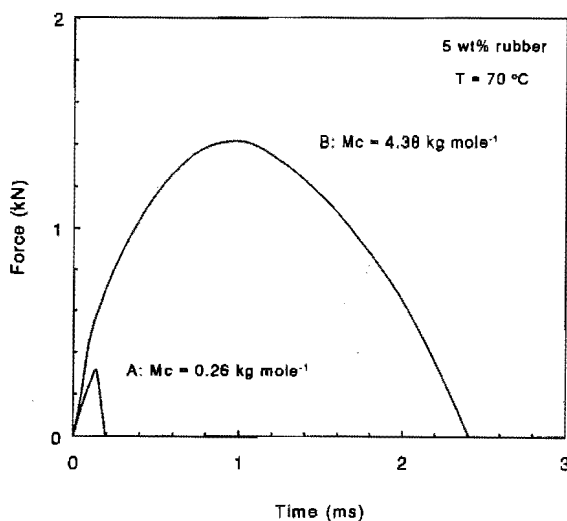


Figure 4.8 Force-time traces of rubber-modified epoxides recorded at 70°C

In *figure 4.8* the recorded force-time traces of two rubber-modified epoxides (5 wt%

rubber: $M_c = 0.26 \text{ kg mol}^{-1}$ and $M_c = 4.38 \text{ kg mol}^{-1}$) are shown measured at 70°C during a notched high-speed tensile test. The striking difference between the G_b values for these two epoxides (curve A: 5 kJ m^{-2} and curve B: 85 kJ m^{-2}) is elucidated in this figure; the maximum force and the strain to break differ considerably for A and B. For the densely crosslinked epoxide (curve A) a brittle fracture is observed; the material is already broken in the elastic region. The fracture process of the less densely crosslinked epoxide clearly corresponds to a ductile failure; after the elastic region a true ductile deformation behaviour occurs indicated by the decreasing slope of the force-time trace which even becomes negative at higher strains.

4.3.6 Optical microscopy

In figure 4.9 optical micrographs are shown of several high-speed fractured rubber-toughened epoxides (neat epoxides do not show a whitened region and are therefore not analyzed).

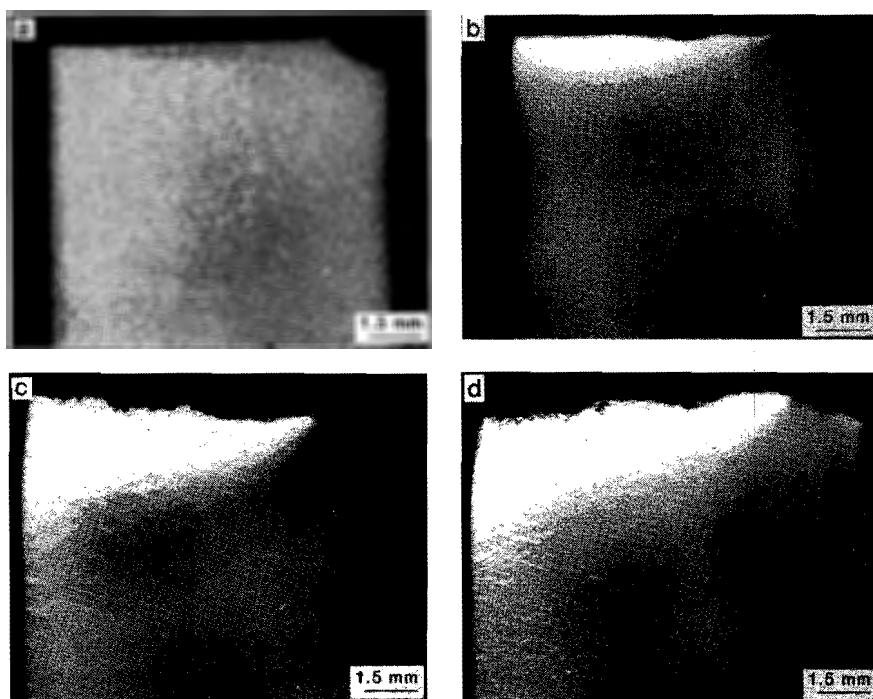


Figure 4.9 Optical micrographs of high-speed fractured rubber-modified epoxides (10 wt%): $M_c =$ (a) 0.88; (b) 1.64; (c) 4.38; (d) 6.79 kg mol^{-1} (reference temperature 70°C)

The micrographs reveal the whitened areas below the fracture surface. Whitening is the result of void formation (particle-matrix interface detachment) and/or deformation¹⁸⁻²². All the micrographs shown in *figure 4.9* are taken from fractured samples measured at 70°C as a reference temperature. Micrographs corresponding to the epoxides coded as A, B, C and D (see *table 4.4*) are shown in *figures 4.9d, 4.9c, 4.9b* and *4.9a*, respectively, (all 10 wt% rubber). Clearly, an increase in M_c results in an increase in whitened volume. Qualitatively, the whitened volume corresponds to the G_h value as given in *figure 4.7c* (70°C).

4.3.7 Critical ligament thickness

In *figure 4.10* a cross-section of *figure 4.7* at room temperature is shown, yielding the values of G_h as a function of the core-shell rubber concentration.

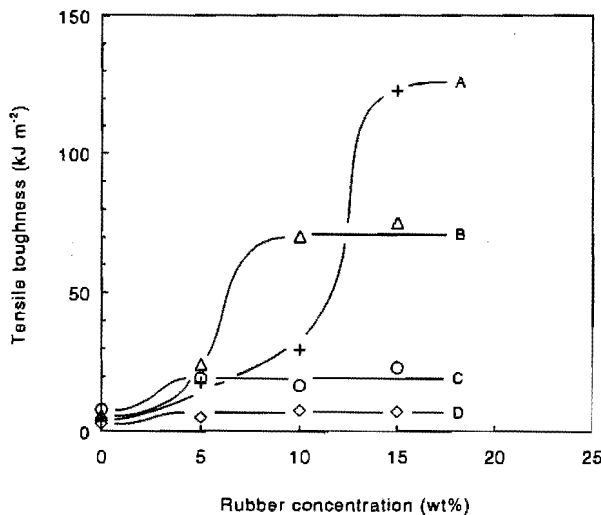


Figure 4.10 Notched tensile toughness of rubber-modified epoxides versus rubber concentration as a function of the epoxide molecular weight: $M_c =$ (A) 6.79; (B) 4.38; (C) 1.64; (D) 0.88 kg mol⁻¹

The brittle-to-ductile transition of the epoxides corresponding to curves C and D is located between 0 wt% and 5 wt% core-shell rubber, hence the corresponding critical matrix ligament thickness is positioned above 0.35 μm for the given testing conditions and cannot be determined accurately. For the epoxides having an M_c of 4.38 kg mol⁻¹ (curve B) and M_c of 6.79 kg mol⁻¹ (curve A), the brittle-to-ductile transition is located

between 5 and 10 wt% rubber, and between 10 and 15 wt% rubber, respectively. If a body-centred lattice is assumed and the average rubber particle diameter is set at $0.2 \mu\text{m}$, the corresponding critical ligament thickness can be estimated to be $0.29 \mu\text{m}$ and $0.21 \mu\text{m}$, respectively.

In figure 4.11 the critical ligament thicknesses for these two epoxides ($M_c = 4.38 \text{ kg mol}^{-1}$ and $M_c = 6.79 \text{ kg mol}^{-1}$; both indicated by a filled circle) are compared with those of the thermoplastic PS-PPE system (indicated by the open circles) as discussed in chapter 3².

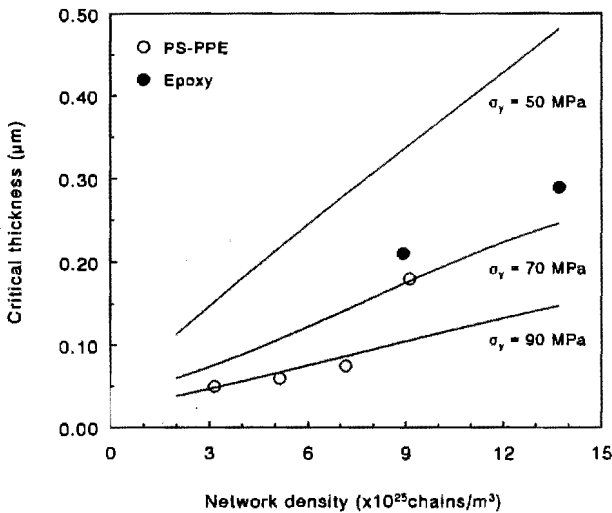


Figure 4.11 Critical ligament thickness versus network density (entanglement and/or crosslink density). The full curves are according to the model. For details, see text

Although the data of the thermosetting system are determined during notched high-speed tensile measurements, the order of magnitude of the value of ID_c is the same as the values displayed for the thermoplastic system determined during slow-speed uniaxial tensile testing. Moreover, there is some overlap between the values of ID_c for both systems at a network density of $9 \times 10^{25} \text{ chains m}^{-3}$.

The full curve in figure 4.11 indicated by $\sigma_y = 70 \text{ MPa}$ is according to the simple, first-order model presented in chapter 3², assuming a constant value of the yield stress of 70 MPa. Clearly, the model predictions agree closely with the experimental

values despite the simplicity of the model. It is worth noting that the model predictions even seem to be valid for high-speed tensile testing indicating the insensitivity of the value of the critical matrix ligament thickness to the testing speed applied. The testing speed and temperature dependency of the critical matrix ligament thickness can be understood in terms of the strain rate and temperature dependency of the yield stress, σ_y (see equation (4.3)). Increasing the strain rate and/or decreasing the temperature results in a decrease of ID_c via an increased yield stress of the matrix material. The σ_y -sensitivity of the critical matrix ligament thickness is shown in *figure 4.11*: three different curves are drawn corresponding to the model predictions of ID_c assuming different values for the yield stress. From the slow-speed fracture toughness data it could be inferred that ID_c for the epoxides coded A and B was positioned above $0.35 \mu\text{m}$. High-speed tensile testing, however, resulted in ID_c 's of $0.21 \mu\text{m}$ and $0.29 \mu\text{m}$, respectively. The lower values of ID_c determined during a high-speed test can be explained in terms of the strain rate dependency of the yield stress. In chapter 5¹⁰ the influence of temperature (and testing speed) on the value of ID_c will be discussed more extensively.

In *figure 4.12* the critical matrix ligament thickness is plotted versus the network density on a different scale, allowing for the incorporation of the critical ligament thickness of polycarbonate (PC; determined via a notched Izod impact test²³).

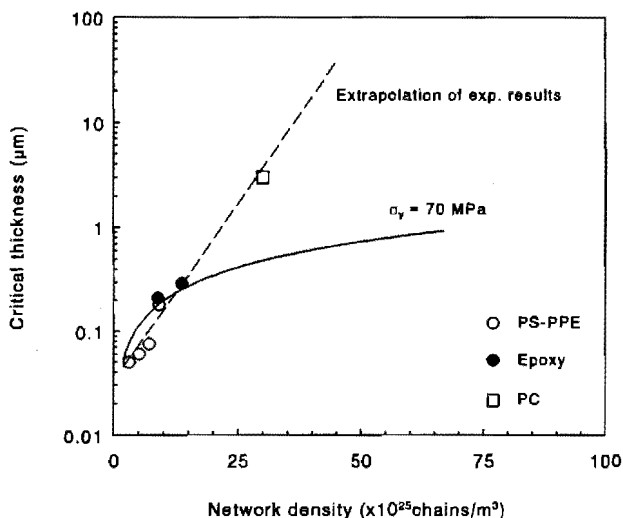


Figure 4.12 Critical ligament thickness versus network density. The full curve is according to the model. For details, see text

The comparison of polycarbonate with the other systems displayed in *Figure 12* is of interest since PC represents one of the most densely entangled thermoplastic polymers, having an ID_c of approximately $3 \mu\text{m}$. The values of ID_c for thermosetting polymers possessing network densities in the range 15×10^{25} - 235×10^{25} chains m^{-3} are not incorporated in *figure 4.12* since it was impossible to determine the value of ID_c using rubbery particles having a diameter of $0.2 \mu\text{m}$ (in this study the same core-shell rubber was used in all systems investigated in order to eliminate the influence of rubber type and particle size). Nevertheless, the prediction of the critical ligament thickness for these densely crosslinked polymers (coded C, D and E) can be estimated to be in the range $1\text{-}10 \mu\text{m}$ indicating that the maximum level of toughness is already obtained after adding just a few percent (non-adhering) rubbery particles. The absolute value of toughness for these densely crosslinked epoxides, however, will be rather low (see *figures 4.3* and *4.10*). Extrapolation (broken curve) to the usually applied highly crosslinked epoxides (with a crosslink density around 200×10^{25} chains m^{-3}) indicates that not much can be expected from rubber-modification, since the critical matrix ligament thickness is to be in the order of a few microns. These aspects are the subject of the current research at our laboratory. The full curve in *figure 4.12* is according to the simple model assuming a constant value of the yield stress of 70 MPa . The model prediction of the critical ligament thickness levels off at high values of the network density and starts to deviate from the experimental trend. This is possibly due to an overestimation of the elastic energy available to generate a brittle fracture. Only a more detailed numerical analysis in a rather large area around the strain localization will probably give conclusive answers concerning this aspect. This is currently one of the topics of study in our laboratory.

4.4 Conclusions

Three series of tests were performed on neat and rubber-toughened epoxides: slow-speed tensile testing, slow-speed (G_{lc}) fracture toughness testing and notched high-speed tensile toughness (G_h) testing. The maximum strain to break of rubber-toughened epoxides (containing non-adhering core-shell particles) increases with an increasing molecular weight between crosslinks (M_c) from 12% ($M_c = 0.88 \text{ kg mol}^{-1}$) up to 70% ($M_c = 6.79 \text{ kg mol}^{-1}$) independent of the volume fraction rubber dispersed in the system. The same deviation between the macroscopic draw ratio (λ_{macro}) and the theoretical draw ratio of a single network strand (λ_{max}) as already observed for the thermoplastic PS-PPE system, is found: $\lambda_{\text{macro}} / \lambda_{\text{max}} = 0.6$. No brittle-to-ductile

transition could be observed with slow-speed uniaxial tensile testing.

Slow-speed (10 mm min^{-1}) fracture toughness measurements (G_{lc}) reveal that the absolute value of G_{lc} of both neat and rubber-toughened epoxides increases with an increasing molecular weight between crosslinks. For neat epoxides G_{lc} ranges from 0.15 kJ m^{-2} ($M_c = 0.26 \text{ kg mol}^{-1}$) to 4.5 kJ m^{-2} ($M_c = 6.79 \text{ kg mol}^{-1}$), while for the rubber-toughened epoxides G_{lc} varies from 0.4 kJ m^{-2} ($M_c = 0.26 \text{ kg mol}^{-1}$) to 14 kJ m^{-2} ($M_c = 6.79 \text{ kg mol}^{-1}$), independent of the rubber concentration. For all epoxides investigated ($9 \times 10^{25} \leq v_c \leq 235 \times 10^{25} \text{ chains m}^{-3}$) in these tests, a brittle-to-ductile transition was observed between 0 and 5 wt% core-shell rubber. Hence, the critical ligament thickness is positioned above $0.35 \text{ }\mu\text{m}$ (corresponding to 5 wt% rubber) under these relatively mild testing conditions of a fracture toughness test.

Since the concept of a real critical ligament thickness should be valid under all testing conditions applied, notched high-speed tensile testing (G_h) at various temperatures was carried out. Analogous to the results obtained from the slow-speed uniaxial tensile testing and the (slow-speed) fracture toughness measurements, the value of G_h of the rubber-toughened epoxides uniquely increases with an increasing molecular weight between crosslinks: G_h varies from 2 kJ m^{-2} ($M_c = 0.26 \text{ kg mol}^{-1}$) up to 120 kJ m^{-2} ($M_c = 6.79 \text{ kg mol}^{-1}$). The critical matrix ligament thickness of two relatively loose crosslinked epoxides were determined to be $0.21 \text{ }\mu\text{m}$ ($M_c = 6.79 \text{ kg mol}^{-1}$) and $0.29 \text{ }\mu\text{m}$ ($M_c = 4.38 \text{ kg mol}^{-1}$) under these severe testing conditions at room temperature. The values of ID_c for the more densely crosslinked epoxides could not be determined due to the inaccuracy introduced by the low rubber volume fraction at which the brittle-to-ductile transition occurred. The values of ID_c of the epoxides, determined by notched high-speed tensile testing, correlate well with the values shown in the previous chapter for the thermoplastic PS-PPE model system determined via slow-speed uniaxial tensile testing clearly indicating the relative insensitivity of the real critical ligament thickness to the testing conditions applied and the nature of the network loci (physical entanglements and/or chemical crosslinks). The experimentally derived values of the critical ligament thickness correlate well with the values predicted by the simple first-order model presented in the previous chapter ². The slight dependency of the critical matrix ligament thickness on the testing conditions applied can be understood in terms of the strain rate and temperature dependency of the yield stress and Young's modulus.

4.5 References

- 1 Van der Sanden, M.C.M., Meijer, H.E.H. and Lemstra P.J. *Polymer* 1993, **34**, 2148
- 2 Van der Sanden, M.C.M., Meijer, H.E.H. and Tervoort T.A. *Polymer* 1993, **34**, 2961
- 3 Treloar, L.R.G. 'The physics of Rubber Elasticity', Clarendon, Oxford, 1975
- 4 Kramer, E.J. and Berger L.L. *Adv. Polym. Sci.* 1990, **91/92**, 1
- 5 Ferry, J.D. 'Viscoelastic Properties of Polymers', John Wiley, New York, 1980
- 6 Nielsen, L.E. *Rev. Makromol. Chem.* 1969, **C3** (1), 77
- 7 Bellenger, V., Verdu, J. and Morel E. *J. Polym. Sci.* 1987, **B25**, 1219
- 8 Williams, J.G. and Cawood M.J. *Polym. Testing* 1990, **9**, 15
- 9 Glad, M.D. and Kramer E.J. *J. Mater. Sci.* 1991, **26**, 2273
- 10 Van der Sanden, M.C.M. and Meijer, H.E.H. *Polymer*, submitted for publication
- 11 Pearson, R.A. and Yee A.F. *J. Mater. Sci.* 1989, **24**, 2571
- 12 Wu, S. *Polymer* 1985, **26**, 1855
- 13 Borggreve, R.J.M., Ph.D. Thesis, Twente University of Technology, The Netherlands, 1988
- 14 Borggreve, R.J.M., Gaymans, R.J., Schuijjer, J. and Ingen Housz, J.F. *Polymer* 1987, **28**, 1489
- 15 Murakami, S. et al. Proc. 34th Int. SAMPE Symp. 1989, 2194
- 16 Bell J.P. *J. Appl. Polym. Sci.* 1970, **14**, 1901
- 17 Garg, A.C. and Mai, Y.-W. *Compos. Sci. Technol.* 1988, **31**, 179
- 18 Kinloch, A.J. and Young, R.J. 'Fracture Behaviour of Polymers', Elsevier, London, 1985
- 19 Parker, D.S., Sue, H.J., Huang, J. and Yee A.F. *Polymer* 1990, **31**, 2267
- 20 Pearson, R.A. and Yee A.F. *J. Mater. Sci.* 1986, **21**, 2475
- 21 Bucknall, C.B. 'Toughened Plastics', Applied Science Publishers, London, 1977
- 22 Li, D., Li, X. and Yee, A.F. *Polym. Mater. Sci. Eng.* 1990, **63**, 296
- 23 Wu, S. *Polym. Eng. Sci.* 1990, **30** (13), 753

Chapter 5*

Influence of Strain rate and Temperature

5.1 Introduction

In chapter 2¹ the concept of a material-specific critical thickness (ID_c) was introduced using (macroscopically) brittle polystyrene (PS). It was demonstrated that a control of the microstructure allowed for an increase of the macroscopic draw ratio (λ_{macro}) from 1% to 60% of the theoretical natural draw ratio (λ_{max}) based on the maximum extension of a single strand of the molecular network structure. In chapter 3² the influence of the physical network structure of the polymeric material on the value of ID_c was investigated using the homogeneously miscible system polystyrene-poly(2,6-dimethyl-1,4-phenylene ether) (PS-PPE), while in chapter 4³ crosslinked epoxides were used to extend the concept to chemical networks.

In the systems with a high network density, notably all chemical networks of chapter 4, the critical ligament thickness could only be determined using relatively extreme testing conditions: i.e. notched high-speed (1 m s^{-1}) tensile testing at different temperatures. Due to the introduction of a crack in the samples stable versus instable crack growth has to be considered. In the case of rubber-toughened polymers, where the rubbery particles are non-adhering to the matrix ('holes'), the introduction of a crack only results in an increase of the *local* strain rate in the matrix ligaments (see chapter 4). Nevertheless, all data concerning the critical thickness, ID_c , obtained under different testing conditions were plotted in one graph and compared with the predictions derived from the simple, energy based, model as proposed in chapter 3. In this study we try to find experimental evidence for this generalization of the basic concept. Especially the influence of testing speed and temperature on the absolute value of the critical matrix ligament thickness will be studied.

* This chapter is reproduced, in part, from:

1. Van der Sanden, M.C.M. and Meijer, H.E.H. *Polymer*, submitted for publication

The expression for the value of the critical matrix ligament thickness in dependence of the relevant material parameters, i.e. network density (ν ; entanglement and/or crosslink density), Young's modulus (E_1) and yield stress (σ_y), is given in equation (5.1) ²:

$$ID_c = \frac{6 (\gamma + k_1 \nu^{1/2}) E_1}{k_2 \nu^{-1/2} \sigma_y^2} \quad (5.1)$$

where γ is the Van der Waals surface energy and k_1 and k_2 are constants ($k_1 = 7.13 \times 10^{-15}$ J chain^{-1/2} m^{-1/2} and $k_2 = 2.36 \times 10^{13}$ chains^{1/2} m^{-3/2}) (ref. 2). Inspection of equation (5.1) reveals that in first approximation the yield stress is the only parameter demonstrating a strong strain rate and temperature dependence below the glass transition temperature of the polymer. (The temperature and strain rate dependence of the Young's modulus is neglected in a first approximation, although its temperature and strain rate dependence is in general comparable with temperature and strain rate dependence of the yield stress. However the yield stress is more dominant in equation (5.1).) Applying the Eyring theory of viscosity ⁴ the strain rate and temperature dependence of the yield stress can be described as:

$$\dot{\epsilon} = A_E \exp \left\{ - \frac{(\Delta E^* - \nu^* |\sigma_y|)}{RT} \right\} \quad (5.2)$$

where $\dot{\epsilon}$ is the strain rate, A_E is a constant, ΔE^* the activation energy, ν^* the activation volume, R the gas constant and T the absolute temperature. Equation (5.2) suggests a linear relationship between yield stress and absolute temperature and a logarithmic dependence of the yield stress on the strain rate. Combining equations (5.1) and (5.2) results in a description of the strain rate and temperature dependence of the critical matrix ligament thickness. In *figure 5.1* the predicted values of the critical matrix ligament thickness are shown as a function of temperature, strain rate and network density. The constants in equation (5.2) are extracted from literature data ⁵ of the yield stress at very low strain rates at room temperature combined with data determined in our laboratory ⁶. For simplification it is assumed that the strain rate dependence of the yield stress is independent of the PS-PPE composition and that the temperature dependence, $(T_g - T)$, of the yield stress is independent of the network density. From *figure 5.1a* it is clear that the critical thickness (for PS-PPE 100-0 as well as for 20-80) increases with a decreasing strain rate and increasing temperature.

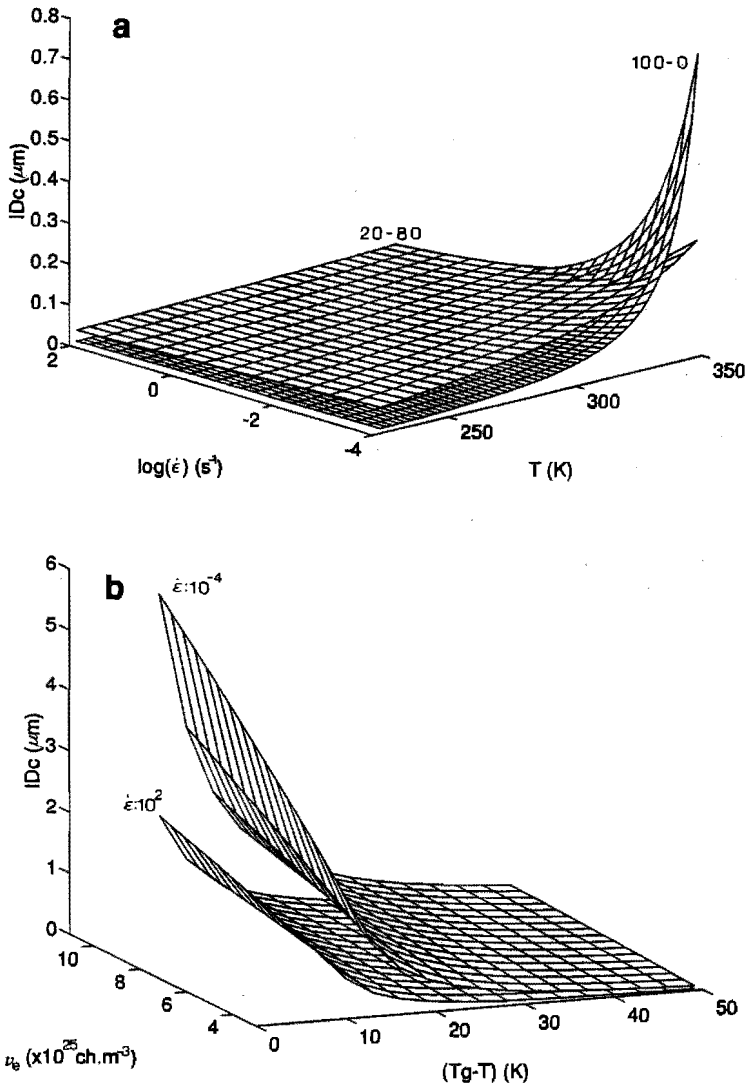


Figure 5.1 Predicted values of the critical matrix ligament thickness as a function of temperature, strain rate and network density: (a) PS-PPE 100-0 and 20-80, (b) $\dot{\epsilon} = 10^{-4} \text{ s}^{-1}$ and $\dot{\epsilon} = 10^2 \text{ s}^{-1}$ and (c) $(T_g - T) = 25 \text{ K}$ and $(T_g - T) = 63 \text{ K}$

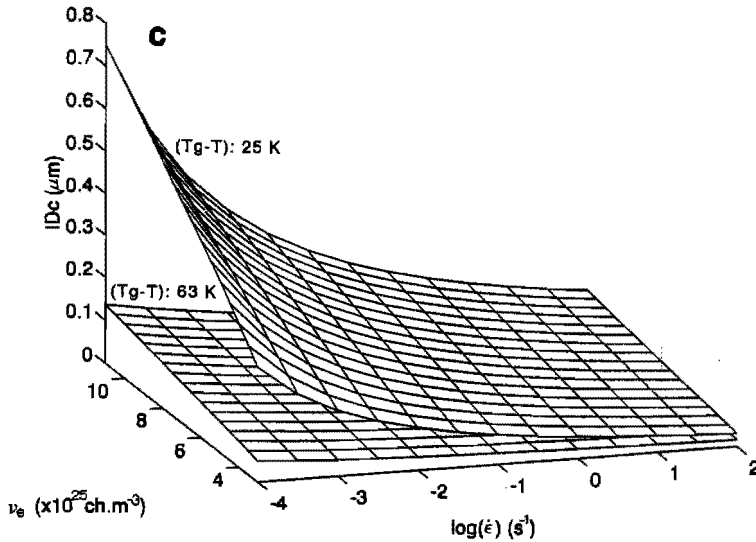


Figure 5.1 (Continued)

The planes shown in *figure 5.1a* intersect at higher temperatures due to the fact that the glass transition temperature of PS (88°C) is much lower than the one of the 20-80 blend (174°C). *Figure 5.1b* clearly reveals the influence of temperature of the value of the critical thickness: slightly dependent on the strain rate applied, the value of ID_c strongly increases, within the region of $0 < (T_g - T) < 25^\circ\text{C}$, if the glass transition is approached. From *figure 5.1c*, finally, it can be inferred that the strain rate dependence of ID_c is only significant if the material is strained close to the glass transition temperature. The network density dependence as already extensively discussed in chapter 3² is obvious in both *figures 5.1b* and *5.1c*.

This study provides the experimental verification of the strain rate and temperature dependence of ID_c using the PS-PPE model system. The values of the critical ligament thickness as determined by uniaxial slow-speed tensile testing at room temperature (see reference 2) are compared with those obtained by notched high-speed tensile testing (1 m s^{-1}) at different temperatures. In order to complete the analysis, high-speed dilatometry (1 m s^{-1}) is used to reveal the change in deformation mechanism from (multiple) crazing to shear deformation at the critical matrix ligament thickness.

5.2 Experimental

5.2.1 Materials

The materials used were (identical to reference 2) polystyrene (DOW, Styron 638), poly(2,6-dimethyl-1,4-phenylene ether) (General Electric Co., PPE-803) and the core-shell rubber with a poly(methyl methacrylate) shell and a styrene-butadiene core (Rohm and Haas Co., Paraloid EXL 3647). The core-shell rubber was an extrusion grade and contained 11 wt% poly(methyl methacrylate). The core-shell rubber particle size was in the range of 0.1-0.3 μm .

5.2.2 Sample preparation

The PS-PPE compounding was carried out as extensively described in chapter 3². Neat PS-PPE blends were prepared via a double extrusion cycle either by diluting a PS-PPE 50-50 master-batch with PS (PS-PPE 80-20 and 60-40 blends) or by direct mixing PS and PPE (100-0, 40-60 and 20-80 blends). Rubber-modified PS-PPE blends with different compositions: 10, 20, 30, 40, 50 and 60 wt% non-adhering core-shell rubber were prepared via the same two step compounding process with the addition of the core-shell rubber in the second extrusion step (processing temperatures: see reference 2). Blend compositions are indicated with a three number code: A-B/C; A: weight fraction PS present in the matrix; B: weight fraction PPE present in the matrix; C: weight fraction core-shell rubber present in the total blend.

Extruded strands were quenched in a water bath and pelletized subsequently. High-speed dilatometry specimens were prepared by injection moulding (Arburg Allrounder 220-75-250) the blends into dog-bone-shaped tensile bars (DIN 53 455, sample thickness: 3 mm). Square plates (length x width x thickness: 60 x 60 x 3 mm) were injection-moulded at temperatures depending on the blend composition (see reference 2). Parallel to the direction of injection moulding specimens were machined with dimensions: length x width x thickness: 60 x 10 x 3 mm. Analogous to the Izod impact test protocol (ASTM D256) the bars were V-shaped single-edge notched in the centre (notched high-speed tensile specimens).

5.2.3 Mechanical testing

Prior to mechanical testing the injection-moulded and machined specimens were annealed at a temperature 20°C below the glass transition temperature of the matrix during 24 hours.

In chapter 2¹ tensile dilatometry has revealed its use to determine the deformation mechanisms of polystyrene. Here, tensile dilatometry has been carried out at 1 m s⁻¹ on the unnotched samples using two contactless electro optical displacement transducers (EODT: Zimmer type 100D; Lenses: model 100-02, 2 mm range). The EODT converts the motion of a black and white edge (target) into a voltage proportional to the displacement in the frequency range from 0 to 400 kHz. Using two EODT's positioned at the edges of the white-painted rectangular part (middle section) of the dog-bone-shaped sample, the absolute displacements of the two edges of the sample could be registered. Assuming that

the relative displacement of the sample in both directions perpendicular to the load direction is equal, the transversal change in cross sectional area could be recorded. The longitudinal strain was obtained from the cross-head displacement of the tensile machine (type Zwick Rel SB 3122). Hence, the volume-strain could be obtained from these measurements as a function of the longitudinal strain.

High-speed notched impact toughness (G_b ; 1 m s^{-1}) is defined as: the energy absorbed during fracture of a single-edge notched (razor-blade tapped) tensile specimen over the original area behind the crack-tip (see reference 3 for a detailed description of the test). The free sample length between the clamps was 20 mm. Impact testing was performed within the range of -75°C to 80°C on a Zwick Rel SB 3122 tensile machine equipped with a climate chamber. At least 5 specimens were fractured for each testing condition in order to obtain an average value of G_b .

5.3 Results and Discussion

The determination of the molecular weight between entanglements (M_e) and entanglement density (v_e) of the various PS-PPE blends from dynamic mechanical thermal analysis has already been described in chapter 3². In table 5.1 the values of M_e and v_e are recapitulated:

Table 5.1 Entanglement molecular weight (M_e) and entanglement density (v_e) of neat PS-PPE blends

Blend composition (PS-PPE)	M_e (kg mol^{-1})	v_e ($\times 10^{25}$ chains m^{-3})
100-0	20	3
80-20	12	5
60-40	8.6	7
40-60	6.7	9
20-80	5.5	11

5.3.1 Unnotched samples

In figure 5.2 the true stress and relative volume change of core-shell rubber-modified pure polystyrene as measured at 1 m s^{-1} (10 s^{-1}) is shown as a function of the

longitudinal strain.

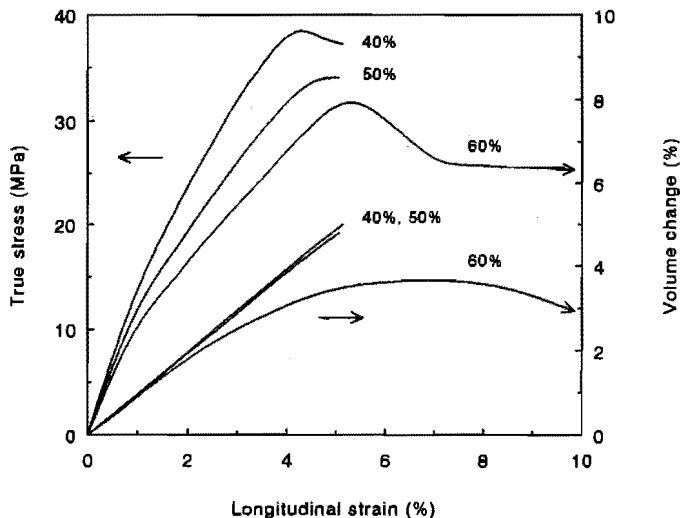


Figure 5.2 Stress-strain and volume-strain curves of rubber-modified PS blends tested at 1 m s^{-1} . Parameter the rubber content

Similar to the slow-speed tensile dilatometry results¹, polystyrene containing up to 50 wt% non-adhering core-shell rubber demonstrates a typically brittle deformation behaviour although the stresses are somewhat increased due to the higher strain rates applied. The slope of the relative volume change versus strain curve is close to unity, indicating a deformation process accompanied by void formation. This void formation can be contributed either to crazing or to the process of particle/interface detachment. Tensile dilatometry can not distinguish between those two processes. If, however, the rubber content is increased to 60 wt% the true stress-strain curve shows the characteristics of a true yield point followed by a constant stress level. Also the slope of the relative volume change versus strain curve deviates from unity and decreases to zero. This latter implies that a shear deformation process occurs in this system. Similar to the slow-speed tensile dilatometry results on core-shell rubber-modified PS the brittle-to-ductile transition is located between 50 and 60 wt% rubber (thus $ID_c \sim 0.05 \mu\text{m}$) for pure PS. At this transition the deformation mechanism changes from crazing to shearing apparently irrespective of the strain rate applied, illustrating the strain rate insensitivity of the value of the critical matrix ligament thickness in the region of low network (entanglement) densities within the investigated strain rate range. However, the macroscopic strain to break of the shear

deforming PS system is only about 80% (not shown in *figure 5.2*), compared to 200% for the slow-speed analysis ¹, indicating that the critical matrix ligament thickness has just been surpassed by the addition of 60 wt% core-shell rubber. Apparently, the local strain rate in the matrix ligament is only slightly influenced by the macroscopically applied strain rate. Since, increasing the macroscopically applied strain rate from $8.3 \times 10^{-4} \text{ s}^{-1}$ (i.e. 5 mm min^{-1}) up to 10 s^{-1} (i.e. 1 m s^{-1}) does not result in a complete brittle fracture of the material as expected from the decrease of ID_c from $0.05 \text{ }\mu\text{m}$ to $0.025 \text{ }\mu\text{m}$ (based on *figure 5.1a*, $T = 298 \text{ K}$, or see equations (5.1) and (5.2)).

5.3.2 Notched samples

1) Tensile toughness data

In *figure 5.3* the influence of temperature on the value of the critical matrix ligament thickness at notched high-speed tensile testing conditions is shown for the various PS-PPE blends filled with different amounts of non-adhering core-shell rubber. As can be inferred from *figure 5.3a* in the range of rubber concentrations tested (0-60 wt%) rubber-modified PS only demonstrates a brittle-to-ductile transition at 60 wt% rubber close to the glass transition temperature of the PS matrix (88°C). Analogous to the critical value of ID as found in slow-speed ¹ and high-speed unnotched uniaxial tensile testing at room temperature (see *figure 5.2*) the brittle-to-tough transition of core-shell rubber-modified PS is found to be at $0.05 \text{ }\mu\text{m}$ for notched high-speed impact testing but now at a temperature of 70°C . Apparently, the introduction of a notch has increased the local strain rate (and, consequently, the value of the yield stress) such that an increase in temperature to 70°C is required to keep $ID_c \approx 0.05 \text{ }\mu\text{m}$ (see *figure 5.4*).

In *figure 5.3b* the notched high-speed impact toughness of the PS-PPE 80-20/X blends is shown. Blends containing less than 20 wt% core-shell rubber are omitted for the sake of simplicity; these materials demonstrate a brittle fracture behaviour in the entire temperature range investigated. Taking 75°C as a reference temperature it can be concluded that upon increasing the rubber concentration the tensile toughness increases. However, increasing the rubber content from 50 to 60 wt% does not result in a further increase of the absorbed energy during notched high-speed fracturing of the sample. Hence, the brittle-to-tough transition of the PS-PPE 80-20 blend at 75°C is located at $0.06 \text{ }\mu\text{m}$. Slow-speed uniaxial tensile testing resulted in the same value of

the critical matrix ligament thickness at room temperature ².

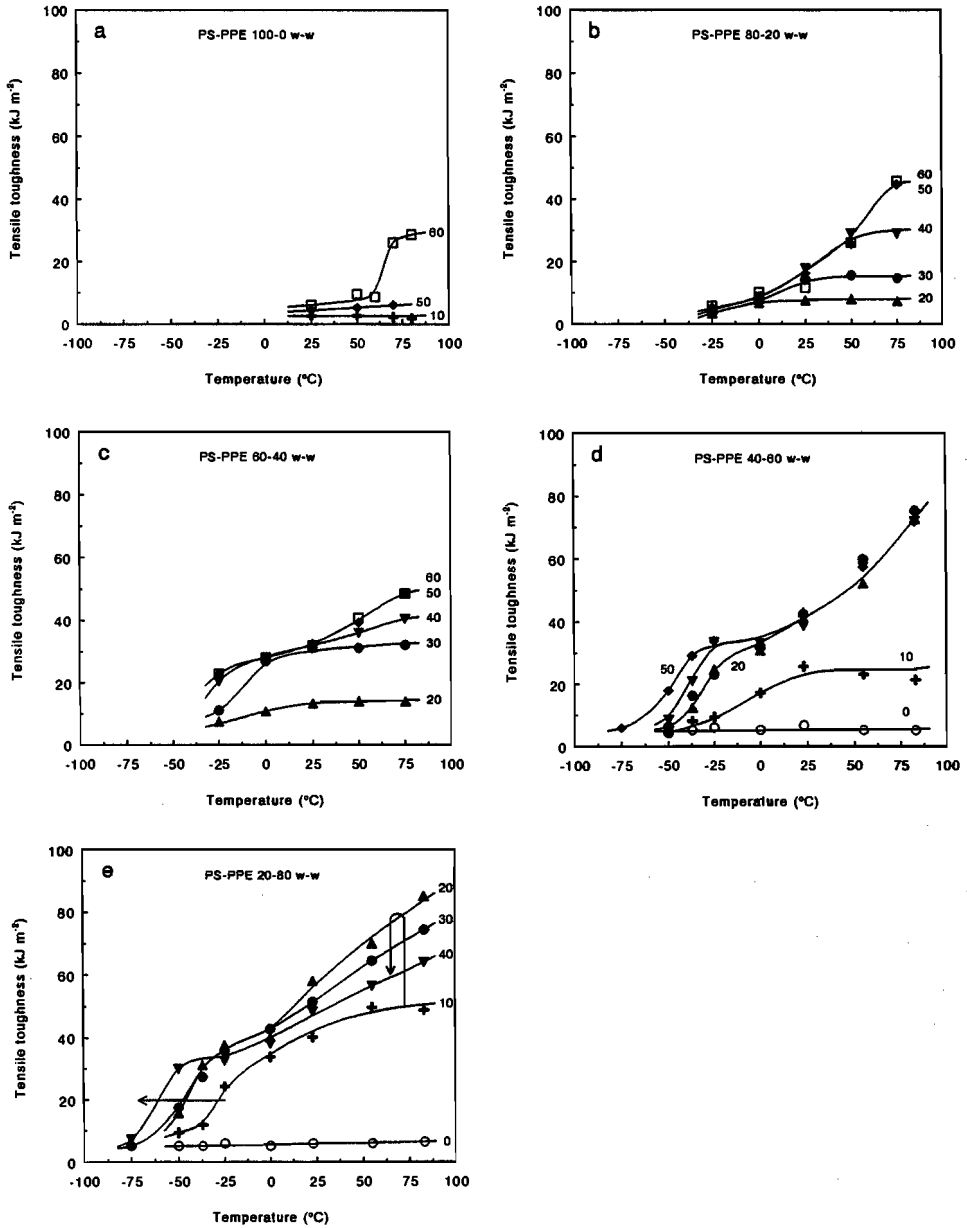


Figure 5.3 Notched tensile toughness of neat and rubber-modified PS-PPE blends vs temperature: (a) 100-0, (b) 80-20, (c) 60-40, (d) 40-60 and (e) 20-80

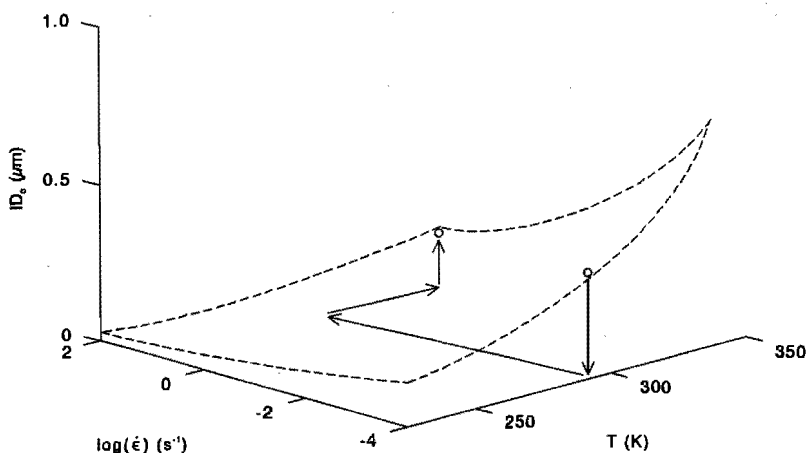


Figure 5.4 Schematic representation of the influence of temperature and strain rate on the critical matrix ligament thickness

As expected (see introduction: *figure 5.1b* and the discussion of *figure 5.3a*), the increase of the yield stress as a consequence of the high speed occurring locally at the notch-tip is counteracted by the increased temperature at which the brittle-to-ductile transition is observed. With increasing temperature the tensile toughness of the 80-20/60 blend increases continuously within the temperature range investigated. This is also reflected in the increased size of the whitened area above and below the fracture surface of the 80-20/X blends with increasing testing temperature (not shown here).

Increasing the PPE content of the matrix (*figure 5.3c*) results in a confirmation of the trends discussed above. For the PS-PPE 60-40 blend the value of the critical matrix ligament thickness at 75°C is positioned around $0.07 \mu\text{m}$ (corresponding to 50 wt% core-shell rubber). At lower temperatures a brittle-to-ductile transition can not be determined due to the fact that no significant distinction can be made between the different levels of tensile toughness.

Figure 5.3d shows the results of the PS-PPE 40-60/X blends. At 75°C the brittle-to-tough transition is located between 10 and 20 wt% core-shell rubber ($\sim 0.17 \mu\text{m}$, assuming that the critical concentration is close to 20 wt% core-shell rubber) since an increase of the rubber concentration (up to 50 wt%) does not result in a higher value of the tensile toughness. Inspection of *figure 5.1b* reveals that a brittle-to-ductile transition can also be observed as a function of temperature at a constant value of

the matrix ligament thickness (i.e. rubber concentration). For example the 50 wt% core-shell rubber-modified PS-PPE blend (40-60/50) shows a brittle-to-tough transition temperature (T_{BT}) of about -50°C (see *figure 5.3d*). Increasing the average matrix ligament thickness, by decreasing the rubber content, results in an increase of the brittle-to-ductile transition temperature.

The PS-PPE 20-80/X blends demonstrate a clear deviation from the general aspects as discussed above (*figure 5.3e*). At 75°C the brittle-to-ductile transition is located between 10 and 20 wt% core-shell rubber ($ID_c = 0.22 \mu\text{m}$, assuming that the critical condition is located close to the 10 wt% rubber-modified PS-PPE blend). Increasing the rubber content above 20 wt% results in a decrease of the tensile toughness at this temperature. Hence, the level of tensile toughness decreases after passing the brittle-to-tough transition. The origin of this decrease is illustrated in *figure 5.5* which shows the recorded force-time traces of the various PS-PPE 20-80/X blends at 75°C .

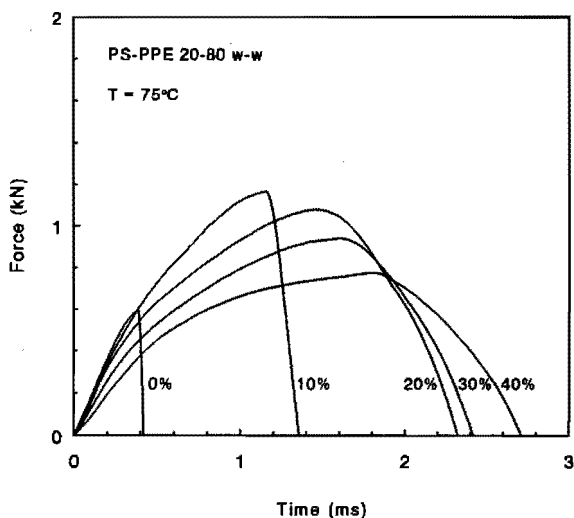


Figure 5.5 Force-time traces of rubber-modified 20-80 blends recorded at 75°C

Clearly the time-to-failure (read: strain to break) continuously increases with an increasing rubber content. The maximum stress on the other hand increases only if the rubber concentration is increased from 0 to 10 wt%, but decreases upon extra rubber addition. Since the tensile toughness shown in *figures 5.3a* up to *5.3e* is correlated with the surface area under the recorded force-time traces (energy), it is clear that the decrease in maximum force upon increasing the rubber content after

passing the T_{BT} , is not fully compensated for by the increased time-to-failure (read: strain). A higher rubber concentration at the brittle-to-tough transition automatically results in a decrease of the macroscopic force of the recorded force-time trace since more 'holes' are present in the material. Consequently, with an increasing rubber concentration an optimum can be observed for the tensile toughness value after passing the brittle-to-tough transition, partly due to an overlap of stress fields ^{7,8}. Macroscopically, this results in a decrease of the recorded forces (stresses). In conclusion, the simple network density dependent strain-to-break argument postulated in chapter 2 results in conclusive data with respect to the value of the critical interparticle distance but can not fully account for the network density dependence of the measured value of the notched tensile toughness. Only detailed micromechanical modelling can provide quantitative answers. This aspect is one of the topics of the present research at our laboratory.

In figure 5.6 the temperature dependence of the critical matrix ligament thickness is shown for the PS-PPE 40-60 and 20-80 blends (compare with figures 5.3d and 5.3e). The theoretical curves of the critical ligament thickness are calculated using yield stress data at room temperature ⁵ (irrespective of the different strain rates applied) and assuming a linear relationship with temperature to a final value of zero at the glass transition temperature.

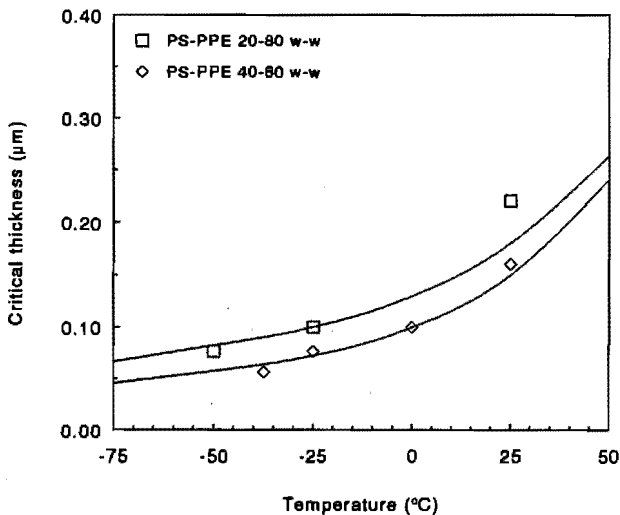


Figure 5.6 Critical matrix ligament thickness vs temperature for two rubber- modified PS-PPE blends: 40-60 and 20-80. The curves are according to the model

The full curves in *figure 5.6*, consequently, represent a cross section in *Figure 1B* at constant strain rate (of 10^2 s^{-1}). From *figure 5.6* it can be inferred that the temperature dependence of ID_c can be predicted satisfactory in a quantitative manner applying the simple model presented in chapter 3² in combination with an Eyring activated flow process despite the fact that the local yield stress in a matrix ligament can not be simply related to a macroscopic yield stress due to the presence of a notch (see discussion of *figure 5.3a*).

2) Visualization of the deformation process

To gain more insight in the deformation process occurring in front of the crack-tip during notched tensile testing in the ductile region pictures were taken at several stages of the process. Since the PS-PPE 20-80/X (for $X > 10$) blends already demonstrate the characteristics of a ductile fracture during notched high-speed tensile testing at room temperature (see *figure 5.3e*) these blends will certainly reveal ductile fracture during slow-speed notched tensile testing (compare *figure 5.1a*).

In *figure 5.7* the deformation process of a PS-PPE 20-80/30 blend is illustrated as observed in the ductile region during a slow-speed notched tensile test (5 mm min^{-1}) at room temperature. The optical micrographs are taken at several stages during the tensile test. Following the deformation process (*figures 5.7a* up to *5.7d*) the size of the deformed region (whitened area) increases to a constant value ahead of the crack-tip. The whitened volume corresponds to the tensile toughness value as already discussed in reference 3.

3) Brittle-to-ductile transitions

In *figure 5.3* brittle-to-tough transitions are clearly visible with increasing temperature or, at a constant temperature, with an increasing rubber concentration. The occurrence of a transition is indicated by a sudden increase of the notched tensile toughness. Inspection of the fractured samples provides an alternative independent determination of the critical situation.

In *figures 5.8a* and *5.8b* micrographs of high-speed fractured notched tensile specimens are shown as observed in the ductile region.

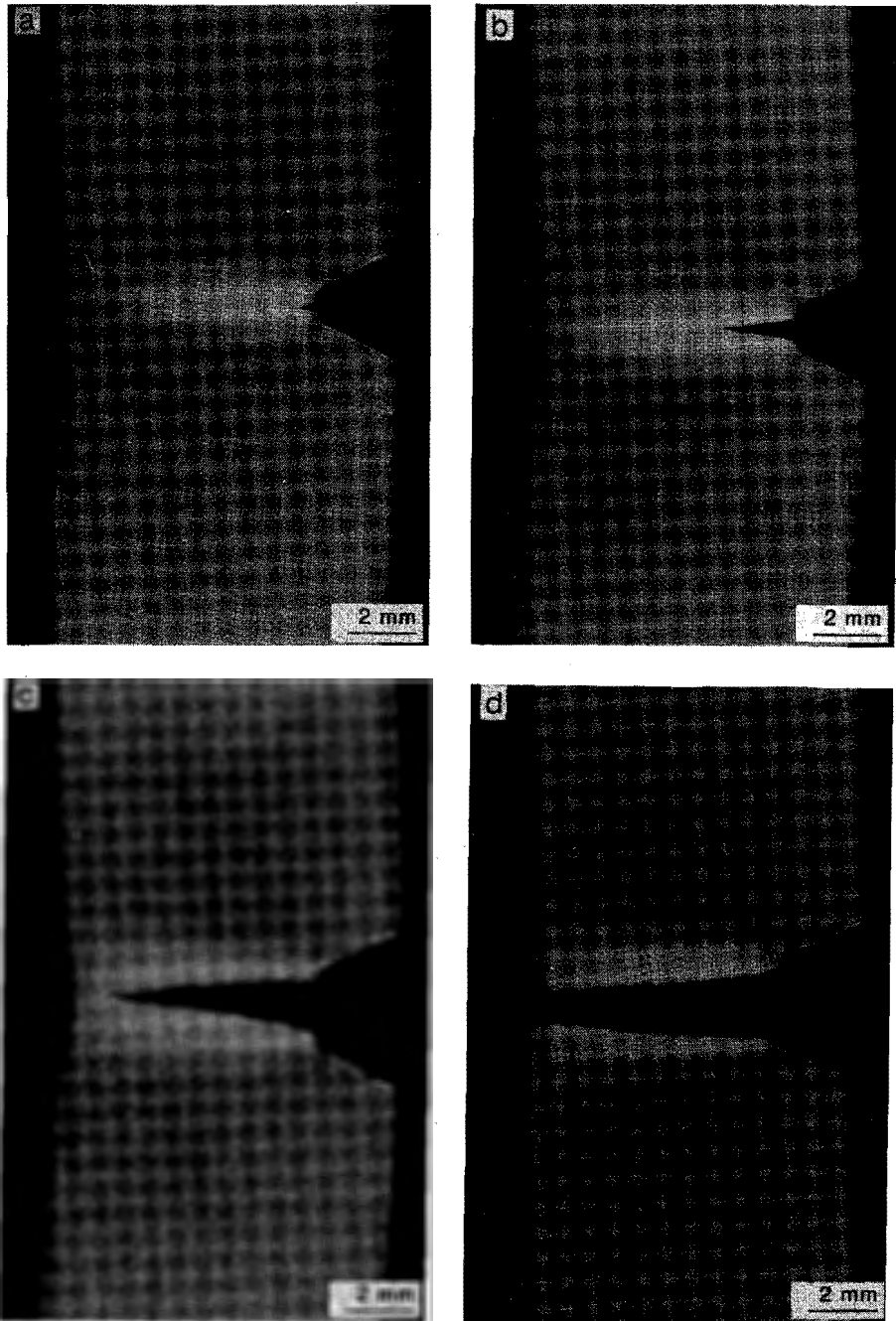


Figure 5.7 Optical micrographs of slow-speed single-edge notched rubber-modified PS-PPE 20-80 blends taken at several stages of deformation (a up to d)

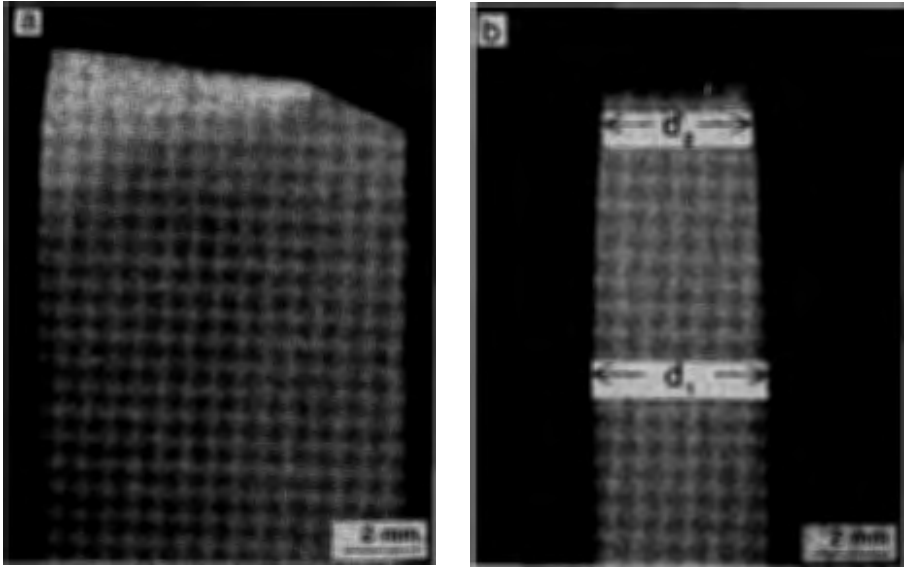


Figure 5.8 Micrographs of a high-speed fractured notched PS-PPE/X blend in the ductile region: (a) side view and (b) on-edge view

In principle the tensile specimens form a neck just below the fracture surface. The dimensions of the neck can be indicated by the values of d_1 and d_2 (see figure 5.8b). In particular the ratio d_1/d_2 represents the strain level locally at the fracture surface. Hence, via a comparison of the ratio d_1/d_2 of the various PS-PPE blends in the ductile region a qualitative insight can be obtained with respect to the influence of network density on the strain level just below the fracture surface of core-shell rubber-modified PS-PPE blends.

In figure 5.9 the ratio d_1/d_2 is plotted versus the rubber concentration for the various PS-PPE blends investigated at 75°C as a reference temperature because most data are present at this (high) temperature in the range of core-shell rubber percentages investigated.

The brittle-to-ductile transitions are revealed by a rather abrupt increase of the ratio d_1/d_2 . If the matrix ligament thickness is below the critical value, the strain to break of the material increases. Interesting to notice is that the strain level at the fracture surface (qualitatively) demonstrates the same network density dependence as the

maximum macroscopic strain to break listed in reference 2. Polystyrene (figure 5.9, curve A) demonstrates the maximum ratio d_1/d_2 in the tough region, i.e. the highest strain level locally at the fracture surface similar to the highest strain to break level for PS reported in reference 2 during slow-speed uniaxial tensile testing of core-shell rubber-modified PS-PPE blends at room temperature. The addition of PPE results in a shift of the brittle-to-ductile transition to lower rubber concentrations, again, analogous to the conclusions derived during the discussion of the unnotched slow-speed measurements presented in chapter 3².

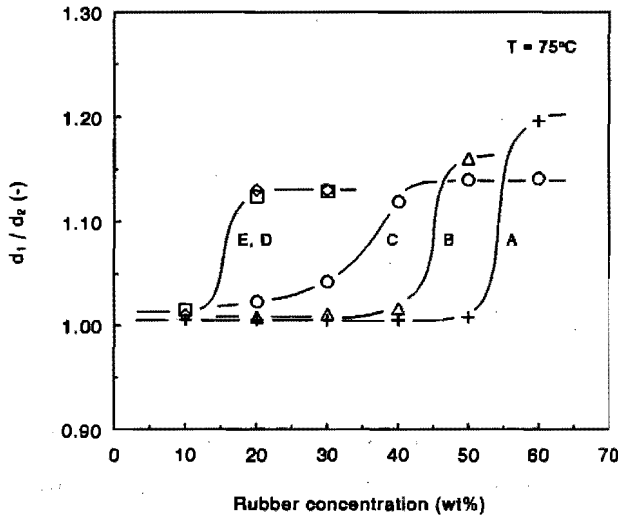


Figure 5.9 Deformation (d_1/d_2) of high-speed fractured notched PS-PPE blends versus rubber concentration with parameter the matrix composition (PS-PPE): (A) 100-0, (B) 80-20, (C) 60-40, (D) 40-60 and (E) 20-80 (reference temperature 75°C)

In order to compare the brittle-to-ductile transitions of the various PS-PPE blends as observed in figure 5.3 in a more convenient way, in figure 5.10 the normalized (relatively to the value in the tough region) value of the tensile toughness is shown versus the rubber concentration at two reference temperatures: 25°C and 75°C.

Only for the PS-PPE 40-60 and 20-80 blends the brittle-to-ductile transitions can be determined at 25°C as a reference temperature. From figure 5.10 (or equally well from figure 5.9) the critical matrix ligament thickness can be determined for the various PS-PPE blends assuming a body-centred-cubic lattice⁹⁻¹¹.

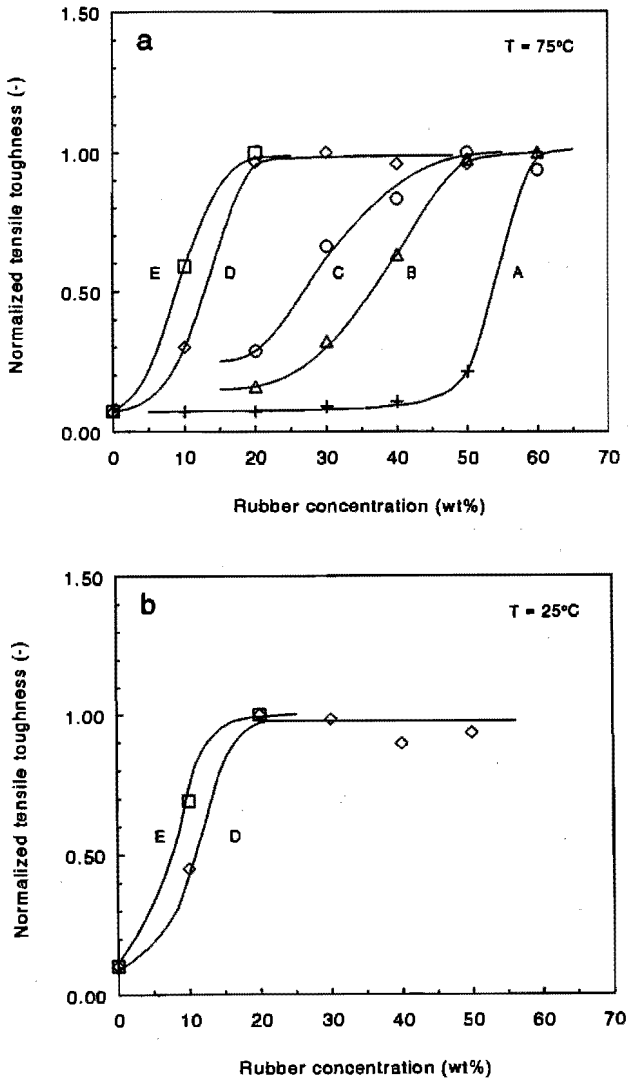


Figure 5.10 Normalized notched tensile toughness versus rubber concentration with parameter the matrix composition (PS-PPE): (A) 100-0, (B) 80-20, (C) 60-40, (D) 40-60 and (E) 20-80: (a) reference temperature 75°C and (b) reference temperature 25°C

In figure 5.11 these values of the critical matrix ligament thickness as determined from a notched tensile test are shown as a function of the network density for the two different reference temperatures (25°C and 75°C).

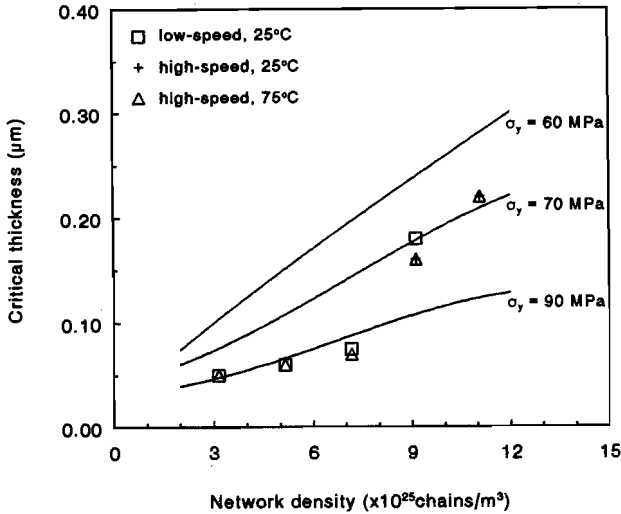


Figure 5.11 Critical matrix ligament thickness versus network density. The full curves are according to the model. For details, see text

For comparison also the critical matrix ligament thicknesses, as determined during slow-speed uniaxial tensile testing at room temperature ², are incorporated in figure 5.11. The values of ID_c determined via slow-speed uniaxial tensile testing compare well with the ID_c data extracted from notched high-speed tensile testing. Apparently, within the investigated strain rate and temperature range the value of ID_c is rather insensitive to changes in testing speed and temperature as could be expected, see figure 5.1. The full curves in figure 5.11 represent the value of ID_c in dependence of the network density as predicted by the simple model (see equation (5.1)), calculated for three different values of the yield stress: 60, 70 and 90 MPa. These values of the yield stress are chosen rather arbitrary since the yield stress in the ligament can not simply be converted into a macroscopic yield stress due to the presence of the notch (see discussion after figure 5.3). Especially in the region of low network densities, ID_c proves to be rather insensitive to changes in the yield stress, thus, it is relatively insensitive to changes in the testing speed or temperature.

The absolute value of the notched tensile toughness is not simply governed by the maximum strain to break but depends on the geometry of the specimen ¹²⁻¹⁷ and the quasi macroscopic effective yield stress (related to the volume fraction of holes). A quantitative prediction in the ductile region can only be made if the stress-state behind the notch-tip is fully understood. A multi-level finite element modelling of the

test sample can result in a more quantitative description of the network density dependence of the value of the notched tensile toughness in the ductile region. This aspect is a major topic of the present research in our laboratory.

5.4 Conclusions

Tensile dilatometry at testing speeds of 1 m s^{-1} reveal that the deformation mechanism of polystyrene in the ductile region ($ID \leq ID_c$) is shear deformation. The critical matrix ligament thickness of polystyrene as determined with uniaxial slow-speed tensile testing at room temperature proves to be valid up to testing speeds of 1 m s^{-1} . A further increase of the local strain rate by the introduction of a razor-blade tapped notch results in a brittle fracture of the 60 wt% rubber-modified polystyrene unless the increase in strain rate is compensated for by an increase in testing temperature to 70°C .

The influence of testing speed and temperature on the value of the critical matrix ligament thickness can be quantitatively understood in terms of the strain rate and temperature dependence of the yield stress (neglecting the strain rate and temperature dependence of the Young's modulus) using the simple model introduced in chapter 3, combined with an Eyring type of strain rate and temperature dependence of the yield stress.

Notched high-speed tensile testing of core-shell rubber-modified PS-PPE blends demonstrates that brittle-to-ductile transitions occur at about the same critical matrix ligament thicknesses as already determined during slow-speed uniaxial tensile testing at room temperature (see reference 2) provided that the testing temperature is increased. Apparently, the increase in yield stress, due to the local high strain rate as a consequence of the introduction of a notch, is counteracted by the increased temperature. The temperature dependence of ID_c according to the model is experimentally verified for PS-PPE 40-60 and 20-80 blends in a temperature range of 50 to 150°C below the glass transition temperature of the polymeric material.

5.5 References

- 1 Van der Sanden, M.C.M., Meijer, H.E.H. and Lemstra, P.J. *Polymer*, in press
- 2 Van der Sanden, M.C.M., Meijer, H.E.H. and Tervoort, T.A. *Polymer*, in press
- 3 Van der Sanden, M.C.M. and Meijer, H.E.H. *Polymer*, accepted for publication
- 4 Eyring, H. *J. Chem. Physics* 1936, 4, 283
- 5 Kambour, R.P. *Polymer Commun.* 1983, 24, 292
- 6 Govaert, L.E., unpublished data
- 7 Bucknall, C.B. 'Toughened Plastics', Appl. Sci. Publ., London, 1977
- 8 Narisawa, I., Kuriyama, T. and Ojima, K. *Makromol. Chem., Macromol. Symp.* 1991, 41, 87
- 9 Borggreve, R.J.M., Gaymans, R.J., Schuijjer, J. and Ingen Housz, J.F. *Polymer* 1987, 28, 1489
- 10 Wu, S. *Polymer* 1985, 26, 1855
- 11 Wu, S. *J. Appl. Polym. Sci.* 1988, 35, 549
- 12 Kinloch, A.J. and Young, R.J. 'Fracture Behaviour of Polymers', Elsevier Appl. Sci. Publ., London, 1985
- 13 Brown, H.R. *J. Mater. Sci.* 1982, 17, 469
- 14 Yap, O.F., Mai, Y.W. and Cotterell, B. *J. Mater. Sci.* 1983, 18, 657
- 15 Williams, J.G. 'Fracture mechanics of polymers', Ellis Horwood-Wiley, Chisester, 1984
- 16 Vincent, P.I. 'Impact tests and service performance of thermoplastics', Plastics Institute, London, 1971
- 17 Hertzberg, R.W. 'Deformation and Fracture Mechanics of Engineering Materials', John Wiley & Sons, New York, 1976

Chapter 6*

A Critical Examination of Multilayered Structures

6.1 Introduction

In chapters 2 and 3^{3,4} the concept of a material-specific thickness, below which brittle, amorphous glassy polymers become ductile, was introduced. It was shown that the value of the critical thickness as well as the maximum level of ductility are both determined by the molecular (network) structure of the polymer. Using thin sheets in stratified structures (with a non-adhering polymer as a spacer) the onset to the sudden increase in macroscopic strain to break was demonstrated while for thin ligaments in between 'holes' (i.e. non-adhering core-shell rubbery particles) it was shown that the macroscopic strain to break of brittle, amorphous polymers can be increased to 60% of the theoretical strain to break based on the stretching of a single entanglement strand of the network structure to its full extension.

Since in chapter 3 attention was focused on the understanding of the phenomenon of the material-specific critical thickness, mainly the core-shell rubber-modified structures were discussed. In this chapter, the deformation behaviour of multilayered tapes based on polystyrene-poly(2,6-dimethyl-1,4-phenylene ether) (PS-PPE) layers alternating with polyethylene (PE) is studied in more detail. Polyethylene is used as a non-adhering spacer possessing a constant high level of ductility at all layer thicknesses³. The number of layers in the tape (and thus the PS-PPE layer thickness, d) can be set by changing the number of mixing elements in the Multiflux static mixer used³ at a constant total tape thickness. However, the viscosity ratio of both components proves to determine the maximum number of elements and thus the limiting layer thicknesses since, finally, viscosity and normal stress difference driven

* This chapter is reproduced, in part, from:

1. Van der Sanden, M.C.M., Buijs L.G.C., De Bie, F.O. and Meijer, H.E.H. *Polymer*, submitted for publication

interfacial instabilities render layer break-up and rupture⁵⁻⁷. As an example, for the system polystyrene/poly(methyl methacrylate) (PS/PMMA) 50/50, with fairly matching flow curves within the shear rate and temperature range applied, a spectacular minimum layer thickness of 40 nm could be achieved: see figure 6.1.

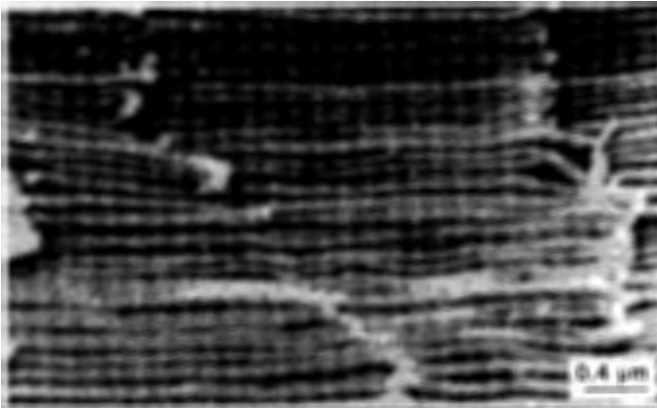


Figure 6.1 SEM micrograph of a multilayered PS/PMMA 50/50 tape: layer thickness: 40 nm

In the PS-PPE/PE systems it was not tried to properly optimize the viscosity ratio (e.g. by choosing different PE types for the different PS-PPE compositions) since attention is focused on the micromechanical explanation of the deformation behaviour found for the different network structures and test geometries.

The motivation for this more detailed investigation on especially the multilayered tapes originated from some stimulating criticism met in the early stage of our research: When we first presented the striking experimental findings concerning the material-dependent critical thickness (read: thinness) in a fast visiting tour in January 1992 to some experts in the area of micromechanics of polymers, both Ed Kramer of Cornell University and Eric Baer of Case Western Reserve University noticed the possible importance of a small level of adhesion that is always present in thin multilayered structures even if immiscible polymer pairs (like PS and PE) are used. This especially could be of influence in the interpretation of the results on the stratified structures. The convincing results of the extremely different macroscopic deformation behaviour of 60 wt% adhering (PS-shell) and non-adhering (PMMA shell) core-shell rubber-modified PS, see reference 3, made the interpretation of the

experimental findings in these systems less ambiguous and, finally, resulted in the simple energy based model that is capable of describing the criterion for macroscopic ductility in crazing and shear deforming polymers (including thermosets!), see chapters 3, 4 and 5^{4,8,9}. The application of this model to predict the change in strain to break of the continuous thin stratified multilayered structures is, however, not that straightforward and needs some additional assumptions. Both aspects are dealt with in this chapter: Using the micromechanical facilities in Case Western Reserve University, the details of the deformation behaviour of our tapes were revealed, while Ed Kramer reworked, after a number of subsequent discussions also at our laboratory, his existing model (Kramer and Berger², that is focused especially on the transition from crazing to shearing) to include the network density effect as found in our previous experiments and is easily applicable to thin films as well.

Several studies have been reported on microlayered structures focusing on unique properties with respect to their optical, barrier and mechanical properties¹⁰⁻¹². The strain to break of multilayered systems containing at least one ductile component can be improved via three routes: (i) A decrease of the layer thickness of the brittle component; this finally results in an elimination of the limiting effect to the overall strain to break^{3,4} while, (ii) the introduction of a considerable degree of adhesion between the layers of the brittle and ductile component can result in a mutual induction of deformation mechanisms in both types of layers^{13,14} and, (iii) also can allow for multiple fracture of each separate brittle layer¹⁵.

In this study the adhesion (G_{IC}) between the PS-PPE and PE layers is investigated by applying a double cantilever beam peel test as described by Bazhenov et al.¹⁶ and optical light microscopy during uniaxial tensile testing is applied to elucidate the deformation mechanism of the PS-PPE/PE tapes. In order to gain some more insight in the phenomenon of interlayer adhesion, a third component (a diblock copolymer) between every individual PS-PPE and PE layer has been introduced to influence the adhesion in a rather extreme and precise manner.

6.2 Experimental

6.2.1 Materials

The materials used were polystyrene (DOW Styron 638), poly(2,6-dimethyl-1,4-phenylene ether) (General Electric Co., PPE-803), low-density polyethylene (PE; DSM, LDPE 1808 AN) and a diblock copolymer

based on polystyrene and hydrogenated isoprene rubber (Shell, Kraton G-1701 X). PS and PPE were mixed in various proportions (100-0, 80-20, 60-40 and 40-60) to set the entanglement density of the PS-PPE blend (see reference 4 for a detailed description of the mixing procedure). The diblock copolymer used ($M_n = 82 \text{ kg mol}^{-1}$, $M_w = 88 \text{ kg mol}^{-1}$) contains about 37 wt% polystyrene.

6.2.2 Sample preparation

PS-PPE and PE were multilayered in different compositions (100/0, 75/25, 50/50, 25/75 and 0/100) using the Multiflux mixer that renders the most perfect baker's transformation of all mixers¹⁷. Laminated tapes with different spacing PE layers were prepared at 200°C (PS-PPE: 100-0), 220°C (PS-PPE: 80-20), 225°C (PS-PPE: 60-40) and 230°C (PS-PPE: 40-60). The total number of continuous layers that could be obtained in a tape varied between 128 (6 mixing elements) and 4096 (11 mixing elements; see comments on the influence of the viscosity ratio in the introduction) while the total tape thickness was kept constant around 0.3 mm. Multilayered tapes will be indicated with a three number code: A-B/C: A-B: PS-PPE composition of the tape; C: weight fraction PE in the tape.

Multilayered tapes containing the diblock copolymer (BC) as a third component were prepared at 200°C for the pure PS/PE system only. Four ingoing layers are required in this case, stacked as: PS/BC/PE/BC. Three different PS/PE ratios were chosen: 75/25, 50/50 and 25/75, while the total amount of block copolymer was 1 wt%.

Small dumb-bell-shaped tensile specimens were machined from the multilayered tapes parallel to the direction of extrusion according to ASTM D 1708.

To avoid any unwanted orientation effects, prior to mechanical analysis all machined tapes were annealed during 24 hours at a temperature 20°C below the glass transition temperature of the PS-PPE phase. Heating of the samples at a temperature of 10°C above the glass transition temperature of the PS-PPE phase revealed a shrinkage of approximately 4%. This value should not have a noticeable influence on the mechanical properties of the tapes^{18,19}.

6.2.3 Interlayer adhesion

The interlayer adhesion of several tapes was measured using a (modified) double cantilever beam (DCB) peel test as described by Bazhenov et al.¹⁶. The conventional DCB test could not be used because this test does not allow for a substantial bending of the beams, which occurred in our situation. Adhesion in the modified DCB test¹⁶ is characterized by the fracture toughness (G_{Ic}), i.e. the energy dissipated during the formation of new surface, given by:

$$G_{Ic} = \frac{F (\sin\Theta_1 + \sin\Theta_2)}{W} \quad (6.1)$$

where F is the peel force, Θ_1 and Θ_2 are the angles between the cantilever beam ends and the direction

of the force applied (see figure 6.2) and W is the width of the sample (5 mm).

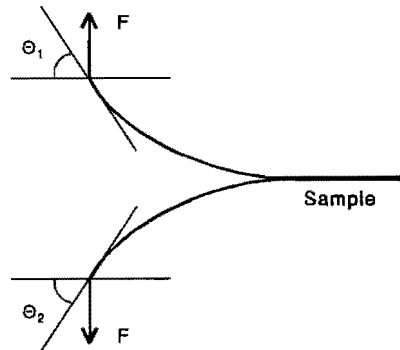


Figure 6.2 Schematic representation of the modified double cantilever beam peel test

Specimens were cut from the extruded tapes with a diamond saw into the desired dimensions: length x width: 90 mm x 10 mm. An initial crack (depth: 10 mm) was made as close as possible to the middle level of the sample using a fresh razor-blade. Subsequently, tabs were glued on the end of both cantilever beams and force was applied (see figure 6.2) using an Instron tensile testing machine equipped with a 5 N load cell at a loading rate of 10 mm min^{-1} . The cantilever beam end angles during crack propagation were determined by taking photographs periodically. Three samples (of the same composition) were tested in order to obtain an average value of G_{Ic} .

6.2.4 Microscopy

Optical reflecting light microscopy (Olympus BH equipped with a C-35 AD-2 Olympus camera) was applied to investigate the fracture surface after measuring the interlayer adhesion in order to verify the crack propagation path.

Scanning Electron Microscopy (SEM) was applied to check the thickness and homogeneity of the PS-PPE layers. Specimens were cut from the centre of the layered specimen, parallel to the direction of extrusion and perpendicular to the layers. The surface was microtomed using a glass knife at liquid-nitrogen temperature, subsequently etched in an oxygen plasma to remove the polyethylene (and rubber-phase of the diblock copolymer) and finally covered with a conducting gold layer.

6.2.5 Mechanical testing

Multilayered tapes were uniaxially strained on a Frank tensile machine (type: 81565 IV) at a cross-head speed of 5 mm min^{-1} ($l_0 = 20 \text{ mm}$). In order to obtain representative data, all experiments were carried out in five-fold for each testing condition.

6.2.6 Microscopy during tensile testing

To visualize the deformation behaviour, deformation was realized using a Minimat (Polymer Laboratories; distance between clamps: 15 mm) mounted on an optical transmission microscope (Olympus BH2). Dumb-bell-shaped tensile specimens were viewed in transmission perpendicular to the tape surface at a low testing speed (5 mm min^{-1}) at Case Western Reserve University (Cleveland). Before testing the top and bottom layers were peeled off (an easy job in the poorly adhering PS-PPE/PE systems) to remove any irregularities and to ensure that all tapes had the same thickness (0.3 mm). During loading pictures were taken at distinct stages of the deformation using an Olympus C-35 AD-2 camera mounted on the microscope. Plastic (shear) deformation, if present, could be visualized with a polarizing filter added to improve the colour contrast.

6.3 Results and Discussion

6.3.1 Interfacial adhesion

Figure 6.3 demonstrates the interlayer adhesion as determined using the (modified) double cantilever beam test of several PS-PPE/PE tapes: 100-0/75, 60-40/75 and 60-40/50 versus the PS-PPE layer thickness*.

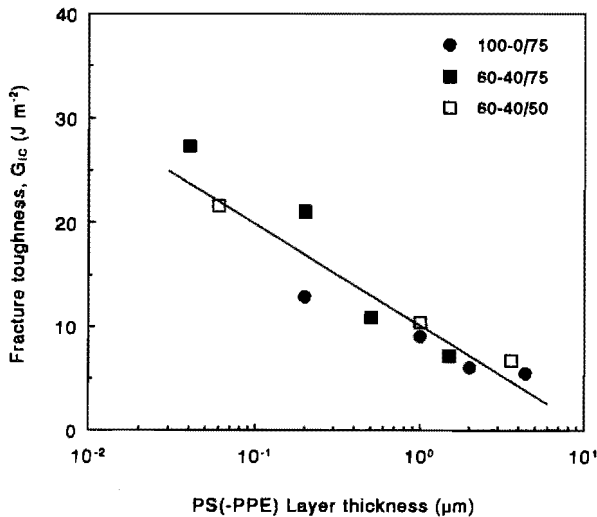


Figure 6.3 Interlayer adhesion (G_{IC}) of 100-0/75, 60-40/75 and 60-40/50 tapes versus the PS-PPE layer thickness

* Multilayered tapes are indicated with a three number code: A-B/C; A-B: PS-PPE composition of the tape; C: weight fraction PE in the tape.

From *figure 6.3* it can be inferred that the G_{Ic} value for all PS-PPE layer thicknesses is very low ($5\text{--}25\text{ J m}^{-2}$) compared with the values published for the PC/SAN system: $100\text{--}1200\text{ J m}^{-2}$ (ref. 16 and 20) and independent of the ratio PS-PPE/PE. The amount of PPE present in the PS-PPE phase does not influence the interlayer adhesion but, surprisingly, the PS-PPE layer thickness has a pronounced influence on the G_{Ic} value: with a decreasing PS-PPE layer thickness the interlayer adhesion increases significantly. Examination of the fracture surfaces of the delaminated samples elucidates the increasing G_{Ic} values with a decreasing PS-PPE layer thickness (see *figure 6.4*; crack path direction: horizontal).

In *figure 6.4a* (100-0/75; PS-PPE layer thickness: $1\text{ }\mu\text{m}$) a clear fracture surface can be observed. Decreasing the PS-PPE layer thickness results in a fracture surface that is covered with torn layers (see *figure 6.4b*) or even demonstrates a large amount of plastic deformation (see *figure 6.4c*). Hence, the increased G_{Ic} interlayer adhesion values are caused by a multiple crack propagation path. Consequently, the G_{Ic} interlayer adhesion obtained from a 100-0/75 tape with a PS-PPE layer thickness of approximately $1\text{ }\mu\text{m}$ (corresponding to the delaminated fracture surface of *figure 6.4a*) is the most representative value: 5 J m^{-2} , which is a very low value as already stated above.

6.3.2 Mechanical testing

Figure 6.5 shows the strain to break of several multilayered PS-PPE/PE tapes (100-0/X, 80-20/X, 60-40/X and 40-60/X) versus the PS-PPE layer thickness. The strain to break of the tape is defined as the strain at which a sharp decrease in stress is observed (see *figure 2.4* of chapter 2) corresponding to the breakage of the PS-PPE layers. In *figure 6.5* only samples with continuous stratified structures are dealt with as verified using scanning electron microscopy.

As can be inferred from *figure 6.5a* (PS-PPE/PE 100-0/X), the strain to break shows an initial upswing at about $1\text{ }\mu\text{m}$ and increases with a decreasing PS-PPE layer thickness. The maximum strain to break is 100% and is observed for the 100-0/75 tape at a thickness of $0.4\text{ }\mu\text{m}$. Tapes containing less than 75 wt% PE have a strain to break of less than 10% (more elements in the mixer resulted in discontinuous layers).

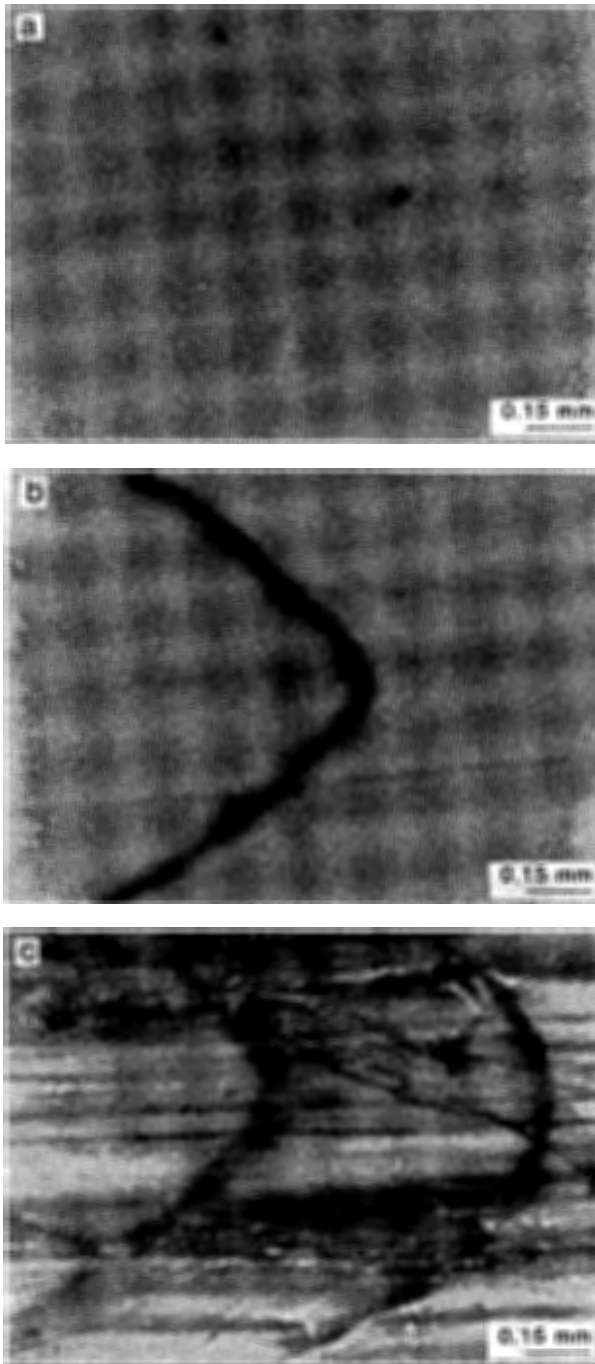


Figure 6.4 Optical micrographs of delaminated PS-PPE/PE tapes: (a) 100-0/75, PS-PPE layer thickness: $1\ \mu\text{m}$, (b) 60-40/75, PS-PPE layer thickness: $0.5\ \mu\text{m}$ and (c) 60-40/75, PS-PPE layer thickness: $0.04\ \mu\text{m}$

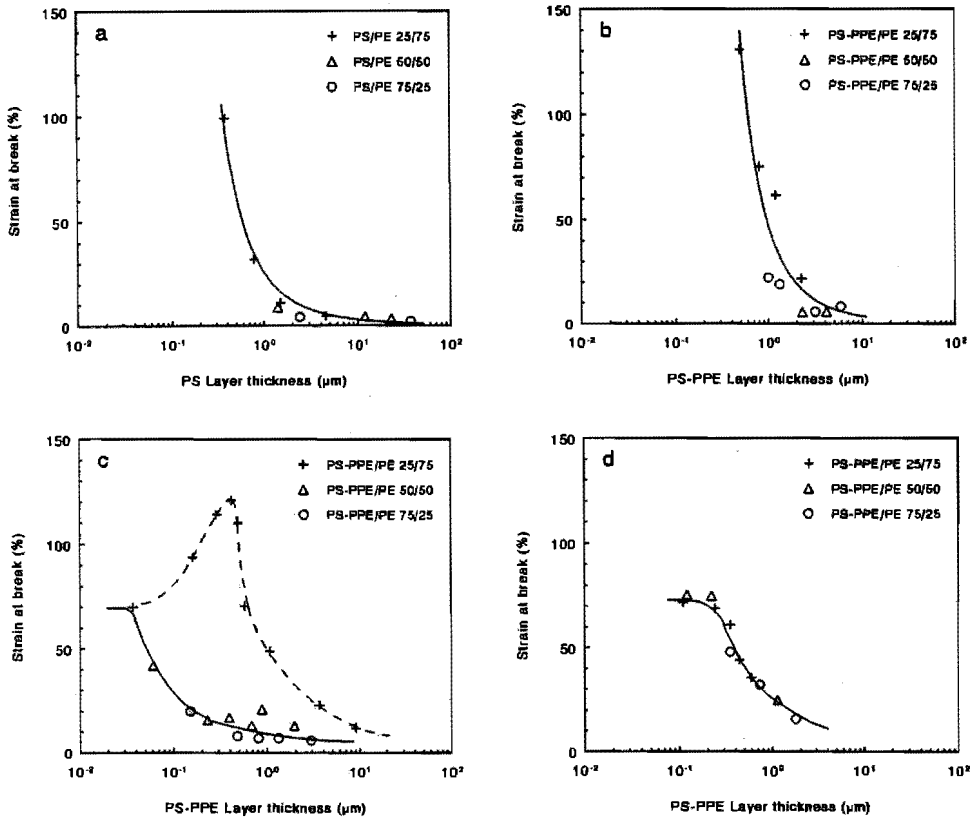


Figure 6.5 Strain at break of several PS-PPE/PE tapes versus the PS-PPE layer thickness: (a) 100-0/X, (b) 80-20/X, (c) 60-40/X and (d) 40-60/X

Adding 20 wt% PPE to the PS phase (PS-PPE/PE 80-20/X; see figure 6.5b) gives roughly the same results (upswing at $\approx 1 \mu\text{m}$) with the exception that the maximum strain to break of the tape is about 130% for the 80-20/75 tape with a PS-PPE layer thickness of $0.5 \mu\text{m}$. (For the 80-20/X tapes the experimentally achievable minimum continuous PS-PPE layer thickness without the occurrence of rupture equals this $0.5 \mu\text{m}$.)

Only increasing the PPE content of the PS-PPE phase above 40 wt% allows for a substantial increase of the maximum number of mixing elements applicable in the static mixer before layer rupture occurs during processing. Consequently, the minimum attainable continuous PS-PPE layer thickness is significantly decreased to

approximately $0.05\ \mu\text{m}$. *Figure 6.5c* shows the strain to break of the 60-40/X tapes versus the PS-PPE layer thickness. The 60-40/75 tape demonstrates initially the same behaviour as already described for 100-0/X and 80-20/X tapes: an initial upswing at about $1\ \mu\text{m}$. However, now also a maximum strain to break ($\approx 125\%$) is observed for a layer thickness of approximately $0.4\ \mu\text{m}$. Below this value the strain to break decreases to 70% at a layer thickness of $0.04\ \mu\text{m}$ (i.e. the minimum achievable experimental PS-PPE layer thickness). The strain to break of the 60-40/50 and 60-40/25 tapes now can be measured up to very thin layers and shows a significant increase if the PS-PPE layer thickness is below $0.1\ \mu\text{m}$. From the optical micrographs taken during deformation (see *figure 6.6*) and the discussion here, it can be stated that there is a distinct difference in the two transitions found for this PS-PPE composition. The apparent brittle-to-ductile transition at the layer thickness of approximately $1\ \mu\text{m}$, as found for the 60-40/75 tape (and the 100-0/75 and 80-20/75 tapes as well), is correlated with the stress transfer mechanism, while the second transition (at $\approx 0.1\ \mu\text{m}$ for the 60-40/X tapes only) coincides with a change in deformation mechanism. Moreover, both the value of the critical thickness and the strain to break below the second transition excellently agree with the data extracted from the core-shell rubber-modified PS-PPE 60-40 blends ⁴.

Finally, for the PS-PPE/PE 40-60/X tapes only a single transition is found for all PS-PPE/PE compositions (see *figure 6.5d*) at a PS-PPE thickness of approximately $0.3\ \mu\text{m}$: a (critical) thickness that again correlates well with the critical matrix ligament thickness as already reported for the 40-60 blend determined with stress-strain measurements of core-shell rubber-modified 40-60 blends ⁴. Also the maximum level of strain to break in the ductile region, i.e. below the critical layer/ligament thickness, agrees perfectly with the maximum macroscopic strain to break of core-shell rubber-modified 40-60 blends (70%) ⁴.

6.3.3 Microscopy during tensile testing

In order to investigate the various transitions observed in *figure 6.5*, uniaxial tensile testing is performed on the 60-40/75 tape at several PS-PPE layer thicknesses on a tensile stage mounted under an optical microscope (Minimat). *Figures 6.6a - 6.6c* show polarized optical transmission micrographs of a 60-40/75 tape having a PS-PPE layer thickness of $1.5\ \mu\text{m}$ taken at distinct strain levels (direction of load is horizontally).

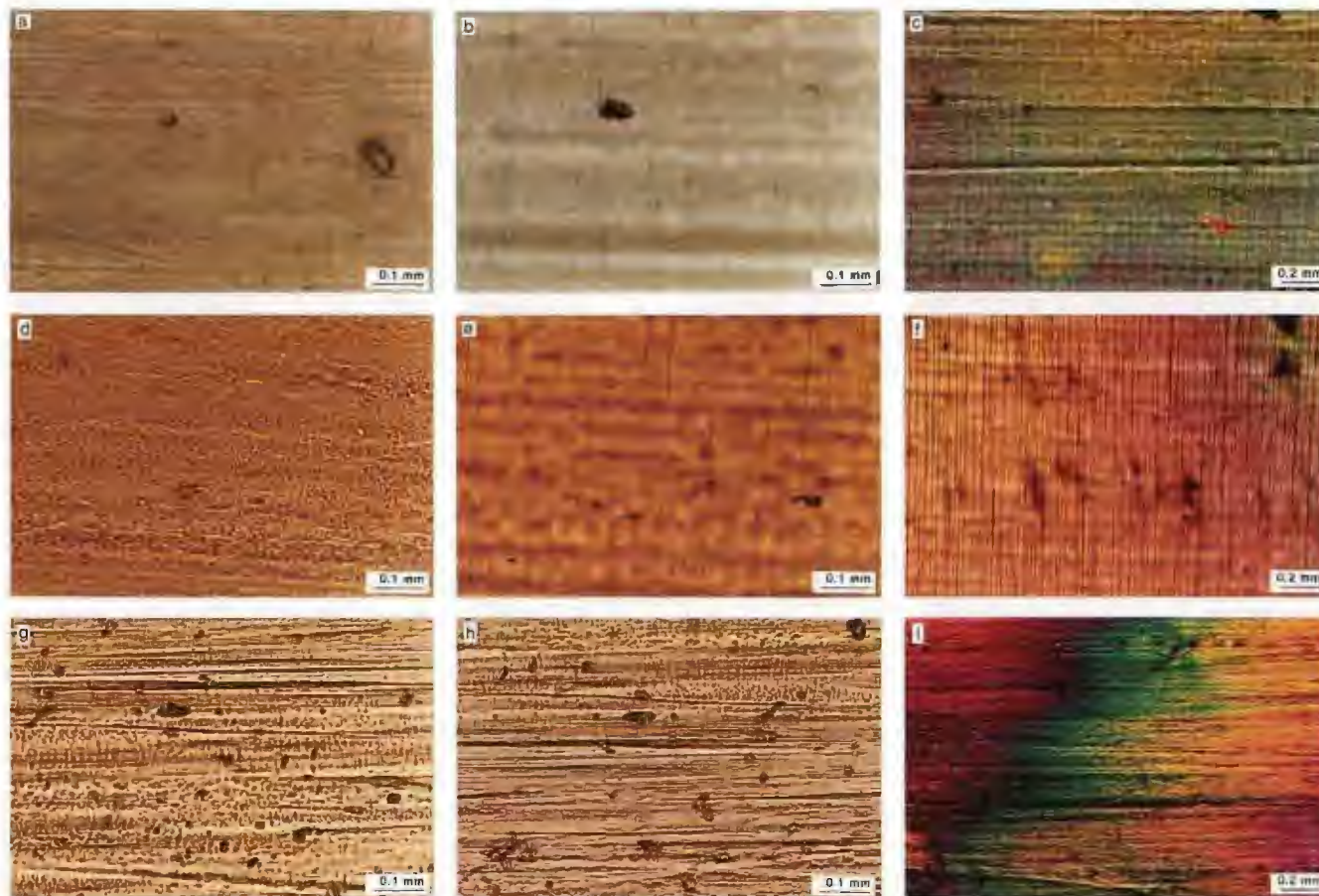


Figure 6.6 Polarized optical micrographs of strained PS-PPE/PE 60-40/75 tapes for several PS-PPE layer thicknesses and strain levels: (a) 1.5 μm , 0% strain, (b) 1.5 μm , 4% strain, (c) 1.5 μm , 8% strain, (d) 0.5 μm , 0% strain, (e) 0.5 μm , 4% strain, (f) 0.5 μm , 8% strain, (g) 0.04 μm , 0% strain, (h) 0.04 μm , 4% strain and (i) 0.04 μm , 13% strain

At 4% strain thin lines are visible perpendicular to the direction of load (see *figure 6.6b*). The black thin lines probably correspond to small cracks preceded by crazes. Increasing the strain results in a strong increase in the number of cracks perpendicular to the load direction (see *figure 6.6c*, 8% strain). Decreasing the PS-PPE layer thickness to $0.5\ \mu\text{m}$ (see *figures 6.6d - 6.6f*, corresponding to the tape possessing a maximum strain to break of approximately 125%) results at the same strain level (e.g. 8%) in: (i) an increase of the number of cracks visible and (ii) a more pronounced visibility of the cracks. A further decrease of the PS-PPE layer thickness ($0.04\ \mu\text{m}$, *figures 6.6g - 6.6i*, below the critical thickness demonstrated in reference 4) drastically changes the optical observations: at any stage during the deformation no cracks can be detected. Moreover, the bright colours that are visible during the deformation under the optical microscope indicate massive plastic (shear) deformation. These microscopic observations demonstrate that a transition occurs from a crack-like deformation (preceded by crazes) at approximately $1\ \mu\text{m}$ to a shearing type of deformation mechanism if the PS-PPE layer thickness is decreased below $0.05\ \mu\text{m}$.

Figure 6.7 shows the stress-strain curves of two 60-40/75 tapes possessing a PS-PPE layer thickness of $0.29\ \mu\text{m}$ (curve A) and $0.04\ \mu\text{m}$ (curve B), respectively.

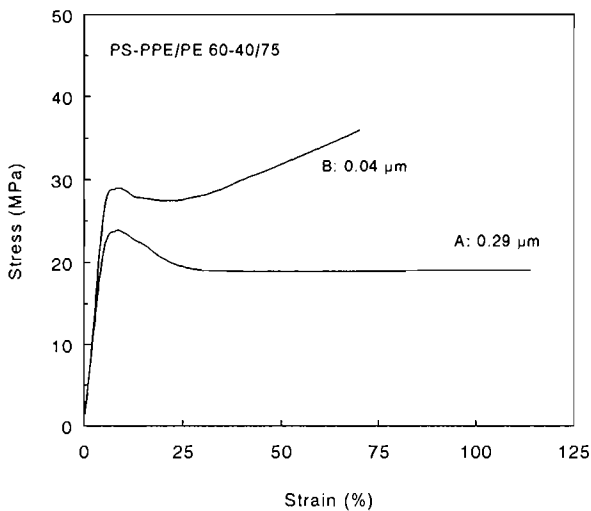


Figure 6.7 Stress-strain curves of PS-PPE/PE 60-40/75 tapes for two different PS-PPE layer thicknesses: (A) $0.29\ \mu\text{m}$ and (B) $0.04\ \mu\text{m}$

Comparing both stress-strain curves confirms the two different deformation mechanisms occurring in both tapes as determined with the optical microscope observations of *figure 6.6*: curve A corresponds to the typical curve of a craze deforming polymer ²¹ (a constant stress level after the yield point; e.g. rubber-toughened polystyrene ²²), while curve B shows the characteristics of a true shear deforming polymer ('strain hardening') ²¹.

6.3.4 Modelling of the first transition

For PS-PPE layer thicknesses comparable with or larger than 0.5 μm cracks are already visible at low strains for the PS-PPE/PE 60-40/75 tape (see *figures 6.6c* and *6.6f*) without causing a fatal macroscopic failure of the tape (see *figure 6.5c*). Similar observations are made in the area of fibre reinforced composites, where a rather stiff (low strain to break) fibre is embedded in a ductile polymeric matrix possessing a strain to break considerably higher than the fibre ^{23,24}. The observation that a fibre embedded in a polymeric matrix can be fractured several times along the fibre before final failure of the composite occurs is explained by the stress transfer mechanism ^{23,24}. This mechanism becomes operative if there is a substantial level of adhesion present between the fibre and the polymeric matrix, expressed by the matrix shear strength or interfacial shear strength (τ_m) whichever is smaller. After breakage of the fibre stress can be build up by stress transfer from the matrix. The process of breakage continues until the transferred stress becomes lower than the strength of the fibre (F_{\max}). A simple force balance results in a correlation between τ_m and F_{\max} on one hand and the critical transfer length (l_c) and the fibre diameter (d_f) on the other hand:

$$\frac{l_c}{d_f} = \frac{F_{\max}}{(2\tau_m)} \quad (6.2)$$

Baer and Moet ¹⁵ carried out a similar analysis for microlayered composites which resulted in a relationship between τ_m , F_{\max} , l_c and t :

$$\frac{l_c}{t} = \frac{F_{\max}}{(2\tau_m)} \quad (6.3)$$

where t is the layer thickness of the brittle component (i.e. the component possessing the lowest strain to break). Equation (6.3) implies that a decrease of the PS-PPE layer thickness (i.e. the 'brittle' component) by a factor two upon the addition of one

extra mixing element in the static mixer results in a decrease of the critical transfer length l_c with the same factor two and, consequently, in an increase of the macroscopic strain to break if it is assumed that the macroscopic strain to break of the multilayered tape is directly correlated with the number of breakages along the length of the tape. Inspection of the transitions at approximately $1 \mu\text{m}$ observed for both the 100-0/75, 80-20/75 and 60-40/75 tapes (see figures 6.5a, 6.5b and 6.5c) experimentally verifies equation (6.3): for PS-PPE layer thicknesses below $10 \mu\text{m}$ an increasing strain to break is observed with a decreasing PS-PPE layer thickness. The addition of an extra mixing element results in a reduction of the PS-PPE layer thickness by half and, consequently, in an increase of the strain to break of the tape roughly by a factor two. For PS-PPE layer thicknesses below $0.5 \mu\text{m}$ (only experimentally achievable for the 60-40/75 tape) the strain to break of the multilayered tape decreases with a decreasing layer thickness. This can be explained by the fact that the deformation mechanism of the PS-PPE layers starts to change from a craze-like deformation into a shearing type of deformation (compare figures 6.6f and 6.6i). The crack-like deformation does not occur for layer thicknesses below $0.05 \mu\text{m}$. Instead the PS-PPE/PE tape fails after complete homogeneous shear deformation of the PS-PPE phase up to the theoretical strain to break (70% for the 60-40 blend ⁴).

For PS-PPE/50 and PS-PPE/25 tapes the stress transfer mechanism as described above seems to be absent (see figure 6.5). This can be subscribed to the fact that upon decreasing the PE content of the tape, fracture of a PS-PPE layer will result in a higher stress level in the neighbouring PE layers. Hence, a fracture of the PE layers is likely to occur immediately after the first fracture of a PS-PPE layer resulting in a fatal failure of the whole tape.

Inspection of figure 6.5d only reveals a single brittle-to-ductile transition at approximately $0.25 \mu\text{m}$, obviously the stress transfer mechanism is not operative in these tapes or coincides with the brittle-to-ductile transition induced by the change in deformation mechanism ⁴.

6.3.5 Increase in interlayer adhesion

Exploiting the stress transfer mechanism (by increasing the interlayer adhesion between PS-PPE and PE) should, finally, result in a PS-PPE/PE tape possessing the

strain to break of pure PE. This hypothesis is verified by the introduction of a third component in the multilayered PS-PPE/PE tapes: a diblock copolymer based on styrene and hydrogenated isoprene rubber. In *figure 6.8* a SEM micrograph is shown of a PS/PE/BC 25/74/1 w/w/w tape having a PS layer thickness of approximately 1 μm .

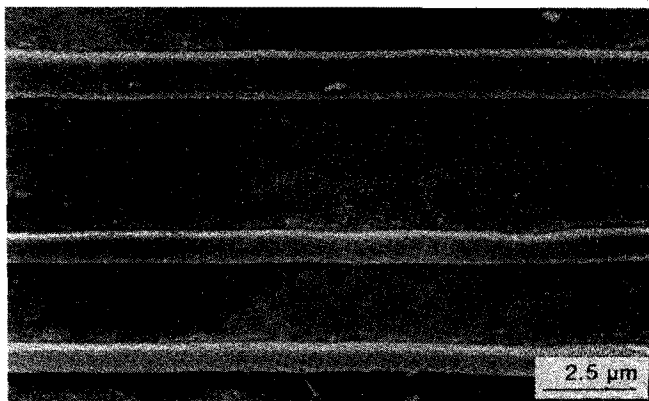


Figure 6.8 SEM micrograph of a multilayered PS/PE/BC 25/74/1 w/w/w tape possessing a PS layer thickness of 1 μm

The diblock copolymer is not detectable on the SEM micrograph (only 1 wt% is present) but it is most likely positioned at the interface with the styrene part of the diblock copolymer positioned in the PS layers and the hydrogenated isoprene rubber block in the PE layers. The presence of the diblock copolymer should increase the interlayer adhesion (and therefore also the interfacial shear strength, τ_m) significantly^{25,26}. Examination of equation (6.3) reveals that an increase in τ_m results in a decrease of the critical transfer length (l_c) at a constant layer thickness. Stress-strain analysis of the tape shown in *figure 6.8* results in a strain to break of 230% (i.e. the strain at break of pure PE) which is considerably higher than the strain to break of the corresponding PS/PE 25/75 tape (no diblock copolymer present) having the same PS layer thickness: 30% (compare *figure 6.5a*).

6.3.6 Modelling of the second transition

In conclusion: generally two transitions are found in the multilayered tapes. The first transition only occurs at a PS-PPE layer thickness of roughly 1 μm if relatively thick PE spacing layers are present. This transition is due to the stress transfer between the

(slightly) adhering layers. The second transition is found if the layers can be made thin enough (which is dependent on the viscosity ratio) and coincides with a change in deformation mechanism from crazing to shearing.

Thus, after a careful and critical evaluation of the results obtained with the stratified structures it can be stated that the concept of a critical thickness, below which brittle polymers become ductile, is not only valid for thin matrix ligaments^{3,4} but is also applicable to thin films (see *figure 6.5c*, transition at 0.05 μm , and *figure 6.5d* with a transition at 0.25 μm). The maximum strain to break in the ductile region could be explained by the theoretical maximum elongation of the polymer network (λ_{max}) and the absolute value of the critical thickness could be quantitatively understood from a simple energy based model (see chapters 3 and 5^{4,9}). This model is, however, only applicable to the thin film experiments if additional assumptions with respect to the volume stored elastic energy are made. It is therefore interesting to reproduce an alternative explanation for the thickness transition in thin films that is focused on the change in deformation mechanism and is derived from the established theory of Kramer for craze growth^{1,2}.

If it is postulated that a craze structure should contain at least two craze fibrils, this minimum thickness (L_{min}), in which the craze structure just can fit, can be calculated from the fastest growing fibril spacing D_0^* (see Appendix 6.A):

$$L_{\text{min}} = \frac{16\Gamma}{\sigma_y(1 - \lambda_{\text{max}}^{-1/2})} + 2h \quad (6.4)$$

where Γ is the surface energy involving the breakage of chains, σ_y is the yield stress, λ_{max} the theoretical maximum extension ratio of the entanglement network and h the thickness of the active zone layer at the craze/bulk interface. Taking for PS: $\Gamma = 0.08 \text{ J m}^{-2}$ (ref. 2), $\sigma_y = 82.8 \text{ MPa}$ (ref. 27), $\lambda_{\text{max}} = 4.2$ (ref. 1) and $h = 25 \text{ nm}$ (ref. 28) results in a value of L_{min} of 80 nm, a value that is rather close to the value derived from the energy based model that resulted in 55 nm.

As Kramer suggested²⁹, a better approximation can be made if not the fastest growing fibril spacing is considered but the fibril spacing less than the fastest growing one to widen at a reduced rate. The transition from crazing to shearing occurs if the craze widening velocity is equal to the velocity of widening a shear deformation zone.

Combining the estimated fibril spacing ($D_{o, tr}$) at which the transition occurs from crazing to shear deformation with the assumption that this minimum thickness contains just two craze fibrils results in a somewhat different expression for $L_{min, tr}$:

$$L_{min, tr} = 4h - h \sqrt{4 - \frac{32\Gamma}{\sigma_y h (1 - \lambda_{max}^{-1/2})}} \tag{6.5}$$

(see again Appendix 6.A for the derivation). Using the same data for PS as used above, results in a value of $L_{min, tr} = 69$ nm, a value that is even closer to the one calculated with the energy based model. The critical thickness for the other PS-PPE blends analyzed in this study according to equations (6.4) (L_{min}) and (6.5) ($L_{min, tr}$) is shown in *figure 6.9* (broken curves; the value of h is assumed to be independent of the PS-PPE composition, which might be incorrect).

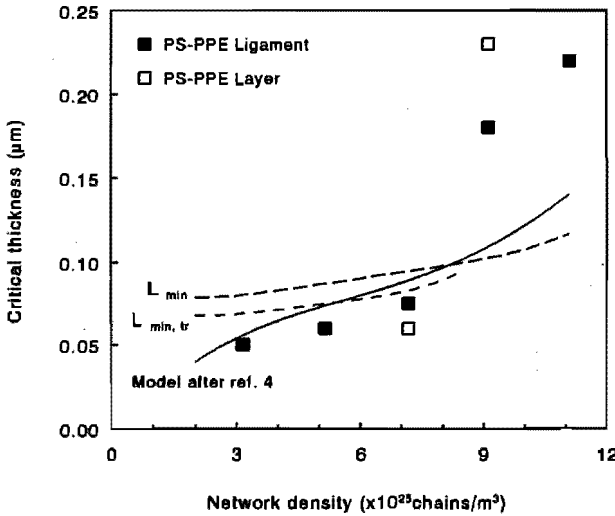


Figure 6.9 Critical thickness versus the matrix entanglement density (v_e) for the various PS-PPE blends. The curves are according to the various models. For details, see text

For comparison the critical thickness according to the energy based model of chapter 3 is also incorporated in this figure (full curve) ⁴. Experimentally, the critical thickness associated with a change in deformation mechanism could only be determined for the 60-40/X and 40-60/X tapes (open squares). The critical matrix ligament thickness

determined via core-shell rubber-modification of the PS-PPE 100-0, 80-20, 60-40 and 40-60 blends is also shown in *figure 6.9*: filled squares. Inspection of *figure 6.9* reveals that all three models result in a satisfying prediction of the critical thickness for the several PS-PPE blends. However, the validity of the model predictions of the critical thickness via equations (6.4) and (6.5) is only limited to polymeric systems where the critical thickness is clearly associated with a change in deformation mechanism. For the epoxide systems discussed in chapter 4⁸, only the energy based model for the critical thickness can be used.

Apparently, the low value of the interlayer adhesion can clearly be noticed with respect to the stress transfer mechanism. However, for the change in deformation mechanism upon decreasing the PS-PPE layer thickness the low level of interlayer adhesion seems to have no profound influence since the critical matrix ligament thickness reported for the non-adhering core-shell rubber-modified 60-40 and 40-60 blends⁴ coincides with the critical PS-PPE layer thickness observed in this study.

6.4 Conclusions

The strain to break of PS-PPE/PE 100-0/75, 80-20/75 and 60-40/75 tapes can be increased significantly by a decrease of the PS-PPE layer thickness (d) to $d \approx 1 \mu\text{m}$. The origin of the increased strain to break of these tapes is explained by a stress transfer mechanism as revealed by optical light microscopy during tensile testing, i.e. PE locally inhibits crack growth after the PS-PPE layer breakage and allows for a multiple fracture of each single PS-PPE layer as a result of the (low) level of interlayer adhesion between PS-PPE and PE ($G_{1c} \approx 5 \text{ J m}^{-2}$). A further decrease of d results (only for the 60-40/75 tape, where the layer thickness can be decreased further without layer rupture) in a maximum strain to break at a layer thickness of $0.4 \mu\text{m}$, followed by a decrease of the strain to break, finally, to a value of 70% at a layer thickness of $0.04 \mu\text{m}$. The latter transition coincides with a change in deformation mechanism (optical light microscopy) and corresponds to the critical thickness as already reported in chapter 3⁴ for the non-adhering core-shell rubber-modified PS-PPE 60-40 blend.

For the PS-PPE/PE 60-40/50, 60-40/25 and 40-60/X tapes only one transition, induced by a change in layer thickness, could be detected that is correlated with a change in deformation mechanism. Again, this transition coincides with a change in

deformation mechanism from multiple cracking (preceded by crazing) to shear deformation as demonstrated for rubber-modified PS-PPE blends where the (local) thickness is controlled by the ligament thickness between the non-adhering rubbery particles. The critical thickness for transitions associated with a change in deformation mechanism is not only predicted satisfactory by the previously introduced energy based model ⁴ but can also be understood from the well established theory of Kramer for craze growth ^{1,2}.

The introduction of a diblock copolymer between the PS and PE layers enables a practical exploitation of the stress transfer mechanism: the stress transfer mechanism already becomes maximum operative at PS-PPE layer thicknesses of approximately 1 μm . This results in a (quasi) macroscopic strain to break of a PS/PE/BC 74/25/1 tape of 230%, i.e. the strain to break of pure PE, where the individual PS layers are fragmented many times along the length of the tape without initiating a fatal macroscopic failure.

6.5 References

- 1 Kramer, E.J. *Adv. Polym. Sci.* 1983, **52/53**, 1
- 2 Kramer, E.J. and Berger, L.L. *Adv. Polym. Sci.* 1990, **91/92**, 1
- 3 Van der Sanden, M.C.M., Meijer, H.E.H. and Lemstra, P.J. *Polymer* in press
- 4 Van der Sanden, M.C.M., Meijer, H.E.H. and Tervoort, T.A. *Polymer* in press
- 5 Wilson, G.M. and Khomami, B. *J. Non-Newt. Fluid Mech.* 1992, **45**, 355
- 6 Wilson, G.M. and Khomami, B. *J. Rheol.* 1993, **37**, 315
- 7 Wilson, G.M. and Khomami, B. *J. Rheol.* 1993, **37**, 341
- 8 Van der Sanden, M.C.M. and Meijer, H.E.H. *Polymer* submitted for publication
- 9 Van der Sanden, M.C.M. and Meijer, H.E.H. *Polymer* submitted for publication
- 10 Radford, J.A., Alfrey, T., Jr. and Schrenk, W.J. *Polym. Eng. Sci.* 1973, **13**, 216
- 11 U.S. Patent 3,711,176, 1973
- 12 Schrenk, W.J. and Alfrey, T., Jr. *Polym. Eng. Sci.* 1969, **9**, 393
- 13 Ma, M., Im, J., Hiltner, A. and Baer, E. *J. Appl. Polym. Sci.* 1990, **40**, 669
- 14 Ma, M., Vijayan, K., Hiltner, A. and Baer, E. *J. Mater. Sci.* 1990, **25**, 2039
- 15 Im J., Baer, E. and Hiltner A. in 'High Performance Polymers', (Eds. E. Baer and A. Moet), pp. 175-198, Hanser Publishers, Munich, 1991
- 16 Bazhenov, S.L., Sellitti, C., Hiltner, A. and Baer, E. *J. Appl. Polym. Sci.* in press
- 17 Meijer, H.E.H. and Janssen, J.M.H. in 'Mixing and Compounding-Theory and Practice', (Vol. Eds. I. Manas-Zloczower and Z. Tadmor), Progress in Polymer Processing Series, Carl Hanser Verlag, Munich, in press
- 18 Nielsen, L.E. and Buchdahl, R. *J. Appl. Phys.* 1950, **21**, 488
- 19 Beardmore, P. and Rabinowitz, S. *J. Mater. Sci.* 1975, **10**, 1763
- 20 Bazhenov, S.L., Sellitti, C., Hiltner, A. and Baer, E. *J. Appl. Polym. Sci.* in press
- 21 Kinloch, A.J. and Young, R.J. 'Fracture Behaviour of Polymers', Elsevier Applied Science, London, 1985
- 22 Bucknall, C.B. 'Toughened Plastics', Applied Science, London, 1977
- 23 Rosen, B.W. *J. ALAA* 1964, **2**, 1985
- 24 Broutman, L.J. and Krock, R.H. 'Modern Composite Materials', Addison-Wesley, Reading, MA, 1967, Chap. 1
- 25 Brown, H.R., Deline, V.R. and Green, P.F. *Nature* 1989, **341**, 221
- 26 Brown, H.R. *Macromolecules* 1989, **22**, 2859
- 27 Kambour, R.P. *Polym. Commun.* 1983, **24**, 292
- 28 Miller, P. and Kramer, E.J. *J. Mater. Sci.* 1991, **26**, 1459
- 29 Kramer, E.J., private communications

Appendix 6.A

6.A.1 The derivation of the critical thickness in films from craze growth analysis according to Kramer (private communications)

The following expression for the fastest growing fibril spacing (D_o^*), that dominates at any tensile stress, S , and maximizes the pressure gradient ($\Delta\sigma$), can be derived from an updated version of the original model of E.J. Kramer^{1,2}:

$$D_o^* = \frac{8\Gamma}{\beta S(1 - \lambda_{max}^{-1/2})} \quad (6.A1)$$

where Γ is the surface energy of the polymeric material, β a constant of the order one (see equation (11) of reference 2), S the average tensile stress on the craze interface and λ_{max} the natural draw ratio of the polymer (compare with equation (13) of reference 2 where it was assumed that $r \approx D_o/2$ and the factor $1/(1 - \lambda_{max}^{-1/2})$ was ignored).

If we assume that it takes about one active zone thickness (h) to build up the hydrostatic tension necessary to stabilize the small radius of curvature on the outsides of the fibrils and that the minimum thickness (L_{min}) into which the fibril structure fits contains two fibrils, L_{min} can be expressed in D_o and h :

$$L_{min} = 2(D_o + h) \quad (6.A2)$$

Combination of equations (6.A1) and (6.A2) finally results in:

$$L_{min} = \frac{16\Gamma}{\beta S(1 - \lambda_{max}^{-1/2})} + 2h \quad (6.A3)$$

which can be rewritten to equation (6.4) if we take β to be 1 and assume the tensile stress S to be equal to the lower yield stress (σ_y) of the polymer.

A better estimation of L_{min} can be made if at the thickness transition not the craze fibril spacing is considered that grows the fastest, but the craze fibril spacing $D_{o,cr}$ that grows at a reduced rate (v), equal to the widening velocity of a shear deformation zone (v_{DZ}). For the craze widening velocity, v , we can write that it scales as (see equation (9) of reference 2):

$$v \sim \left(\frac{h \Delta\sigma}{\sigma_{fc}} \right)^n \quad (6.A4)$$

where σ_{fc} is a flow stress of the material in the active zone at a certain reference strain rate and n is an exponent (>1) which describes the stress dependence in the active zone.

The widening velocity of a shear deformation zone is assumed to possess the same power law:

$$v_{DZ} \sim (S/\sigma_y)^n \quad (6.A5)$$

where S is the average stress on the bulk/deformation zone interface and σ_y is the yield stress at the same reference strain rate as above. Assuming that the two exponents n are equal the transition occurs if $v = v_{DZ}$:

$$\Delta\sigma = \frac{\sigma_{fc} S}{\sigma_y h} \quad (6.A6)$$

At the transition we assume that $S \approx \sigma_y$, which with equations (6.A2) and (6.10), (6.11) and (6.12) (where $r \approx D_o/2$ is replaced by $r \approx D_o/(2*(1 - \lambda_{max}^{-1/2}))$) analogous to the additional factor introduced in equation (6.A1) of reference 2, leads to the following quadratic equation:

$$\left(\frac{L_{min}}{2h} - 1\right)^2 - B\left(\frac{L_{min}}{2h} - 1\right) + C = 0 \quad (6.A7)$$

where B and C are the following dimensionless parameters:

$$B = \frac{2\beta\sigma_y}{\sigma_{fc}} \quad (6.A8)$$

and

$$C = \frac{8\Gamma}{\sigma_{fc} h (1 - \lambda_{max}^{-1/2})} \quad (6.A9)$$

The smallest solution of equation (6.A7) corresponds to the material thickness ($L_{min, tr}$) smaller than the one that contains two craze fibrils and grows the fastest (equation (6.A3)). If it is assumed that $\sigma_{fc} \approx \sigma_y$ this solution can be written as:

$$L_{min, tr} = 4h - h \sqrt{4 - \frac{32\Gamma}{\sigma_y h (1 - \lambda_{max}^{-1/2})}} \quad (6.A10)$$

which is equation (6.5).

Chapter 7*

Critical Thickness of Diluted Entanglement Networks

7.1 Introduction

The phenomenon of a critical thickness (ID_c), below which brittle amorphous glassy polymers become ductile, has been extensively discussed in previous chapters 2, 3 and 5 for thermoplastic⁸⁻¹⁰, and chapter 4 for thermosetting¹¹ polymers, respectively. Below ID_c a maximum macroscopic strain to break can be observed comparable with the theoretical strain to break of stretching the molecular (entanglement and/or crosslink) network to its full extension ($\sim \lambda_{max}$). Via an energy based criterion⁹ the absolute value of ID_c could be predicted and expressed in terms of entanglement density (v_e) and natural draw ratio (λ_{max}):

$$ID_c = \frac{6(\gamma + k_1 v_e^{1/2}) E_1}{\lambda_{max} \sigma_y^2} \quad (7.1)$$

where γ is the Van der Waals surface energy, k_1 a constant ($k_1 = 7.13 \times 10^{-15}$ J chain^{-1/2} m^{-1/2}, ref. 9), E_1 the Young's modulus and σ_y the true yield stress.

In chapter 3⁹, equation (7.1) is simplified by introducing the most elementary form of the network density dependency of the maximum network draw ratio: $\lambda_{max} = k_2 v_e^{-1/2}$, where k_2 is a constant. A somewhat more detailed analysis of this dependency reveals that²:

$$\lambda_{max} = \frac{l_e}{d} \quad (7.2)$$

where l_e is the chain contour length and d is the entanglement mesh size while both l_e

* This chapter is reproduced, in part, from:

1. Van der Sanden, M.C.M. and Meijer, H.E.H. *Polymer*, submitted for publication

and d can be expressed in terms of entanglement density ²:

$$l_e = \frac{\rho N_A}{M_0 \nu_e} l_0 \quad (7.3)$$

$$d = k_3 \left(\frac{\rho N_A}{\nu_e} \right)^{1/2} \quad (7.4)$$

where ρ is the density, N_A Avogadro's number, l_0 the length of a fully extended chain unit of molecular weight M_0 and k_3 a constant which is polymer dependent ². Since equations (7.3) and (7.4) contain constants that are polymer dependent (l_0 , M_0 and k_3), a given value of ν_e as measured via the plateau modulus in the melt ⁹ does not automatically correspond with a unique value of λ_{\max} .

In this study, the validity of equation (7.1) will be experimentally verified using physical entanglement networks based on different types of polystyrene (PS) and poly(2,6-dimethyl-1,4-phenylene ether (PPE). PS and PPE form a homogeneously miscible system, where PPE possesses a relatively high network density, $\nu_e = 13.2 \times 10^{25}$ chains m^{-3} , and PS a relatively low value of ν_e : 3.2×10^{25} chains m^{-3} . At the same value of ν_e , networks will be compared that consist of PPE and PS_l (where PS_l can not participate in the network structure due to the fact that the molecular weight falls well below the entanglement molecular weight) with networks that are based PPE and PS_h where PS_h can be part of the entanglement network structure. The previously introduced core-shell rubber (non-adhering to the PS-PPE matrix) is applied in order to set the local average ligament thickness ⁸.

7.2 Experimental

7.2.1 Materials

The materials used were poly(2,6-dimethyl-1,4-phenylene ether) (PPE; polymerized as described in ref. 12 using toluene as a solvent), high molecular weight polydisperse polystyrene (PS_h ; DOW), low molecular weight polystyrene (PS_l ; radically polymerized) and the core-shell rubber (poly(methyl methacrylate) shell, styrene-butadiene core, Rohm and Haas Co., Paraloid EXL 3647) that was used throughout this series. The weight-average molar mass of PPE was verified with g.p.c. (CHCl_3): $M_w = 120 \text{ kg mol}^{-1}$ and the glass transition temperature was checked with d.s.c.: $T_g = 220^\circ\text{C}$, I.V.: 0.86 dl g^{-1} (CHCl_3 , 25°C). PS_h was an experimental type containing no additives with a $T_g = 100^\circ\text{C}$ (d.s.c.) and a $M_w = 200 \text{ kg mol}^{-1}$ (g.p.c.: CHCl_3). The low molecular weight PS_l was prepared according to the

method described by Rempp and Merrill (80°C) and subsequently characterized by g.p.c.: $M_w = 3.5$ kg mol⁻¹ (well below the entanglement molecular weight of both PS_h, 19.1 kg mol⁻¹, ref. 5 and 9, and PPE, 4.5 kg mol⁻¹, ref. 5 and 9) and d.s.c.: $T_g = 80^\circ\text{C}$.

7.2.2 Sample preparation

Two series of PS_i-PPE and PS_i-PPE blends containing different amounts of core-shell rubbers (0 - 60 wt%) were prepared by casting mixtures of the three polymeric components dissolved in chloroform (10 wt% solutions). Subsequently, the films (with a final average thickness of 0.3 mm) were dried under vacuum conditions at a temperature of 100°C during 48 hrs. Small dumb-bell shaped tensile specimens were machined from the films according to ASTM D 1708.

7.2.3 Scanning Electron Microscopy

Scanning Electron Microscopy (SEM; Cambridge Stereo Scan 200) was applied in order to check the rubber particle distribution in the prepared PS-PPE blends. Specimens were prepared by fracturing the samples at liquid-nitrogen temperature. Subsequently, the samples were coated with a conducting gold layer.

7.2.4 Mechanical testing

Slow-speed tensile testing was performed on a Frank tensile machine (type 81565) at a cross-head speed of 5 mm min⁻¹ at room temperature. All measurements were carried out in five-fold.

7.3 Results and Discussion

7.3.1 Network density and natural draw ratio

In order to compare rubber-modified blends based on PS_h-PPE with blends having a PS_i-PPE matrix at the same entanglement density, the correlation between network density and concentration PPE must be determined for both dilution methods. The experimental determination of the network density of blends based on PS_h and PPE has already been described in chapter 3⁹. Prest and Porter¹³ have derived an empirical relationship between the weight fraction PPE (χ) in the PS_h-PPE blend and the network density of the miscible blend:

$$v_e(\chi) = v_{e(\text{PS})} (1 + 3.2\chi) \quad (7.5)$$

where $v_{e(\text{PS})}$ is the network density of PS_h: 3.2×10^{25} chains m⁻³ (ref. 9). This correlation is illustrated in *figure 7.1* (full curve).

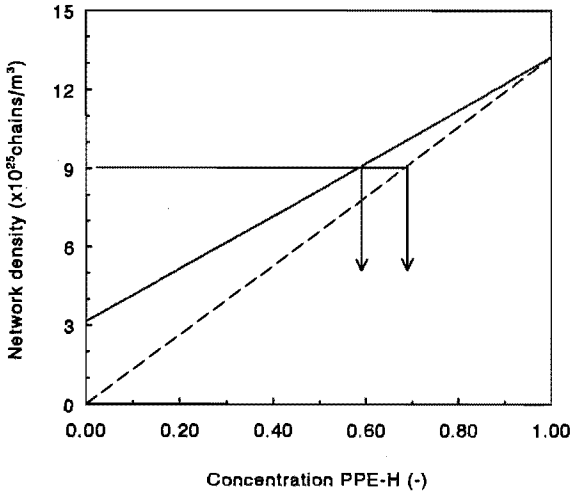


Figure 7.1 Network density versus concentration PPE for PS_h -PPE and PS_f -PPE blends. For details, see text

If the entanglement network of PPE is diluted by the addition of low molecular weight PS, the latter component can not participate in the entanglement network since the molecular weight is lower than the M_e of neat PPE (4.5 kg mol^{-1}). Hence, the entanglement density of the blend can simply be described as:

$$v_e(\chi) = \chi v_{e(\chi=1)} \quad (7.6)$$

where $v_{e(\chi=1)}$ is the network density of neat PPE: $13.2 \times 10^{25} \text{ chains m}^{-3}$. The value of v_e as a function of the concentration PPE ($=\chi$) is shown in figure 7.1 for the PS_f -PPE blend (broken curve).

As already demonstrated by Donald and Kramer ⁵, the value of the natural draw ratio of a PS-PPE blend does not only depend on the network density of the system but also on the 'dilution method'. Therefore, it is interesting to compare the values of λ_{\max} of the PS_h -PPE system with the values of λ_{\max} of PS_f -PPE blends as a function of the concentration PPE (i.e. χ). For both types of blends values of $\lambda_{\max}(\chi)$ can be obtained from data reported by Donald and Kramer ⁵ using equations (7.2), (7.3) and (7.4) where the corresponding values of v_e can be obtained from equations (7.5) and (7.6). In figure 7.2 the $\lambda_{\max}(\chi)$ values extracted from these literature data are shown for both types of blends: the full curve corresponds to the PS_h -PPE blends, the broken curve represents the v_e -dependency of the natural draw ratio for the PS_f -PPE system.

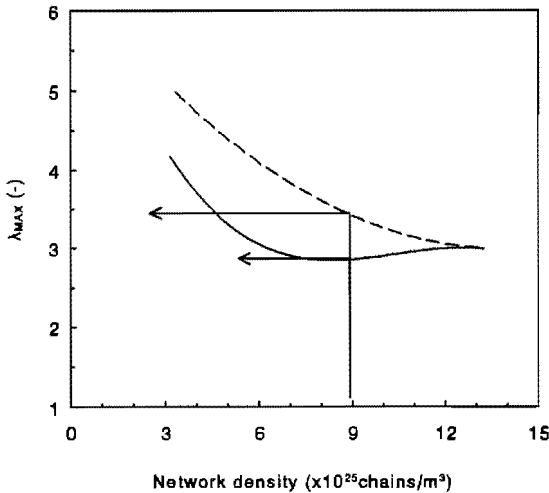


Figure 7.2 Natural draw ratio versus network density for PS_h -PPE and PS_f -PPE blends. For details, see text

For two different blends possessing the same network density (9×10^{25} chains m^{-3} , chosen arbitrary but within the realisable range) but with a different value of λ_{max} the critical thickness is determined and verified with equation (7.1). The blend compositions corresponding to this network density of 9×10^{25} chains m^{-3} can be determined from figure 7.1 and result in: PS_h -PPE: 40-60 and PS_f -PPE: 30-70. The corresponding values of λ_{max} are: 2.9 and 3.5, respectively, see figure 7.2.

Before mechanical analysis the homogeneity of the spatial rubber particle distribution for both types of core-shell rubber-modified PS-PPE blends is verified, see figure 7.3. For both dilution methods the rubber particle distribution proves to be rather homogeneous, independent of the rubber concentration.

7.3.2 Slow-speed tensile testing

The critical thickness of PS-PPE blends is indicated by a sudden increase in strain to break on a macroscopic scale for slow-speed uniaxial tensile testing (see ref. 8). In figure 7.4 the macroscopic strain to break of the two blends is demonstrated as a function of the rubber concentration.

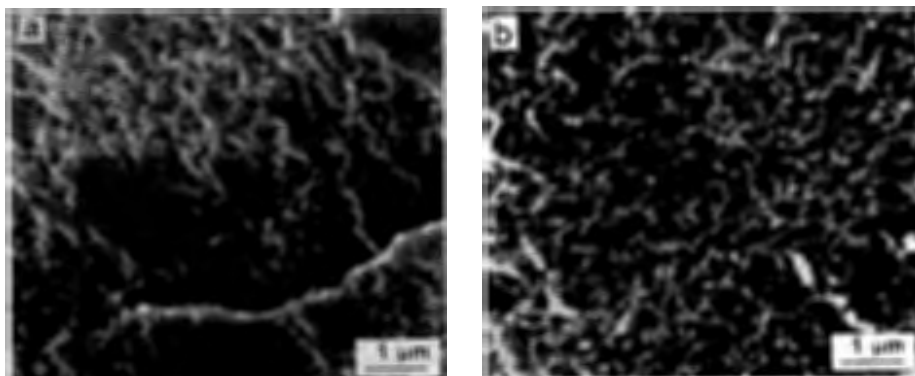


Figure 7.3 SEM micrographs of (a): a 40 wt% core-shell rubber-modified PS_n -PPE 40-60 blend; and (b): a 60 wt% core-shell rubber-modified PS_r -PPE 30-70 blend

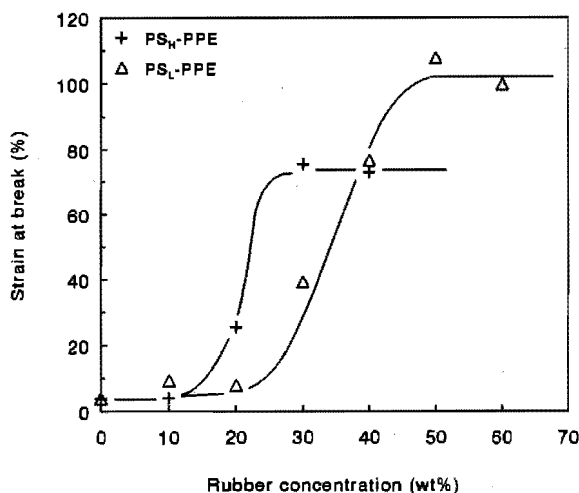


Figure 7.4 Strain to break of core-shell rubber-modified PS_n -PPE 40-60 and PS_r -PPE 30-70 blends

For the PS_n -PPE 40-60 blend a sudden increase in strain to break is observed at a rubber concentration of 20 wt% (see figure 7.4). Assuming a body-centred-cubic lattice⁸ for the spatial rubber particle distribution the critical average surface-to-surface interparticle distance (ID_c) can be calculated from the critical rubber concentration (20 wt%) and average rubber particle size (i.e. $0.2 \mu\text{m}$) and equals $0.15 \mu\text{m}$. As expected, this value agrees well with the value of ID_c already reported in

chapter 3⁹ for the extruded PS-PPE 40-60 blend: $ID_c = 0.18 \mu\text{m}$. However, for the PPE network diluted by the addition of low molecular weight PS the brittle-to-ductile transition occurs at a significantly higher rubber concentration (35 wt%), i.e. a lower value of ID_c ($0.09 \mu\text{m}$). In *table 7.1* the values ID_c as predicted by the energy based model (equation (7.1)), using $\gamma = 40 \text{ mJ m}^{-2}$ (ref. 2) and assuming a constant yield stress of 70 MPa and a Young's modulus of 3 GPa) are listed for both PS_h-PPE 40-60 and PS_l-PPE 30-70 blends and compared with the experimentally determined values.

Table 7.1 Predicted and experimental values of ID_c and the macroscopic draw ratio for PS-PPE blends ($v_e = 9 \times 10^{25} \text{ chains m}^{-3}$)

Blend composition	ID_c (model) (μm)	ID_c (exp.) (μm)	$0.6 \lambda_{\text{max}}$ (-)	λ_{macr} (-)
PS _h -PPE: 40-60	0.14	0.15	1.74	1.75
PS _l -PPE: 30-70	0.11	0.09	2.1	2

Clearly, the model predictions show not only a qualitative but also a quantitative agreement with the experimentally determined values of ID_c .

The macroscopic strain to break in the ductile region (λ_{macr}), below the critical thickness, has been demonstrated to correlate with the natural draw ratio via: $\lambda_{\text{macr}} = 0.6 \lambda_{\text{max}}$ (ref. 8, 9 and 11). In *table 7.1* the values of λ_{macr} and of $0.6 \lambda_{\text{max}}$ are listed. These data clearly confirm the previously found relationship between the macroscopic maximum draw ratio and the molecular network structure.

7.4 Conclusions

Two different dilution methods of a high molecular weight PPE entanglement network are compared. The critical thicknesses (below which polymers become macroscopically tough) of PS_h-PPE 40-60 and PS_l-PPE 30-70 blends, with a constant network density of $9 \times 10^{25} \text{ chains m}^{-3}$ but with different values of the natural draw ratio (2.9 and 3.5, respectively), have been experimentally determined to be $0.15 \mu\text{m}$ and $0.09 \mu\text{m}$, respectively. The energy based criterion for the explanation of the

phenomenon of the critical thickness as introduced in chapter 3⁹ results in a satisfying quantitative agreement with the experimentally determined values of ID_c . The values of the maximum macroscopic strain correspond to the maximum network strain in a similar way as found for all polymer systems previously studied within this thesis: $\lambda_{\text{macr}} / \lambda_{\text{max}} = 0.6$.

7.5 References

- 1 Kramer, E.J. *Adv. Polym. Sci.* 1983, **52/53**, 1
- 2 Kramer, E.J. and Berger, L.L. *Adv. Polym. Sci.* 1990, **91/92**, 1
- 3 Henke, C. and Kramer, E.J. *J. Polym. Sci., Polym. Phys. Edn.* 1984, **22**, 721
- 4 Donald, A.M. and Kramer, E.J. *J. Polym. Sci., Polym. Phys. Edn.* 1982, **20**, 899
- 5 Donald, A.M. and Kramer, E.J. *Polymer* 1982, **23**, 461
- 6 Donald, A.M. and Kramer, E.J. *Polymer* 1982, **23**, 1183
- 7 Glad, M.D. and Kramer, E.J. *J. Mater. Sci.* 1991, **26**, 2273
- 8 Van der Sanden, M.C.M., Meijer, H.E.H. and Lemstra, P.J. *Polymer*, 1993, **34**, 2148
- 9 Van der Sanden, M.C.M., Meijer, H.E.H. and Tervoort, T.A. *Polymer*, 1993, **34**, 2961
- 10 Van der Sanden, M.C.M. and Meijer, H.E.H. *Polymer*, submitted for publication
- 11 Van der Sanden, M.C.M. and Meijer, H.E.H. *Polymer*, in press
- 12 Rempp, P. and Merrill, E.W. 'Polymer Synthesis', Huethig & Wepf Verlag, Basel, 1986
- 13 Prest, W.M. and Porter, R.S. *J. Polym. Sci. (A-2)* 1972, **10**, 1639

Chapter 8*

Influence of Dispersed Rubbery Phase

8.1 Introduction

In the previous chapters¹⁻⁶ the ultimate toughness of amorphous glassy polymers has been discussed extensively in terms of a network density. Below a critical thickness of the polymeric material (ID_c), the maximum degree of ductility (as dictated by the network structure) can be obtained on a macroscopic scale. The local thickness of the polymeric material was controlled by the use of thin films separated by sheets of a non-adhering (ductile) polymeric spacer or via the use of a non-adhering core-shell rubber (i.e. 'holes'). However, in practice often a compatibilized system (that automatically results in a significant degree of adhesion between the rubbery particles and the matrix) is applied in order to obtain a fine dispersion of the rubbery phase (via a lowering of the interfacial tension)⁷⁻⁹. Small particles (size d) result in a more efficient decrease of the average distance between the particles (ID) at a dispersed phase volume fraction (Φ_r), since:

$$ID = d \left\{ \left(\frac{k \pi}{6 \Phi_r} \right)^{\frac{1}{3}} - 1 \right\} \quad (8.1)$$

where k is a constant depending on the spatial rubber particle distribution (e.g. $k = 2$ for a body-centred cubic lattice) and the rubber particle size distribution.

The energy based model, introduced in chapter 3¹ and extended in chapter 5³, describing the phenomenon of a critical thickness was derived for non-adhering rubbery particles yielding a 'holey' system. If the rubbery particles were firmly

* This chapter is reproduced, in part, from:

1. Van der Sanden, M.C.M., De Kok, J.M.M. and Meijer, H.E.H. *Polymer*, submitted for publication

attached to the matrix, a pronounced influence was found experimentally⁵: PS filled with 60 vol% of non-adhering rubbery particles (poly(methyl methacrylate) shell) revealed a ductile deformation behaviour with a macroscopic strain at break of 200%, while upon replacing the non-adhering particles by 60 vol% adhering particles (polystyrene shell) a brittle fracture with a strain at break < 5% was found. No explanations were sought up to now in the previous chapters, e.g. using the above mentioned simple model. However, the energy available for a local brittle catastrophic fracture will certainly be influenced by the presence of an interaction between the rubbery phase and the matrix. In literature several studies have been reported on the influence of the mechanical properties of the elastomeric filler on the occurrence and/or shift of brittle-to-ductile transitions¹⁰⁻¹⁷. However, in most of these studies more than one parameter was changed at the same time resulting in less unambiguous conclusions.

This study aims at providing a better understanding of the influence of the properties of the dispersed rubbery phase on the critical thickness. Polycarbonate (PC) was chosen as a model matrix, filled with non-adhering core-shell rubbers as a reference while furthermore spherical Ethylene-Propylene-Diene Monomer (EPDM) rubber particles were used. The EPDM rubber contains a low amount of maleic anhydride groups providing a certain degree of adhesion with the PC matrix. The mechanical properties of the dispersed rubbery phase can be controlled independently by the use of Electron Beam (EB) irradiation after manufacturing the specimens. EB irradiation strongly induces crosslinking of the EPDM phase¹⁸ while the PC matrix remains virtually unaffected (at least up to irradiation doses not exceeding 400 kGy). Slow-speed uniaxial tensile testing combined with tensile dilatometry and notched high-speed impact testing are used to reveal the influence of the mechanical properties of the EPDM phase on the critical thickness of polycarbonate. Finally, the influence of adhesion between the elastomer and the matrix on the value of the critical thickness will be discussed in terms of the energy based model.

8.2 Experimental

8.2.1 Materials

The materials used were polycarbonate (PC; General Electric Co., Lexan 141), Ethylene-Propylene-Diene Monomer rubber (EPDM; Exxon, Exxclor VA 1801) and a core-shell rubber (CS) with a styrene-butadiene core and a poly(methyl methacrylate) (PMMA) shell and a constant average particle size of

0.2 μm (Rohm and Haas Co.; Paraloid EXL 3647; d.s.c., $T_g = -78^\circ\text{C}$). The polycarbonate was a general-purpose grade: d.s.c., $T_g = 150^\circ\text{C}$; g.p.c. (THF), $M_n = 18.5 \text{ kg mol}^{-1}$ and $M_w = 45.5 \text{ kg mol}^{-1}$. The EPDM rubber contains 50-60 wt% ethylene, 50-40 wt% propylene and 0.2-2 wt% maleic anhydride (substituted at the diene monomer functionality).

8.2.2 Sample preparation

Before blending, the PC granules were dried at a temperature of 100°C during 36 hours under vacuum conditions. Blends of PC and EPDM rubber were prepared in a double-cycle extrusion process in compositions varying from 5, 10, 15 and 25 wt% EPDM on a 25 mm co-rotating twin-screw extruder (Werner and Pfleiderer ZSK 25) with a standard screw geometry at an average barrel temperature of 260°C . A master-batch of PC/EPDM 75/25 w/w was prepared in the first extrusion step and the desired PC/EPDM ratio was set in the second step by the addition of pure PC. Blends of PC and CS rubber were prepared using the same processing conditions in three different compositions (5, 10 and 15 wt% rubber) in a double-cycle extrusion process, where the CS rubber is already added in the first process step. Tensile specimens (DIN 53 455) were injection-moulded at a temperature of 260°C on a Stubbe SKM 75-80 injection moulding machine. Notched high-speed tensile samples were machined from injection-moulded plates (300°C , Arburg Allrounder 220-75-250; length x width x thickness: 60 x 12 x 3 mm) and subsequently V-shaped single-edge notched in the centre of the bar according to the Izod impact protocol (ASTM D256).

8.2.3 Microscopy

Scanning Electron Microscopy (SEM; Cambridge Stereoscan 200) was applied to investigate the morphology of the injection-moulded specimens. Specimens were cut at the centre of the injection-moulded tensile bars parallel to the direction of extrusion. Subsequently, the surface of the specimens was microtomed using a glass knife at liquid-nitrogen temperature. After microtoming, the sample was etched in an oxygen plasma to remove the rubbery phase and, subsequently, coated with a conducting gold layer.

8.2.4 Irradiation

Slow-speed tensile specimens and notched high-speed tensile specimens were irradiated to various doses: 0, 25, 50, 100 and 200 kGy. Irradiation was carried out with a 3 MeV 'van de Graaff' electron beam accelerator at the Interfaculty Reactor Institute (IRI, Delft), in air at room temperature. In order to investigate the influence of EB irradiation on the mechanical properties of the EPDM elastomer, governed by the crosslink density, also compression-moulded plates of EPDM rubber (thickness: 3 mm) were irradiated to the same doses and under the same circumstances as the tensile specimens. Shielding effects due to the presence of the PC matrix in the blends are neglected. Consequently it is assumed that the EPDM rubber in the blends will possess the same mechanical properties as the neat (irradiated) EPDM rubber.

8.2.5 Dynamic mechanical thermal analysis

Dynamic shear moduli of the irradiated EPDM rubber plates were measured in torsion using rectangular-shaped specimens (length x width x thickness: 60 x 10 x 3 mm) in the temperature range of -90°C up to +40°C. A Rheometrics RDS II spectrometer was used at a constant frequency of 10 rad s⁻¹ and a maximum strain of 0.5%.

8.2.6 Molar mass measurements

Gel permeation chromatography (g.p.c.) was used to determine the relative number-average molar mass (M_n) and the mass-average molar mass (M_w) of irradiated PC samples. G.p.c. was performed on a Waters apparatus consisting of a 510 pump, a wisp 712 injector and a differential refractometer. Three columns were used: 10⁵, 10⁴ and 10³ μ -Styragel (40°C), calibrated with monodisperse polystyrene standards using tetrahydrofuran (THF; 0.6 ml min⁻¹) as the eluent. Irradiated PC was dissolved in THF, filtered and injected in the columns.

8.2.7 Mechanical testing

Before mechanical testing tensile specimens were annealed at 100°C during 24 hours under vacuum conditions to remove any unwanted traces of water.

Slow-speed tensile testing was performed on a Frank tensile machine (type 81565) at a strain rate of 8x10⁻⁴ s⁻¹ at room temperature. All measurements were carried out in five-fold. Slow-speed tensile dilatometry as applied in this investigation, is described in chapter 2⁵.

Notched high-speed tensile testing has been performed on a Zwick Rel SB 3122 tensile machine equipped with a climate chamber in the temperature range of -75°C up to 50°C at a cross-head speed of 1 m s⁻¹ (free sample length: 20 mm). The tensile toughness (G_h) is defined as the integrated area under the recorded force-displacement curve of a high-speed fractured single-edge notched (razor-blade tapped) specimen divided by the original area behind the notch tip².

Finally, in order to visualize the influence of spatial particle (or: hole) distribution on the deformation behaviour of PC, thin PC films (thickness: 7 μ m) were used containing spatially random distributed pores of a diameter of 3 μ m (14 vol%) running, perpendicular to the surface of the film, through the film (Cyclopore[®]). The Cyclopore[®] films were strained using a Minimat (Polymer Laboratories; distance between clamps: 15 mm) mounted on an optical transmission microscope (Olympus BH2). Rectangular-shaped specimens were viewed in transmission perpendicular to the film surface at a test speed of 5 mm min⁻¹. During loading pictures were taken at distinct stages of the deformation using an Olympus C-35 AD-2 camera mounted on the microscope. Plastic deformation was visualized with a polarizing filter added to improve the colour contrast.

8.3 Results

The critical thickness of polycarbonate (ID_c) can be calculated using the expression that was introduced and verified in chapter 3¹ for physical networks and in chapter 4 for chemical networks², that was extended in chapter 5³ to include temperature and strain rate effects and, finally, was investigated in chapter 7⁴ for two different types of physical networks:

$$ID_c = \frac{6 (\gamma + k_1 v^{1/2}) E_1}{k_2 v^{-1/2} \sigma_y^2} \quad (8.2)$$

where γ is the Van der Waals surface energy, k_1 and k_2 are constants ($k_1 = 7.13 \times 10^{15}$ J chain^{-1/2} m^{-1/2} and $k_2 = 2.36 \times 10^{13}$ chains^{1/2} m^{-3/2} (ref. 19)), E_1 is the Young's modulus, v is the network density (entanglement and/or crosslink density) and σ_y is the yield stress. The strain rate and temperature dependence of ID_c can be predicted via the strain rate and temperature dependence of the yield stress using the well known Eyring theory of viscosity²⁰:

$$\dot{\epsilon} = A_E \exp \left\{ - \frac{(\Delta E^* - v^* |\sigma_y|)}{RT} \right\} \quad (8.3)$$

where $\dot{\epsilon}$ is the strain rate, A_E is a constant, ΔE^* the activation energy, v^* the activation volume, R the gas constant and T the absolute temperature. The temperature and strain rate dependence of the Young's modulus, E_1 is neglected in first approximation (which might be incorrect). (The temperature dependence of the Young's modulus can be estimated from a strict harmonic approximation of an elastic solid^{21,22}, resulting in roughly the same temperature dependence as found for the yield stress.) For polycarbonate all constants of equations (8.2) and (8.3) are known from literature: $v = 30 \times 10^{25}$ chains m⁻³ (ref. 23,24), $E_1 = 2300$ MPa, $\gamma = 40$ mJ m⁻² (ref. 19), $\ln(A_E) = 8.95 \times 10^{-5}$ (ref. 25), $\Delta E^* = 335$ kJ mol⁻¹ (ref. 25) and $v^* = 1.69 \times 10^3$ m³ mol⁻¹ (ref. 25). In *figure 8.1* the calculated critical thickness of polycarbonate is plotted as a function of temperature and strain rate (combination of equations (8.2) and (8.3)).

Increasing the temperature or decreasing the strain rate results in an increase of the critical thickness as already discussed for the polystyrene-poly(2,6-dimethyl-1,4-phenylene ether) model system in chapter 5³.

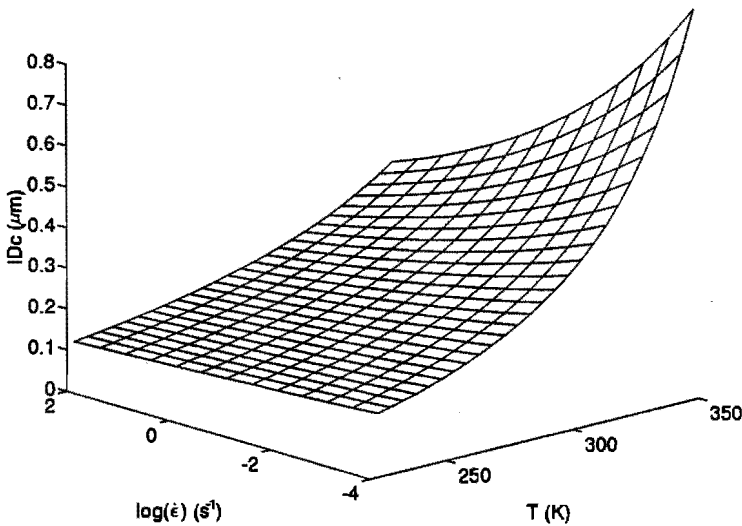


Figure 8.1 Model predictions of the critical ligament thickness of polycarbonate as a function of temperature and strain rate

However, if adhesion prevails a considerable influence of the mechanical properties of the elastomer on ID_c is to be expected because the matrix ligaments are separated by adhering rubbery particles that can transfer stress from the surroundings to the ligament under consideration. As a result, the stored elastic energy¹ can change due to (i) a change in matrix volume supplying the energy, (ii) a contribution of elastic energy stored in the rubbery particles and (iii) a change in strain energy density within the matrix ligament as a consequence of the altered stress state. Before investigating the influence of adhesion between the elastomer and the matrix, and/or the cavitation stress of the elastomer, on the critical thickness of polycarbonate, the uniaxial tensile testing results will be discussed briefly.

8.3.1 Slow-speed tensile testing

Slow-speed uniaxial tensile tests were performed on pure PC and EPDM rubber-modified polycarbonate blends. In *figure 8.2* some typical results are given, showing only the initial part of the curves of pure PC (100/0) and PC/EPDM 90/10.

As expected, since pure PC is a tough polymer under these relatively mild testing conditions (unnotched, strain rate: $8 \times 10^{-4} \text{ s}^{-1}$) and in accordance with the other results

of this test on the more dense networks (PS-PPE 20-80¹ and epoxides²), no ductile-to-brittle transitions (i.e. abrupt changes in the strain to break) can be detected.

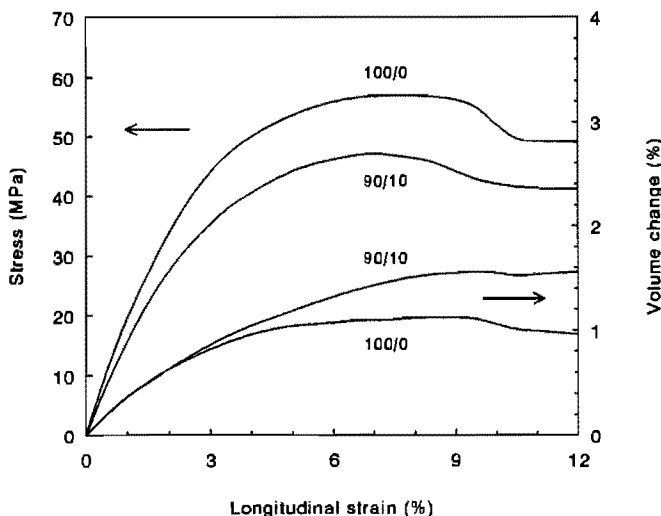


Figure 8.2 Initial stress-strain and volume-strain curves for PC/EPDM 100/0 and 90/10

Neat PC and PC/EPDM 90/10 both reveal a ductile deformation behaviour with a strain at break that equals 80% (not indicated in figure 8.2) which is again about 60% of the theoretical draw ratio (compare ref. 2,3,5).

The volume change as a function of strain reveals for neat PC a deformation mechanism that, after passing the elastic region, occurs at a constant volume. This can most certainly be ascribed to the shear deformation mechanism well known to be operative in polycarbonate¹³. Adding 10 wt% EPDM rubber to PC only results in a slight deviation of the $\Delta V/V_0$ curve above a strain level of 3% (see figure 8.2) probably due to the cavitation and/or detachment of the rubbery particles.

8.3.2 Notched, high-speed tensile testing

1) Unirradiated blends

The notched, high-speed tensile test results of PC/EPDM blends are displayed in figure 8.3a. For comparison also the notched tensile toughness data of the PC/CS

rubber blends are shown in *figure 8.3b*.

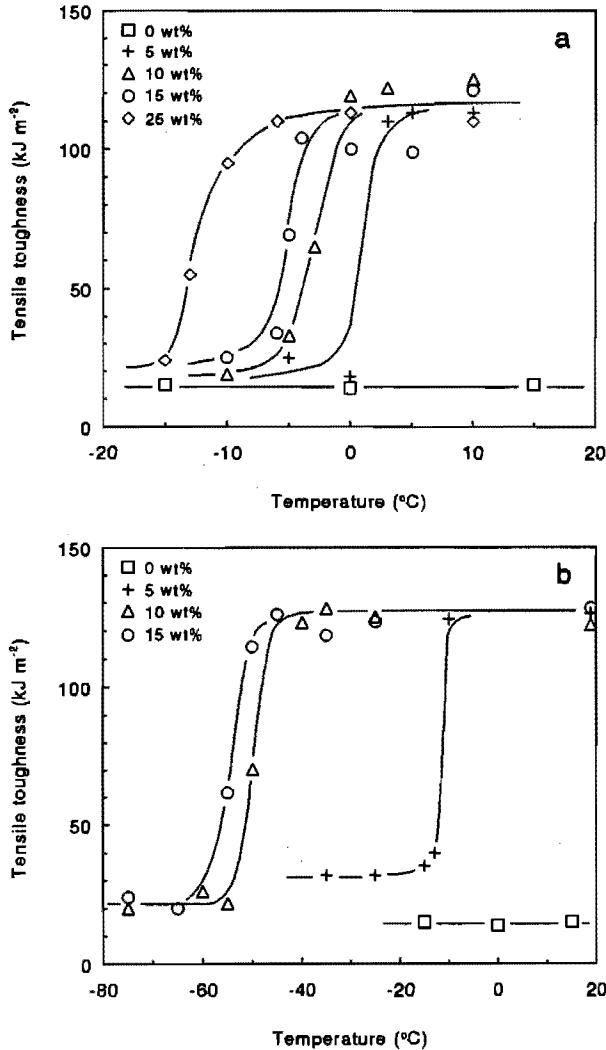


Figure 8.3 Notched tensile toughness (G_n) of neat and rubber-modified PC blends vs temperature, parameter: rubber content: (a) PC/EPDM; and (b) PC/CS

Neat PC reveals a brittle fracture over the entire temperature range investigated with a value of the notched tensile toughness (G_n) of approximately 10 kJ m^{-2} . In contrast with the slow-speed results, brittle-to-ductile transitions can clearly be observed under notched high-speed testing conditions for both types of PC/rubber blends. As can be inferred from *figures 8.3a* and *8.3b*, the level of ductility in both the brittle and the

tough region -if present- are roughly independent of the rubber concentration or type of rubber (adhering EPDM rubber or non-adhering CS rubber), while with an increasing rubber content the brittle-to-ductile transition temperature (T_{BT}) shifts to lower temperatures, from $+2^{\circ}\text{C}$ to -13°C for 5 wt% to 25 wt% EPDM rubber and from -16°C to -50°C for 5 wt% to 10 wt% core-shell rubber. Adding more than 10 wt% core-shell rubber does not result in a further significant lowering of the brittle-to-ductile transition temperature since the glass transition temperature of the core-shell rubbery particles is approached. Clearly, the holes from the core-shell rubbers are much more effective in impact modifying PC than the EPDM spheres added. This can be due to their smaller particle size (roughly two times smaller than the EPDM rubber particles, see *figure 8.4* and *table 8.1*) and to the absence of adhesion in the PC/Core-shell rubber system.

The values of the (critical) interparticle distance that correspond to the transitions observed in *figures 8.3a* and *8.3b* can be calculated from the rubber volume fraction and the average particle size (see equation (8.1)). In *figure 8.4* SEM micrographs are shown of microtomed surfaces of the four different PC/EPDM blends.

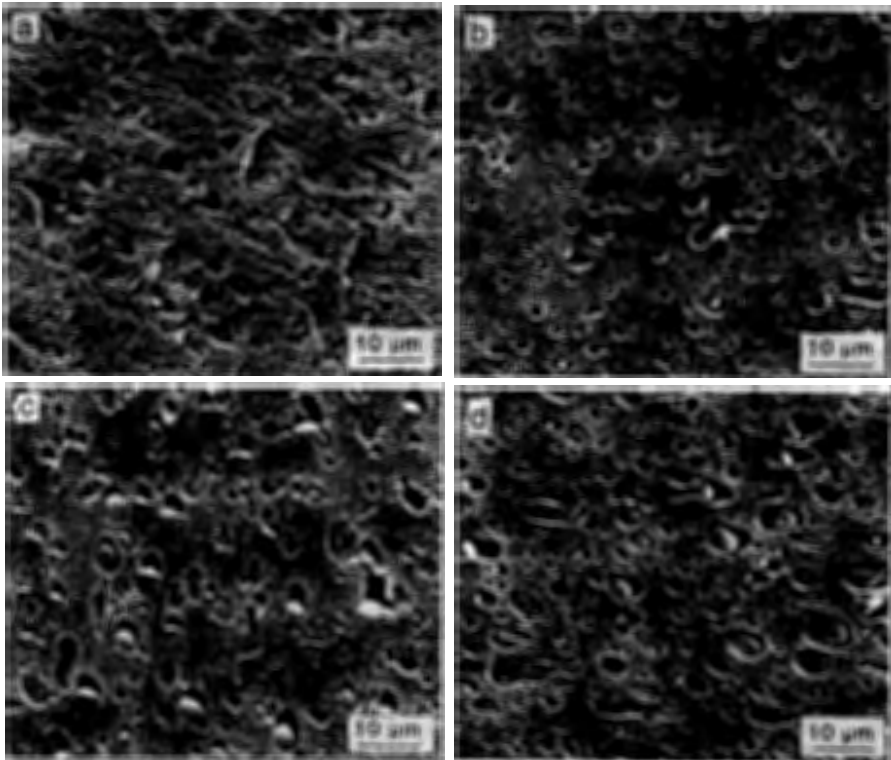


Figure 8.4 Morphology PC/EPDM blends: (a) 95/5; (b) 90/10; (c) 85/15; (d) 75/25

The average particle size is fairly constant over all compositions. This is probably due to the double-cycle extrusion process used that only dilutes the same 75/25 blend. Apparently, in this second step the average particle size hardly changes. The estimated weight-average particle sizes (d_w , obtained from SEM micrographs) of the various PC/CS and PC/EPDM blends are listed in *table 8.1* combined with the corresponding values of ID, calculated using equation (8.1).

Table 8.1 Weight-average particle size (d_w) and ID of the various PC/rubber blends

Blend composition (PC/rubber)	d_w (μm)	ID (μm)
PC/EPDM: 95/5	0.38	0.67
PC/EPDM: 90/10	0.36	0.43
PC/EPDM: 85/15	0.38	0.35
PC/EPDM: 75/25	0.42	0.26
PC/CS: 95/5	0.2	0.35
PC/CS: 90/10	0.2	0.24
PC/CS: 85/15	0.2	0.18

In *figure 8.5* the brittle-to-ductile transition temperature is plotted as a function of the value of the critical thickness of polycarbonate thus determined (i.e. a cross section of *figures 8.3a* and *8.3b*) and is compared with the predicted values according to the model: broken curve (i.e. a cross section at a strain rate of 10 s^{-1} in *figure 8.1*).

Compared to the PC/EPDM blends, the PC/CS blends have a larger critical ligament thickness at a constant temperature (e.g. $0.24 \mu\text{m}$ versus $0.35 \mu\text{m}$ at -10°C) or, alternatively, shift the T_{BT} to lower temperatures at a constant value of the interparticle distance (e.g. -10°C versus -50°C at $0.24 \mu\text{m}$). Hence, analogous to the PS results⁵, adhesion between the rubbery phase and the matrix influences the critical thickness of PC in a negative sense. Clearly, the model predictions strongly deviate from the experimentally determined values of ID_c , especially at higher temperatures (i.e. high values of ID_c). This can be ascribed to the fact that the validity of the simple model is restricted to values of ID_c comparable with or lower than the hole

diameter (see figure 7 of ref. 26). (For the basic model the stored elastic energy is assumed to be correlated with a spherical volume ($\sim(ID_c)^3$). This is a too naive assumption, especially if the distance between particles is higher than the particle size applied or if adhesion between matrix and dispersed phase is present.)

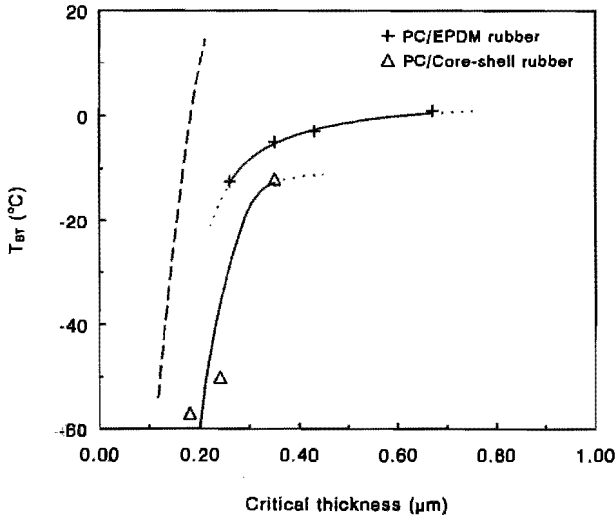


Figure 8.5 Brittle-to-tough transition temperature, T_{BT} , of PC/EPDM and PC/CS blends as a function of the critical ligament thickness. The broken curve is according to the model

2) Irradiated blends

To explore the influence of the mechanical properties of the elastomer on the brittle-to-ductile transition of polycarbonate in a controlled manner, electron beam irradiation of the PC/EPDM blends has been performed. EB irradiation induces crosslinks in the EPDM rubber, as reflected in the dynamic shear modulus of neat EPDM rubber, see figure 8.6.

EPDM rubber has a glass transition temperature of -40°C , above which a rubbery plateau is found (figure 8.6, curve A). Irradiation of EPDM rubber results in an increase in height of this plateau.

The plateau modulus (G_{No}) can be correlated with the average molecular weight

between crosslinks (M_c) using classical rubber elasticity theory ²⁷:

$$M_c = \frac{\rho RT}{G_{No}} \quad (8.4)$$

where ρ is the density, R the gas constant and T the reference temperature. Hence, an increasing value of G_{No} with increasing irradiation dose corresponds to a decreasing value of M_c .

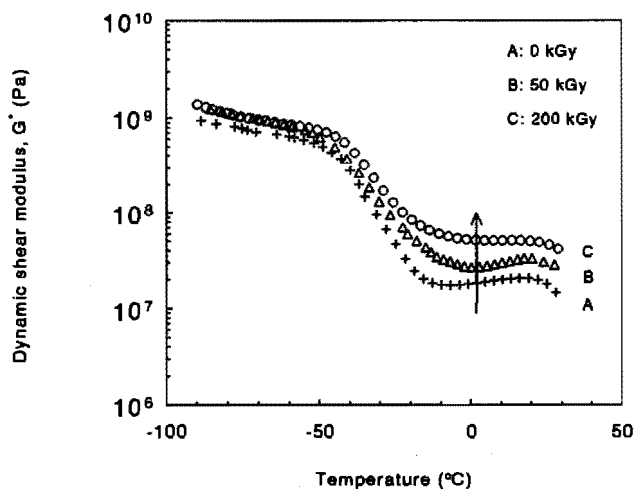


Figure 8.6 Dynamic shear modulus, G' , of irradiated EPDM rubber versus temperature for three different irradiation doses

According to Gent and Tompkins ²⁸ the Young's modulus (or: shear modulus) of a rubber is directly correlated with the cavitation stress. Thus EB irradiation results in an increasing cavitation stress of the rubber, which will certainly influence the brittle-to-ductile transition of the blend provided that the adhesion remains unchanged.

The influence of EB irradiation on neat polycarbonate has been verified via g.p.c. measurements, see *table 8.2*, and notched high-speed tensile toughness measurements, see *figure 8.7a*. Clearly, within the range of irradiation doses applied ($0 \leq \text{dose} \leq 200$ kGy) the molecular weight of PC and the value of the notched tensile toughness are hardly influenced by irradiation since the G_n value of all PC samples roughly equals 10 kJ m^{-2} .

Table 8.2 G.p.c. data of irradiated polycarbonate samples

Irradiation dose (kGy)	M_n (kg mol ⁻¹)	M_w (kg mol ⁻¹)
0	19	48
50	19	46
100	17	45
200	18	43

In figures 8.7b to 8.7e the notched high-speed tensile toughness of the irradiated PC/EPDM blends is demonstrated as a function of temperature for various irradiation doses. The unirradiated PC/EPDM 95/5 blend (figure 8.7b) reveals a brittle-to-ductile transition temperature, T_{BT} , of approximately 2°C, while irradiation results in a shift to higher values, finally, up to +13°C for an irradiation dose of 200 kGy. The value of G_h in both the brittle and the ductile region is independent of the irradiation dose applied, similar to the independency of the value of G_h in the brittle or tough region with a varying rubber concentration (compare with figures 8.3a and 8.3b).

The notched high-speed tensile data of the other PC/EPDM rubber blends all show roughly this same trend (compare figures 8.7b, 8.7c, 8.7d and 8.7e): irradiation results in a shift of T_{BT} to higher temperatures ($\Delta T_{BT} \approx 15^\circ\text{C}$) independent of the absolute value of T_{BT} and the rubber concentration present in the blend. Besides, the values of G_h in both the brittle and the ductile regions remain unaffected by the irradiation dose applied. To illustrate these effects, the values of T_{BT} are plotted versus the dynamic shear modulus, G^* , of the EPDM rubber-phase in figure 8.8a.

Clearly, T_{BT} increases with an increasing G^* and the slopes of the T_{BT} versus G^* curves are apparently independent of the rubber concentration. At a constant G^* , T_{BT} decreases with increasing rubber concentration (i.e. a decreasing ID, see figure 8.8b) similar to the conclusion arrived at during the discussion of figures 8.3a, 8.3b and 8.5.

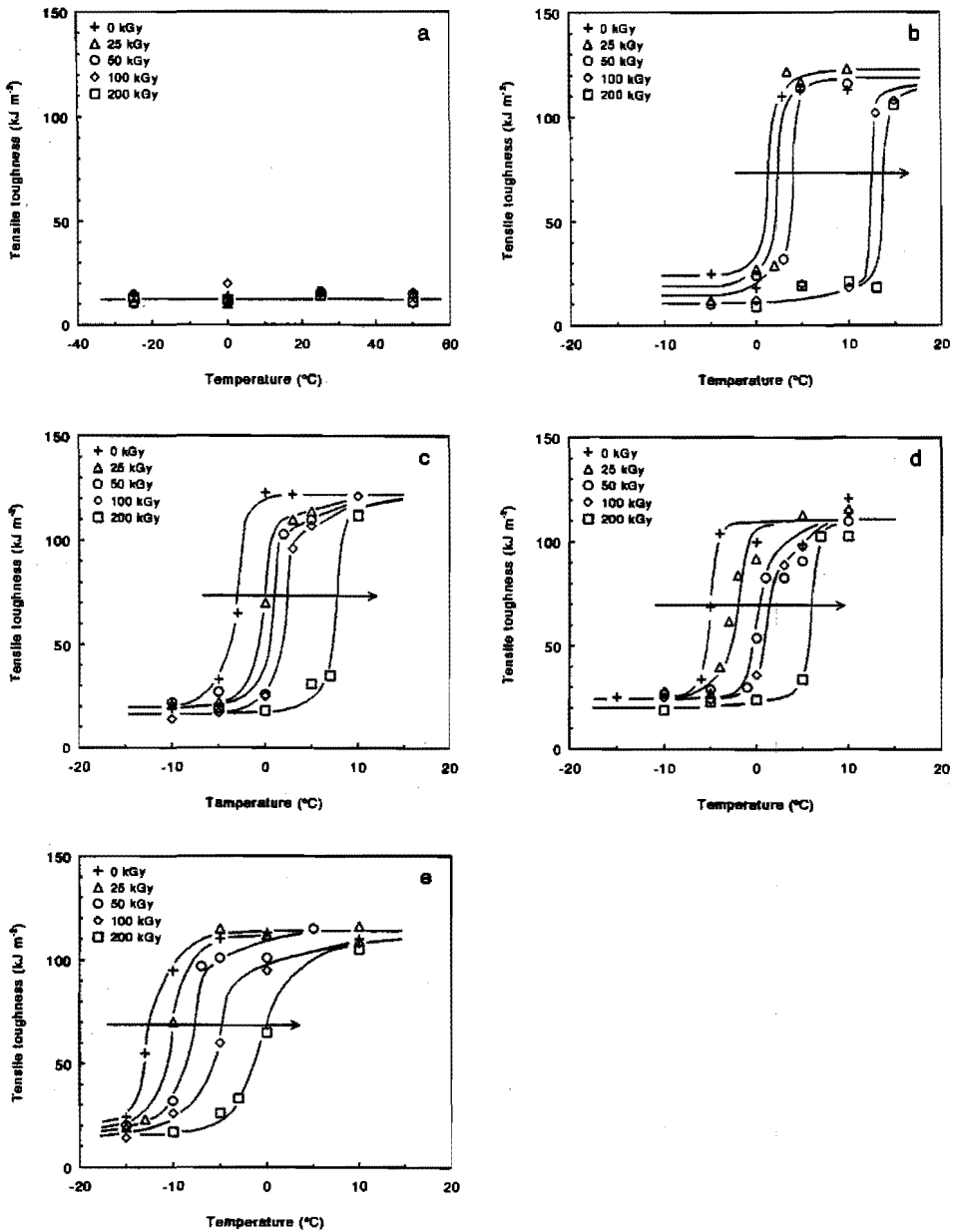


Figure 8.7 Notched tensile toughness of PC/EPDM blends versus temperature with parameter the irradiation dose: (a) 100/0; (b) 95/5; (c) 90/10; (d) 85/15; and (e) 75/25

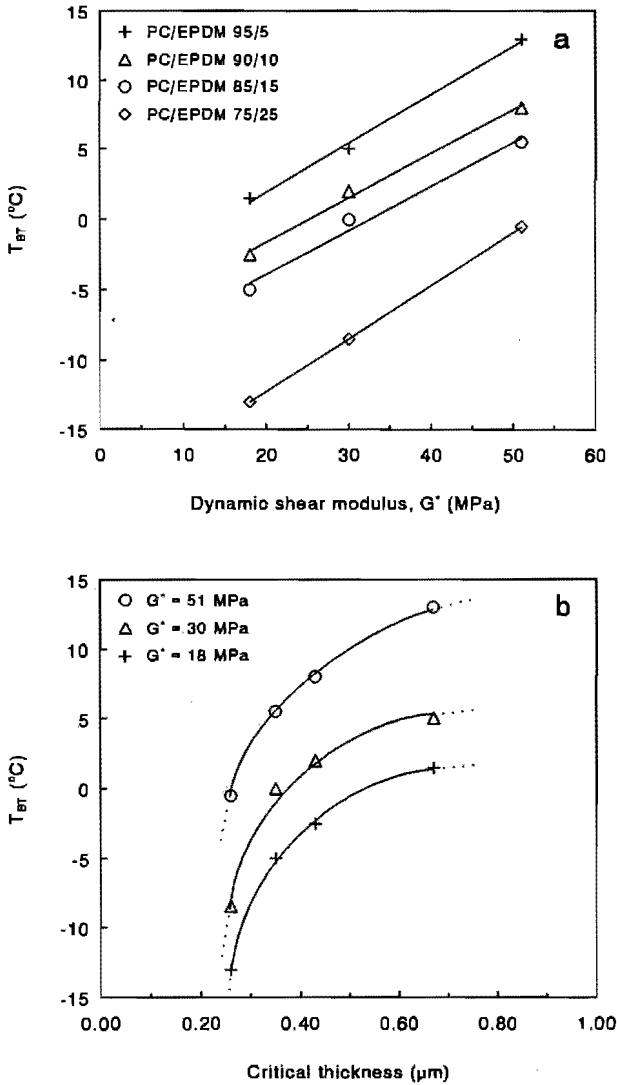


Figure 8.8 Brittle-to-tough transition temperature of PC/rubber blends versus (a) the dynamic shear modulus, G^* , of the EPDM rubber (parameter the EPDM rubber content); (b) the critical interparticle distance, ID_c (parameter: the dynamic shear modulus of the rubber); and (c) as (b) on a different scale

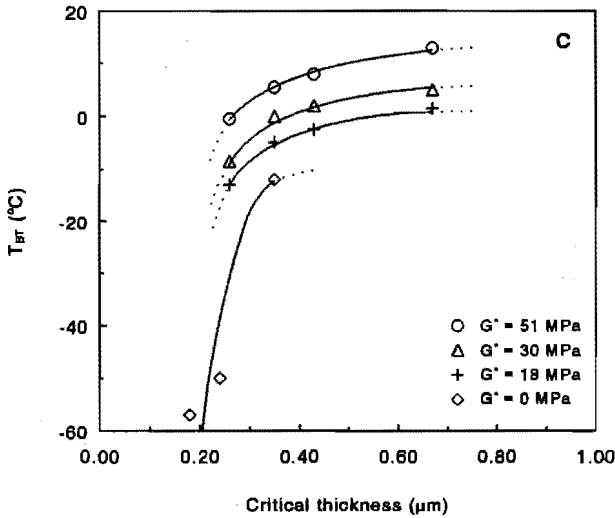


Figure 8.8 (Continued)

Figure 8.8c contains the same data as shown in figure 8.8b plotted on a different scale allowing for the incorporation of $T_{BT} - ID_c$ data for the PC/CS blends extracted from figure 8.5 ($G' = 0$ MPa). According to Morbitzer and Grigo²⁹, the high degree of ductility of PC is related to its low γ -relaxation temperature (-100°C). Hence, it would be interesting to check this hypothesis using PC filled with real holes (foam) generating an average ligament thickness corresponding to a T_{BT} below -100°C ($\leq 0.1 \mu\text{m}$; extrapolation of figure 8.8c).

8.4 Discussion

In this thesis attention has mainly be focused on the understanding of the *ultimate* toughness of polymeric materials. Most conclusive evidence resulted from influencing the microstructure of amorphous polymers -given their molecular network structure- by the addition of holes using non-adhering core-shell rubber of a well-defined small size ($0.2 \mu\text{m}$). From the PS/CS systems we already know how dramatic a small change of adhesion can be⁵, therefore this aspect has been chosen as the main issue here. Moreover, the PC/EPDM blends investigated are somewhat more directly related to practical blend systems that usually include adhesion between the two distinct phases. One of the reasons for this -ultimately undesired- adhesion is that small particles of a dispersed phase obviously only can be obtained during melt mixing if the two fluids are compatibilized by the addition of (block) copolymers or

by their in-situ formation³⁰. For the PC/EPDM blends the resulting particle size proved to be fairly constant and of the order of 0.4 μm .

Following Borggreve et al.¹⁰, who investigated the toughness of the polyamide-6/EPDM system thoroughly, results of different systems can be easily compared if particle size and volume fraction are combined and converted into the interparticle distance, using equation (8.1). Comparing *figures 8.3* and *8.5* it is clear that, after correcting for their particle size, pronounced differences between the holey, non-adhering, systems (PC/CS) and adhering systems (PC/EPDM) exist, in favour of the holes. This trend is in accordance with the early PS/CS results and is subsequently confirmed by the irradiation experiments where selectively the cavitation strength of the dispersed EPDM phase is influenced without changing the morphology of the blend investigated (see *figure 8.8*).

The question arises whether the simple universal (but, consequently, naive) model at least qualitatively can deal with these findings. As was clearly shown, the model predictions for the critical thickness of polycarbonate are considerably lower than the experimentally determined values already for the PC/CS system and did not show the pronounced temperature influence for the PC/EPDM system (see *figure 8.5*). Apart from these apparent defects, the introduction of adhesion and the subsequent increase of the cavitation stress systematically decreased the experimental critical thickness, see *figures 8.5* and *8.8*. It is assumed that rubber particle cavitation and/or detachment occur during or after the initiation of (localized) deformation. Since, if cavitation and/or detachment of the particles were to occur before initiation of (localized) deformation, the stress state at the onset of plastic deformation would not be influenced by the particle cavitation and/or particle/matrix detachment stress and, consequently, the stored elastic energy would be equal to the stored elastic energy of a ligament bordered by holes and, therefore, no influence of particle/matrix detachment and/or particle cavitation stress should be observed on the value of the critical matrix ligament thickness. As mentioned, adhesion influences the volume of stored elastic energy, adds the energy stored in the dispersed phase and, finally, influences the local stress state in the matrix ligament. Since only detailed micromechanical analyses can deal with the first two aspects (which is a topic of current research at our laboratory) here only the last aspect will be discussed qualitatively focusing on the experimental trends found. Replacing a hole by an adhering rubbery particle and, subsequently, increasing the cavitation and/or

detachment stress of the rubbery phase results in a more pronounced triaxial stress state in the matrix ligament. Hence the available stored elastic energy (U_{av}) will be directly influenced while the energy required to create a potential brittle fracture surface in the highly strained fibrils (U_{re}) is not changed. The strain energy density in the matrix (W_s) is given by ³¹:

$$W_s = \left(\frac{1}{2E_1}\right) [\sigma_1^2 + \sigma_2^2 + \sigma_3^2 - 2\nu_m(\sigma_1\sigma_2 + \sigma_1\sigma_3 + \sigma_2\sigma_3)] \quad (8.5)$$

where σ_1 , σ_2 and σ_3 are the three principle stresses and ν_m is the Poisson's ratio of the polymeric matrix ($\nu_m = 0.4$ for polycarbonate). For the uniaxial stress situation where the matrix ligaments are bordered by holes it was in first order assumed that the strain energy density in the volume concerned ($(\pi/6) \cdot (ID)^3$) is equal to the strain energy density at the equator of the hole at the matrix/hole interface:

$$W_{s, hole} = \frac{\sigma_y^2}{2E_1} \quad (8.6)$$

where σ_y is the uniaxial yield stress of the matrix. In the case of adhering rubbery particles (where it is assumed that cavitation and/or detachment occur after yielding of the matrix) it can be assumed that two of the three principle stresses are equal but not zero: $\sigma_2 = \sigma_3 = k \sigma_1$ and constant throughout the matrix volume supplying the stored elastic energy. In order to express the three principle stresses (σ_1 , σ_2 and σ_3) in terms of the uniaxial yield stress (σ_y), a Von Mises yield criterion ³¹ is taken:

$$\sigma_y = \sqrt{\frac{(\sigma_1 - \sigma_2)^2 + (\sigma_3 - \sigma_1)^2}{2}} \quad (8.7)$$

Hence, the value of W_s (equation (8.5)) can be expressed in the ratio of $\sigma_2/\sigma_1 = \sigma_3/\sigma_1 = k$ (with $0 \leq k \leq 1$) and normalized with the strain energy density of a matrix ligament bordered by holes, $W_{s, hole}$ ($k = 0$), see figure 8.9.

Clearly, the strain energy density strongly increases with an increasing degree of triaxiality, i.e. with an increasing cavitation stress (that is proportional to the shear modulus ²⁸) and/or particle/matrix interface detachment stress. Consequently, a lower value of the critical ligament thickness results.

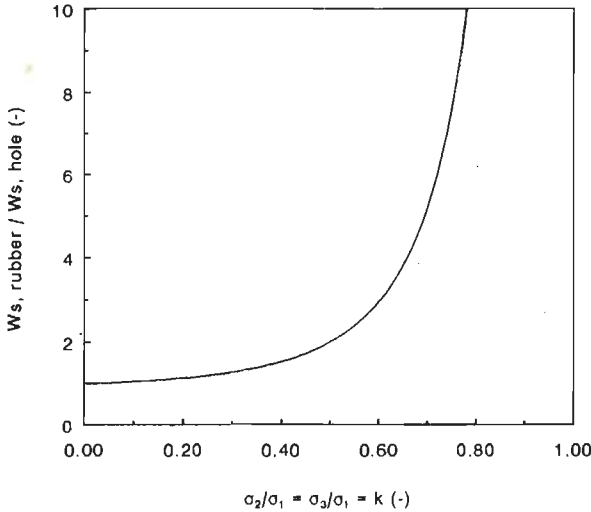


Figure 8.9 Normalized strain energy density of a matrix ligament bordered by adhering rubbery particles versus the degree of triaxiality, $\sigma_2 / \sigma_1 = \sigma_3 / \sigma_1 = k$

Combined with the increasing matrix volume supplying stored elastic energy and the (small) contribution of the elastic energy stored in the dispersed phase, that also both result in a lower value of the critical thickness, now, qualitatively the influence of the changing properties of the adhering dispersed elastomer on the brittle-to-ductile transition can be justified. However, in order to derive a more quantitative prediction of the strain energy density and, consequently, also the critical thickness, the local stress state within the matrix ligament should be clarified more completely. This will also result in a more funded estimation of the matrix volume that is supposed to supply the available stored elastic energy in dependence of both the level of interaction between the elastomer and the matrix and the properties of the elastomer. Eventually, these (so-called multi-level finite element, MLFE) calculations could result in predicted values of the notched tensile toughness in both the brittle and ductile region.

8.4.1 An illustrative example

The complexity of the problems to be solved using the necessary non-uniform stress and strain fields in these calculations are illustrated in *figure 8.10* where thin polycarbonate films containing pores running perpendicular to the film surface throughout the complete film, are viewed under an optical microscope during straining (direction of load: horizontal).

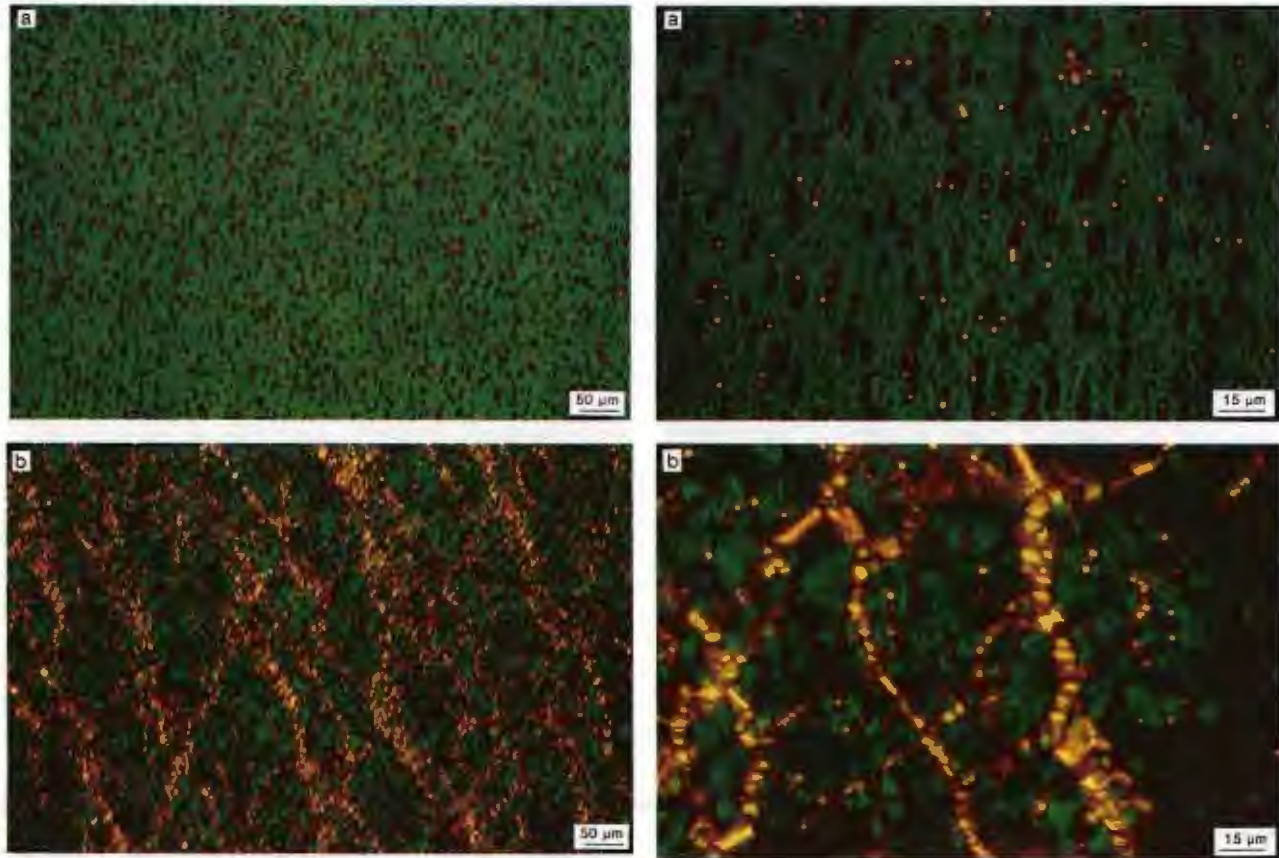


Figure 8.10 Polarized optical micrographs of strained porous PC films: (a) 0% strain; (b) 10% strain

The bright spots visible in *figure 8.10a* correspond to the holes that are aligned parallel to the direction of observation. Since the pores in these films are randomly distributed, regions with a higher pore density can be easily recognized. Straining the PC film up to 10% (see *figure 8.10b*) results in the development of a shear band type of deformation pattern. The initiation and development of these deformation bands is clearly correlated with the inhomogeneous distribution of the pores: a higher pore density results in a higher probability of a deformation band to be initiated from this position.

8.5 Conclusions

Neat and EPDM rubber-modified polycarbonate (PC) deform via shear deformation up to 60% of the theoretical draw ratio (i.e. a strain to break of 80%). Notched high-speed tensile testing of rubber-modified PC as a function of temperature reveals the occurrence of a brittle-to-ductile transition with increasing temperature. At a constant ligament thickness, T_{BT} increases upon replacing holes (i.e. non-adhering core-shell rubbery particles) by adhering EPDM rubbery particles. The model predictions of the brittle-to-tough transitions of polycarbonate are much lower than the experimentally determined values, especially in the region of high ID_c values (i.e. high temperatures).

Electron Beam (EB) irradiation of the PC/EPDM blends results in a controlled crosslinking of the dispersed EPDM rubber-phase while the PC matrix remains unaffected. The crosslinking of the rubbery phase results in a shift of T_{BT} to higher temperatures. A maximum shift of the brittle-to-ductile transition temperature (+15°C) is observed for the highest irradiation dose applied (200 kGy) independent of the rubber concentration present in the polycarbonate matrix (5 - 25 wt%). A clear correlation is established between the rubber cavitation stress (proportional to the dynamic shear modulus, G^*) and the observed T_{BT} : with increasing G^* the brittle-to-tough transition temperature increases.

Only qualitatively, the observed dependence of the brittle-to-tough transition temperature (or: critical thickness) on the rubber cavitation and/or particle interface detachment stress can be understood in terms of an increased strain energy density in the matrix ligament as a result of an increased triaxiality of the local stress state due to the presence of adhering rubbery particles compared to the situation where the matrix ligament is bordered by holes. Moreover, the matrix volume containing the

stored elastic energy is most likely to be influenced by the replacement of holes (e.g. non-adhering rubbery particles) by adhering rubbery particles. The results clearly demonstrate the necessity to comprehend the local stress state around matrix ligaments bordered by adhering elastomeric particles which can result from (multi-level) finite element calculations.

8.6 References

- 1 Van der Sanden, M.C.M., Meijer, H.E.H. and Tervoort, T.A. *Polymer* 1993, **34**, 2961
- 2 Van der Sanden, M.C.M. and Meijer, H.E.H. *Polymer*, in press
- 3 Van der Sanden, M.C.M. and Meijer, H.E.H. *Polymer*, submitted for publication
- 4 Van der Sanden, M.C.M. and Meijer, H.E.H. *Polymer*, submitted for publication
- 5 Van der Sanden, M.C.M., Meijer, H.E.H. and Lemstra, P.J. *Polymer* 1993, **34**, 2148
- 6 Van der Sanden, M.C.M., Buijs, L.G.C., De Bie, F.O. and Meijer, H.E.H. *Polymer*, submitted for publication
- 7 Grace, H.P. *Chem. Eng. Comm.* 1983, **14**, 225
- 8 Elmendorp, J.J. Ph.D. Thesis, Delft University of Technology, The Netherlands, 1986
- 9 Elemans, P.H.M. Ph.D. Thesis, Eindhoven University of Technology, The Netherlands, 1989
- 10 Borggreve, R.J.M. Ph.D. Thesis, University of Twente, The Netherlands, 1988
- 11 Borggreve, R.J.M., Gaymans, R.J. and Schuijjer, J. *Polymer* 1989, **30**, 71
- 12 Borggreve, R.J.M., Gaymans, R.J. and Eichenwald, H.M. *Polymer* 1989, **30**, 78
- 13 Parker, D.S., Sue, H.-J., Huang, J. and Yee, A.F. *Polymer* 1990, **31**, 2267
- 14 Li, D., Li, X. and Yee, A.F. *Polym. Mat. Sci. Eng.* 1990, **63**, 296
- 15 Keskkula, H., Kim, H. and Paul, D.R. *Polym. Eng. Sci.* 1990, **30** (21), 1373
- 16 Wu, S. *Polymer* 1985, **26**, 1855
- 17 Yee, A.F. *J. Mater. Sci.* 1977, **12**, 757
- 18 Van Gisbergen, J.G.M. Ph.D. Thesis, Eindhoven University of Technology, The Netherlands, 1991
- 19 Kramer, E.J. and Berger, L.L. *Adv. Polym. Sci.* 1990, **91/92**, 1
- 20 Eyring, H. *J. Chem. Phys.* 1936, **4**, 283
- 21 Zwicker, C. 'Physical Properties of Solid Materials', Pergamon, London, 1954
- 22 Tabor, D. 'Gases, Liquids and Solids', Cambridge Univ. Press, Cambridge, 1985
- 23 Donald, A.M. and Kramer, E.J. *J. Mater. Sci.* 1981, **16**, 2967
- 24 Donald, A.M. and Kramer, E.J. *J. Mater. Sci.* 1981, **16**, 2977
- 25 Bauwens-Crowet, C., Bauwens, J.C. and Homès, G. *J. Polym. Sci. (A-2)* 1969, **7**, 735
- 26 Van der Sanden, M.C.M., Meijer, H.E.H. and Lemstra, P.J. *Progr. Colloid Polym. Sci.*, in press
- 27 Ferry, J.D. 'Viscoelastic Properties of Polymers', Wiley, New York, 1980
- 28 Gent, A.N. and Tompkins, D.A. *J. Polym. Sci. (A-2)* 1969, **7**, 1483
- 29 Morbitzer, L. and Grigo, U. *Angew. Makromol. Chem.* 1988, **162**, 87
- 30 Janssen, J.M.H. Ph.D. Thesis, Eindhoven University of Technology, The Netherlands, 1993
- 31 Williams, J.G. 'Stress Analysis of Polymers', Longman, London, 1973

Chapter 9*

The Influence of Network and Microscopic Structure

9.1 Introduction

As demonstrated by Kramer et al. (see section 1.5), a *systematic* investigation on a wide variety of different types of polymers can result in a clear understanding of the strain to break (read: toughness) of amorphous glassy polymers from a molecular point of view, on at least a microscopic scale such as the craze extension ratio and the draw ratio in a shear deformation zone. The network density is the key parameter in these investigations since with a decreasing network (entanglement and/or crosslink) density both the theoretical and the experimental **microscopic** draw ratio strongly increase. Intriguing in this context is that routes towards other ultimate properties like stiffness and strength, at least for flexible semi-crystalline polymers like polyethylene, also fully depend on the on the drawability of the network. Analogously, in the search for the ultimate toughness the maximum attainable draw ratio can be chosen as a discriminating parameter since toughness can be roughly defined as the product of deformation stress and strain to break. The first parameter is relatively constant within the class of amorphous glassy polymers, while the latter shows some apparent contradictions; since on a macroscopic scale the experimental strain to break is in most cases more than two decades lower than the maximum strain of the molecular network. Strikingly in this context is the theoretical draw ratio of polystyrene (PS) that equals 320% and is experimentally verified by Kramer et al. on a microscopic scale to be 300% (see section 1.6), while macroscopically the strain to break of polystyrene roughly equals only 1-3%.

* This chapter is reproduced, in part, from:

1. Van der Sanden, M.C.M., Meijer, H.E.H. and Lemstra, P.J. *J. Coll. Pol. Sci.* 1993 in press
2. Van der Sanden, M.C.M., Moonen, H.H.P., Jansen, B.J.P. and Meijer, H.E.H. *Polymer* 1993, in preparation

In the research discussed in this thesis these discrepancies were investigated and a universal approach for the macroscopic toughness of amorphous polymeric systems was aimed at using a systematic experimental approach covering the complete class of polymeric networks. This approach has resulted in a possibility to estimate the ultimate toughness of polymeric systems and a theory that is capable of defining directions for further research in the development of controlled toughness.

9.2 The Phenomenon of a Material-Specific Critical Thickness

While the large microscopic draw ratio is found on the scale of local deformation mechanisms such as craze fibrils or shear deformation zones, the low macroscopic draw ratio is operative on a scale of a few millimetres. Hence, a decrease of the macroscopic sample dimensions should eventually result in an increase of the macroscopic strain to break. In chapter 2 of this thesis, the macroscopic dimensions of PS have been decreased in one (thin films) or two dimensions (ligaments). Both approaches finally resulted in a sharp increase of the macroscopic strain to break at a certain critical thickness of less than $1\ \mu\text{m}$. Below this critical size, either given by the film thickness or by the average distance between the added non-adhering rubbery particles, the macroscopic draw ratio reaches values comparable with the theoretical strain to break (see *figure 9.1*, network density of $3 \times 10^{25}\ \text{chains m}^{-3}$).

In chapters 3 and 4 of this thesis both the network density dependence of the critical thickness and the maximum macroscopic toughness (strain to break) were investigated for the class of thermoplastic and thermosetting polymers, respectively. The results of these experiments and the corresponding theoretical curves are summarized in *figures 9.1* and *9.2*.

The macroscopic draw ratios below the material-specific critical thickness clearly fit the broken curve given by 60% of the theoretical draw ratio (see *figure 9.1*). Obviously, the maximum macroscopic toughness is influenced by the existence of a distribution in network densities (any other network arguments only would lead to higher predicted values). For a given network density, the maximum draw ratio is independent of the type of network as physical entanglements and chemical crosslinks both act as 'nodes of enhanced friction' on the time scale of a deformation process (typically a few seconds or less), and no chain slippage and/or disentanglement can occur at the testing temperatures applied.

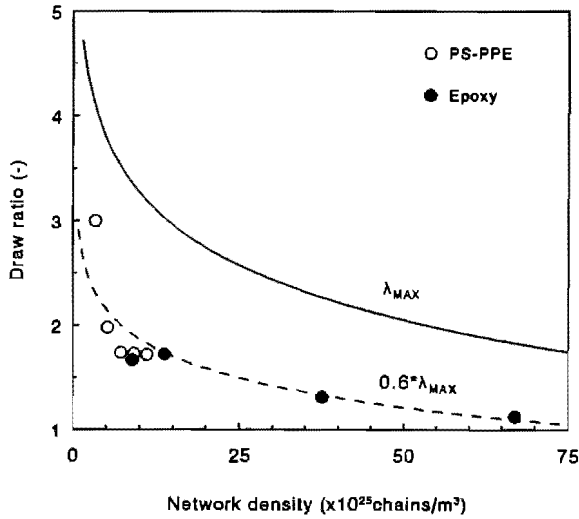


Figure 9.1 Draw ratio versus network density (entanglement and/or crosslink density). For details, see text

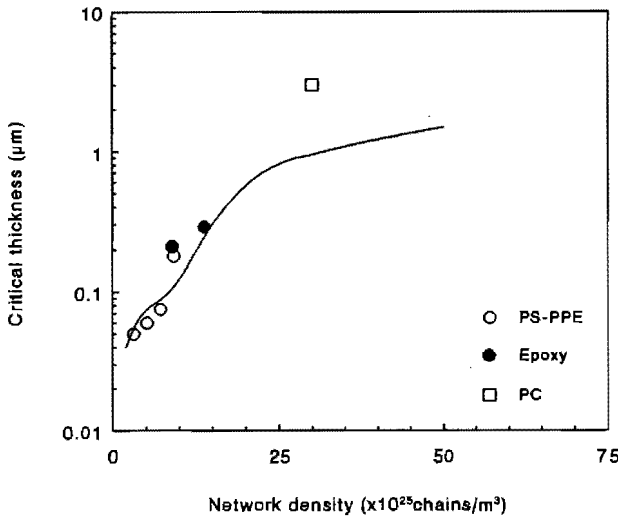


Figure 9.2 Critical thickness versus network density (entanglement and/or crosslink density). For details, see text

Similar to the maximum macroscopic draw ratio, the critical thickness is dependent on the network density of the polymer. With an increasing network density the critical thickness, below which the maximum degree of macroscopic ductility is observed, increases (see figure 9.2). Given the intrinsically time- and temperature-dependent

response of polymeric materials, for all thermosetting and for some of the more densely entangled thermoplastic polymers this critical thickness could only be determined under severe testing conditions like a notched high-speed impact test conducted at low temperatures.

The physical explanation for the occurrence and network density dependence of a critical dimension was given in chapter 3 and originates from an energy based criterion for brittle fracture assuming that deformation will always be initiated locally. The stored elastic energy within a matrix ligament is compared with the required fracture surface energy to generate a brittle fracture of this ligament. If the stored elastic energy equals, or is higher than, the fracture surface energy required, brittle fracture will occur locally and extend throughout the complete sample; if the stored elastic energy is lower than the fracture surface energy, a macroscopic ductile fracture behaviour occurs. The results of the most simplified calculations concerning this fracture criterion were already shown in *figure 9.2*: full curve. Given the simplicity of the model a surprisingly good correlation is observed between the predicted values and the experimental data. Extrapolation of the predicted curve to network densities of 200×10^{25} chains m^{-3} (typical for standard crosslinked thermosetting polymers) reveals that the critical thickness of these samples is of the order of a few micron. Hence, the addition of only a few percent of rubber to these systems already results in their maximum macroscopic toughness. However, the absolute toughness of this class of materials is of course limited.

The influence of extrinsic parameters on the value of the critical thickness could be relatively well understood on basis of the energy based criterion proposed. Via the well-known temperature and strain rate dependence of (mainly) the yield stress, the critical thickness could be predicted (see chapters 5 and 8). As an example, in *figure 9.3* the temperature and strain rate dependence of the critical thickness is shown for various polymers with a different network density (ν).

With an increasing temperature and a decreasing strain rate the critical thickness strongly increases. This is experimentally verified for the thermoplastic polystyrene-poly(2,6-dimethyl-1,4-phenylene ether) (chapter 5) and polycarbonate (chapter 8) model systems. Polymers with a network density higher than 11×10^{25} chains m^{-3} only reveal a brittle-to-ductile transition under relatively severe testing conditions.

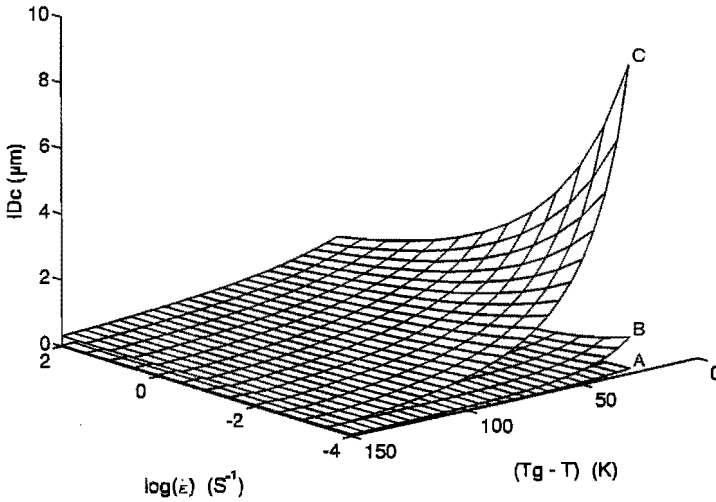


Figure 9.3 Model predictions of the critical ligament thickness as a function of temperature and strain rate: $\nu = (A) 3 \times 10^{25}$; $(B) 30 \times 10^{25}$; $(C) 300 \times 10^{25}$ chains m^{-3}

In practice, the final local ligament thickness is often the result of a (compatibilized) melt-mixing process resulting in adhesion between the two distinct phases. The presence of adhesion between the dispersed rubbery phase and the matrix influences the local stress state in the ligament. Therefore, a significant influence of the degree of adhesion and/or cavitation stress of the rubbery particle on the value of the critical thickness was found, see figure 9.4. The decreased cavitation stress as indicated by the dynamic shear modulus of the rubbery phase results in an increase of the critical thickness at a given temperature or, alternatively, for a given ligament thickness, in a decrease of the brittle-to-tough transition temperature. Qualitatively, the influence of particle/matrix interface detachment, and/or particle cavitation, stress could be understood on basis of the naive energy based model, although only a detailed micromechanical analysis can result in a more quantitative prediction of the critical thickness for these situations.

These experiments clearly demonstrate the positive influence of a decreased cavitation stress of the elastomeric filler and the beneficial absence of adhesion between the elastomer and the matrix in obtaining the ultimate toughness. This in clear contrast with earlier findings (see section 1.7.2) if only an intermediate toughness is pursued, e.g. via the introduction of a multiple crazing mechanism, where

improved adhesion can influence the macroscopic toughness in a favourable manner. The optimal particle sizes reported for craze-deforming materials (see section 1.7.2) are not relevant with respect to the ultimate toughness of amorphous polymers, since in principle no limitations exist for a minimum hole size in the ultimate toughening concepts presented here.

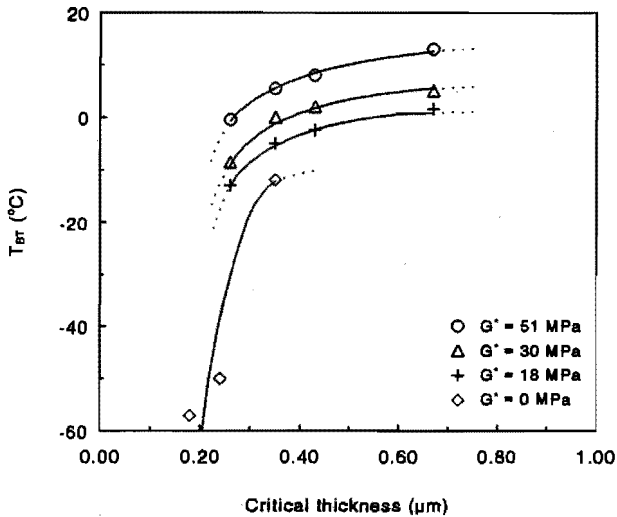


Figure 9.4 Brittle-to-tough transition temperature (T_{BT}) of PC/rubber blends versus the critical thickness of PC (parameter: the dynamic shear modulus of the dispersed rubbery phase)

9.3 Polystyrene Sub-micron Engineering Foam

Based on the above understanding of ultimate macroscopic toughness the elegance of developing sub-micron, or even nano-sized, polymeric structures emerges. One of the most brittle of all amorphous polymers, polystyrene, manifests itself as a very ductile polymer below a local thickness of $0.05 \mu\text{m}$ (see figures 9.1 and 9.2). This offers a challenging perspective in developing macroscopically tough polystyrene by adding holes in order to create the required (local) critical thickness. Generally foams are materials with low stiffness and strength that are not very tough. This is due to the too large cell diameters used. In figure 9.5 the foam density of polymers is plotted versus the cell diameter for different values of the (critical) intercellular distance.

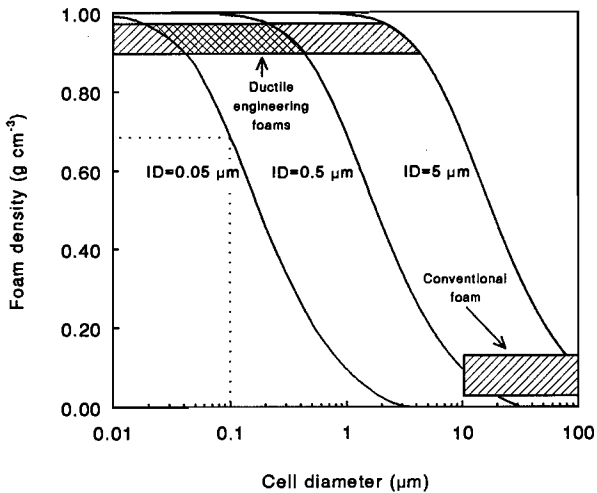


Figure 9.5 Foam density as a function of the cell diameter for different values of the critical intercellular distance (according to equation (8.1))

Traditional PS foams possess typical cell diameters of $50 \mu\text{m}$, gas volume fractions of 95 vol%, consequently densities of 0.05 g cm^{-3} (50 kg m^{-3}), and therefore wall thicknesses of a few micron or larger. Consequently, they do not show any ductile macroscopic properties knowing that the critical thickness for PS is $0.05 \mu\text{m}$ (see figure 9.5). Only the development of PS foam with cell diameters smaller than $0.1 \mu\text{m}$ can result in extremely ductile foam-like structures, without a considerable loss of stiffness (i.e. concentrations of gas lower than 30 vol%). Logically, a lower limit exists in the cell size that can be applied, since, finally, on a molecular scale also density fluctuations exist while most amorphous glassy polymers do not reveal a macroscopic ductile fracture behaviour as a consequence of these (locally) thin ligaments. The curve corresponding to a wall thickness of $0.5 \mu\text{m}$ (figure 9.5) is valid for the typical critical thickness of polycarbonate at low temperatures under notched high-speed impact conditions (see chapters 3 and 8), while the $5 \mu\text{m}$ curve corresponds to relatively densely crosslinked thermosets.

In order to investigate toughness of these sub-micron foams, e.g. for PS, a new method to produce these foams has been explored based on the use of a physical blowing agent (glycerol) that (i) can be very finely distributed in the PS matrix with the aid of a compatibilizer (maleic anhydride modified ethylene-propylene/

polystyrene block copolymer) and (ii) can be subsequently selectively evaporated using microwave irradiation (1 minute, at a microwave source of 500 Watt). The cell sizes and wall thicknesses are manageable via an independent and accurate control of the temperature of the PS matrix close to the glass transition temperature, thus allowing the necessary flow but preventing unwanted coalescence. *Figure 9.6* shows some preliminary results using this method.

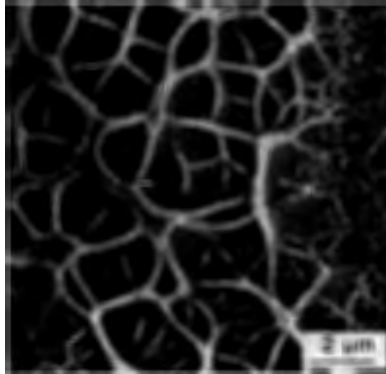


Figure 9.6 Scanning electron micrograph of a cryogenically fractured, foamed PS sample (using glycerol as a blowing agent) foaming time: 1 minute

The process is not yet fully optimized and the fracture surface reveals a too large distribution in cell sizes (see *figure 9.6*). Consequently, these structures do not reveal the maximum macroscopic ductile fracture behaviour yet. However, this technique provides a first step in the development of sub-micron foam-like structures and further research in our laboratory is aimed at its improvement.

Summary

Ultimate properties of polymeric materials (stiffness, strength and toughness) are major topics of research. Nowadays, ultimate stiffness and strength can be directly related to the structure and arrangement of molecular chains and are experimentally confirmed for a selected range of polymers.

A thorough understanding of the parameters governing the ultimate macroscopic toughness of amorphous glassy polymers, however, was still lacking.

Toughness is, in a first approximation, proportional to the total energy involved in deformation up to fracture, i.e. the area under the stress-strain curve. Since the stress at which amorphous glassy polymers deform is within the limited range of 50-80 MPa and the strain to break varies in a much wider range (1-150%), the strain to break can be used as a discriminating parameter. On a microscopic level (i.e. inside deformation areas) a satisfying correlation has been established between the local strain and the strain to break based on stretching the molecular network to its full extension. The molecular network is characterized by the molecular weight between nodes of enhanced friction, i.e. entanglements for thermoplastic polymers and crosslinks for thermosetting polymers. On a macroscopic scale the strain to break is often two decades below the expected strain to break. This paradox is the issue for this thesis.

In this study, the concept of a *critical thickness* is introduced below which amorphous glassy polymers deform up to their maximum draw ratio (read: toughness) given by their equilibrium polymer-specific molecular network density. A decrease of the sample dimensions in one (thin films) or two (thin ligaments) dimensions results in a sharp increase of the macroscopic strain to break up to a value comparable with the draw ratio (λ_{\max}) of the molecular network. For example, the strain to break of polystyrene (PS) can be increased from 1% up to 200% by decreasing the (local) specimen size below 0.05 μm . The (local) specimen dimensions can be easily controlled via the use of thin films (separated by non-adhering spacers) or by the introduction of (preferably) non-adhering rubbery particles. The average distance

between the rubbery particles determines the local thickness in the latter case. Below the critical thickness, all amorphous glassy polymers deform via shear yielding, as demonstrated with tensile dilatometry.

An explanation for the phenomenon of a critical thickness is postulated based on an energy criterion for brittle fracture. If deformation is initiated locally, deformation will continue throughout the complete sample only if catastrophic fracture of fibrillated ligaments is prohibited anywhere in the sample. Decreasing the size of the sample finally results in an equilibrium between the stored elastic energy in the sample (i.e. ligament) and the (brittle fracture) surface energy of the fibrillated sample (ligament) which is deformed up to λ_{\max} . A further decrease of the ligament thickness prohibits brittle fracture of the fibrillated ligament for the testing conditions applied. Hence, macroscopically ductile deformation behaviour prevails and ultimate toughness is obtained.

The critical thickness (ID_c) has been experimentally determined for a wide range of thermoplastic and thermosetting polymers and proves to be highly dependent on the molecular network density showing no differences between the two types of networks, which can be understood from the typical time-scale of the experiments. ID_c varies from 0.05 μm for polystyrene (low network density) up to a few micron for relatively densely crosslinked thermosets. This material-dependent critical thickness can be quantitatively understood from the energy-based criterion via the network density dependence of (i) the natural draw ratio (λ_{\max}) and (ii) the brittle fracture surface energy.

The influence of extrinsic variables on the absolute value of the critical thickness can be predicted relatively easy via a strain rate and temperature dependence of the yield stress and Young's modulus of the amorphous glassy polymer.

Any adhesion between the matrix and the dispersed elastomer added to create the desired local thickness in most practical (melt-mixed) systems (lowering of interfacial adhesion), and any subsequent increase in the elastomer cavitation stress, influence the value of the critical thickness in an unfavourable manner: the critical thickness decreases with an increasing degree of adhesion and/or cavitation stress of the elastomer or, alternatively, the brittle-to-tough transition temperature shifts to higher temperatures at a constant ligament thickness.

Based on these findings one of the most ductile amorphous glassy polymers proves to be polystyrene that reveals its ultimate ductility in a non-adhering holey morphology only if the local thickness is below the critical value of $0.05 \mu\text{m}$. Hence, the development of sub-micron foam-like structures based on PS offer a challenging prospect in confirming the findings in this thesis. An onset towards the development of these nano-sized structures has been made.

Samenvatting

De uiterste stijfheid, sterkte en taaigheid zijn al geruime tijd speerpunten in het onderzoek naar polymeren of polymere materialen. Terwijl experimenteel en modelmatig is aangetoond dat stijfheid en sterkte gekorreleerd kunnen worden aan de moleculaire structuur en ordening van polymeerketens, ontbreekt een eenduidig begrip van de parameters die de uiterste taaigheid en slagvastheid van polymeren bepalen.

De mate waarin materialen meer of minder taai zijn is in eerste benadering evenredig met de hoeveelheid opgenomen energie tijdens deformatie tot breuk, dus met het oppervlak onder de spannings-*rek* curve. De spanning waarbij polymeren plastisch deformerend varieert slechts binnen een beperkt gebied van 50 tot 80 MPa, terwijl de *rek-bij-breuk* orden van grootte kan verschillen. Vandaar dat *rek*, in eerste instantie, als een indicatie voor taaigheid beschouwd kan worden. Op mikroskopische schaal is in de deformatiegebieden een opmerkelijk goede overeenkomst gevonden tussen de gemeten maximale *rek* en die gebaseerd op het volledig verstrekken van het moleculaire netwerk, gekarakteriseerd door het molekuulgewicht tussen netwerkknooppunten: fysische verstrengelingen voor thermoplasten en chemische verknoppingen voor thermoharders.

In dit onderzoek wordt het concept van een *kritische dikte* geïntroduceerd waarbeneden alle amorfe glasachtige polymeren maximaal deformerend tot hun natuurlijke verstrekkingsgraad, gegeven door de polymeer-specifieke evenwichtsnetwerkdichtheid, bereikt is. Een lokale verlaging van de afmetingen van de testmonsters in één (dunne films) of twee (ligamenten) dimensies resulteert in een scherpe toename van de makroskopische *rek-bij-breuk* tot een waarde welke vergelijkbaar is met de natuurlijke verstrekkingsgraad van het polymere netwerk (λ_{\max}). Zo kan bijvoorbeeld de *rek-bij-breuk* van polystyreen (PS) verhoogd worden van 1% tot 200% door een verlaging van de (lokale) monstergrootte tot beneden 0.05 μm , gekontroleerd door het toepassen van dunne films (gescheiden door niet-hechtende tussenlagen) of door het innemen van, bij voorkeur niet-hechtende, rubberdeeltjes (resulteert in dunne ligamenten). De gemiddelde afstand tussen de rubberdeeltjes

bepaalt in het laatste geval de lokale dikte. Beneden de kritische dikte, gaat de enorme rektoename gepaard met een verandering in deformatiemechanisme en deformerende alle amorfe glasachtige polymeren in afschuiving. Dit is aangetoond met metingen van de relatieve volumeverandering tijdens rekdeformatie.

Een verklaring voor het bestaan van een kritische dikte is opgesteld gebaseerd op een energie-kriterium voor brose breuk. Lokaal geïnitieerde deformatie kan alleen door het gehele monster plaatsvinden wanneer breuk in elk van de tot fibril gedeformeerde ligamenten wordt voorkomen. Een verlaging van de monsterdimensies resulteert uiteindelijk in een balans tussen de -lokaal- opgeslagen elastische energie in een ligament en de (brosse breuk) oppervlakte-energie in het reeds tot λ_{\max} -gerekte daarmee verbonden fibril. Een verdere verlaging van de ligamentdikte voorkomt brose breuk van fibrillen onder alle experimenteel toegankelijke testomstandigheden. Hierdoor wordt er makroskopisch een duktiële deformatie waargenomen en wordt de ultieme taaiheid behaald.

De kritische dikte (ID_c), welke voor een groot aantal thermoplastische en thermohardende polymeren experimenteel is bepaald, is sterk afhankelijk van de netwerkdichtheid en onafhankelijk van het type netwerk. Dit laatste kan worden begrepen uit het feit dat op de typische tijdschaal van een deformatietest geen ontarring van ketens kan plaatsvinden waardoor fysische verstrengelingen en chemische knooppunten in een netwerk zich identiek gedragen. ID_c varieert van $0.05 \mu\text{m}$ voor polystyreen (lage netwerkdichtheid) tot een aantal micrometers voor relatief hoogvernette thermoharders. De materiaalafhankelijkheid van de kritische dikte kan kwantitatief worden begrepen op basis van het energiekriterium voor brose breuk via een netwerkdichtheid-afhankelijkheid van (i) de natuurlijke verstrekkingsgraad (λ_{\max}) en (ii) de oppervlakte-energie.

De invloed van extrinsieke variabelen op de absolute waarde van de kritische dikte kunnen relatief eenvoudig voorspeld worden via een reksnelheid- en temperatuur-afhankelijkheid van de vloeispanning en Young's modulus van het amorfe glasachtige polymeer.

Bij blends die via een smeltmengproces worden gerealiseerd is voor een goede verdeling en verkleining van de (rubber)fase in de matrix, die wordt toegevoegd om (lokaal) de ligamentdikte in te stellen, een goede interactie tussen disperse fase en

matrix wenselijk (verlaging grensvlakspanning). Echter, deze interactie tussen de matrix en de disperse rubberfase, en een eventuele verhoogde cavitatiespanning van de rubberfase, beïnvloeden de waarde van de kritische dikte in ongunstige zin: de kritische dikte (ID_c) neemt af bij gelijke bros-taai overgangstemperatuur (T_{BT}) met een toenemende mate van hechting en/of cavitatiespanning van de rubberfase (ofwel omgekeerd: T_{BT} neemt toe bij een konstante ID).

Op basis van dit onderzoek blijkt dat polystyreen intrinsiek een van de meest duktiele amorge glasachtige polymeren is. De ultieme taaiheid van dit polymeer wordt echter op een makrosopisch niveau uitsluitend verkregen wanneer het materiaal gevuld is met een groot aantal niet-hechtende rubberdeeltjes, waarbij de gemiddelde lokale interdeeltjesafstand beneden de kritische waarde van $0.05 \mu\text{m}$ is. In dit perspectief vormt de ontwikkeling van een fijncellige schuimstructuur met celwanddikten kleiner dan 1 micrometer, een uitdaging teneinde de konklusies van dit onderzoek te bevestigen. De ontwikkeling van deze structuren op nanometerschaal is geïnitieerd.

Acknowledgements

I would like to thank all those who have contributed to the realization of this thesis: In particular, I am grateful to both my promotors, Prof. Han Meijer and Prof. Piet Lemstra, who have given me the opportunity to initiate and complete this thesis work. I have enjoyed their stimulating and creative way of thinking, which for certain, have marked the directions of research. Dr. Rein Borggreve is acknowledged for his critical comments not only during the preparation of the manuscript of this thesis, but also during the development of the research projects on which this thesis is based on.

Special gratitude is addressed to the graduate students that performed the major part of the experimental work described in this thesis: Peter Adriaansen, François de Bie, Jeroen Crevecoeur, Robert van Deursen, Stefan Dusée, Sascha van Etten, Bernd Jansen, Peter Koets, Johan Kuypens, Hélène Moonen, Rob Schulkes and Irene Tauber. Louison Buijs is acknowledged for his enthusiastic cooperation and assistance during his postgraduate education course at the Institute for Continuing Education ('AIO-2 onderzoekersopleiding'). Prof. Jan Bussink, Leon Govaert, John de Kok and Theo Tervoort are gratefully acknowledged for their valuable comments and remarks during the numerous discussions that have taken place during this thesis work. Many thanks to Herman Ladan and Gerard Schepens for their kind assistance in the field of (SEM)photography.

Prof. Ed Kramer of the Department of Materials Science and Engineering and the Materials Science Center of Cornell University (Ithaca) is acknowledged for his inspiring enthusiasm during a number of discussions and his comments on the interpretation of the experimental work and help with the subsequent modelling.

Profs. Eric Baer and Anne Hiltner from the Center for Applied Polymer Research (CAPRI) at the Case Western Reserve University in Cleveland are gratefully acknowledged for providing the necessary facilities in the field of in-situ visualization of deformation processes.

Prof. Robert Legras and Dr. Etienne Ferain of the Université Catholique de Louvain,

Belgium, are acknowledged for providing the Cyclopore® membranes.

Special thanks to Prof. Derek Heikens who has introduced me into the complex field of fracture mechanics during many of his private lectures especially during the initial stage of the research project described in this thesis.

Finally, I want to thank my family and friends, and in particular Margot, for supporting me during this thesis work.

This research has partly been sponsored by the Foundation for Polymer Blends (SPB).

Curriculum Vitae

The author of this thesis was born in Valkenswaard, The Netherlands, on January 10th, 1966. After finishing secondary school in 1984 (Atheneum-B, Hertog Jan College, Valkenswaard), he studied Chemical Technology at the Eindhoven University of Technology, The Netherlands. In 1989 he obtained his Master Degree, Cum Laude, after completing a thesis report on electron beam irradiation of polymer blends under supervision of Prof.dr. P.J. Lemstra.

In the same year he entered a Ph.D. program in Materials Science at the Centre for Polymers and Composites (CPC) at the Eindhoven University of Technology under supervision of Prof.dr.ir. H.E.H. Meijer. This centre introduced the author into the necessary disciplines, i.e. chemistry and mechanical engineering, required to complete the study presented in this thesis.

As from January 1994, the author will join the research group of Prof.dr. A.J. Heeger and Prof.dr. P. Smith at the University of California, Santa Barbara (UCSB) where he will be active in the field of optical and electrical conductive polymers.

Stellingen

behorende bij het proefschrift

Ultimate Toughness of Amorphous Polymers

van Marco van der Sanden

1. De uiterste taatheid van polymere materialen wordt slechts door twee parameters bepaald: de netwerkdichtheid en de kritische dikte.
Dit proefschrift.
2. Lucht is de optimale slagvastheidsverbeteraar voor polymeren. Voor dit type disperse fase geldt geen zogenaamde optimale deeltjesdiameter zoals gerapporteerd door Wu en Dijkstra et al. Derhalve kan met behoud van stijfheid en sterkte ultieme taatheid worden verkregen op makroskopische schaal.
Dit proefschrift, Hoofdstukken 8 en 9
Wu, S. *Polym. Eng. Sci.* 1990, 30 (13), 753
Dijkstra, K., Oostenbrink, A.J. and Gaymans, R.J. Proc. 8th Int. Conf. 'Deformation Yield and Fracture of Polymers', Cambridge, 1991, p.39.1
3. Een optimum in slagvastheid zoals waargenomen door Murakami et al. voor rubber-gemodificeerde epoxiden is misleidend, omdat de afname in slagvastheid met een toenemend molekulgewicht tussen verknopingen veroorzaakt wordt door het feit dat het materiaal lokaal niet beneden de kritische dikte is. Wanneer een amorf glasachtig polymeer (lokaal) beneden de kritische dikte is wordt een toenemende taatheid waargenomen met een toenemend molekulgewicht tussen netwerkverknopingen.
Murakami, S., Watanabe, O., Inoue, H., Ochi, M., Shiraishi, T. and Shimbo, M. *Polymer* 1992 33 (3), 572
Dit proefschrift, Hoofdstuk 4
4. De door Wu voorgestelde optimale entanglementdichtheid voor een maximale slagvastheid is onjuist, daar ultieme taatheid van amorge glasachtige polymeren slechts verkregen wordt wanneer het materiaal volledig via afschuiving deformeert. Dit laatste wordt slechts bereikt wanneer het materiaal (lokaal) voldoende dun is (beneden de kritische dikte).
Wu, S. *Polymer International* 1992, 29, 229
Dit proefschrift, Hoofdstuk 9
5. De relatief lage dichtheid van poly(hydroxyboterzuur) (PHB) granules in de *Alcaligenes eutrophus* bacterie, wordt, in tegenstelling tot de bewering van Mas et al., niet veroorzaakt door de aanwezigheid van 40% water maar door het feit dat PHB amorf is.
Mas, J., Pedrós-Alió, C. and Guerrero, R. *J. Bacteriol.* 1985, 164, 749
De Koning, G.J.M. and Lemstra, P.J. *Polymer* 1992, 33, 3292

6. Bij het dispersief mengen van niet-mengbare vloeistof-vloeistof systemen zijn tijdschalen van essentieel belang. Quasi-evenwichtsbeschouwingen, zoals het kritisch capillair getal waarbij een gedispergeerde druppel juist breekt, zijn slechts van beperkte waarde.
Grace, H.P. *Chem. Eng. Comm.* 1982, **14**, 225
Janssen, J.M.H. and Meijer, H.E.H. *J. Rheol.* 1993, **37** (4), 597
7. Het optimum in rek-bij-breuk zoals waargenomen door Argon et al. voor polystyreen/polybutadieen-rubber blends bij 1.1 gew.% rubber komt, merkwaardig genoeg, niet overeen met later door dezelfde groep gepubliceerde data waar het optimum is verschoven naar 4 gew.% rubber.
Gebizlioglu, O.S., Beckham, H.W., Argon, A.S., Cohen, R.E. and Brown, H.R. *Macromolecules* 1990, **23**, 3968
Spiegelberg, S.H., Argon, A.S. and Cohen, R.E. *J. Appl. Polym. Sci.* 1993, **48**, 85
8. Omdat men in de literatuur kan vinden dat polystyreen onder invloed van elektronenbestraling kan vernetten, onveranderd blijven of zelfs degraderen, afhankelijk van de experimentele uitvoering is een uitgebreide en vooral volledige beschrijving van het experimentele gedeelte van een wetenschappelijke publikatie uitermate belangrijk.
Henke, C.S. and Kramer, E.J. *J. Polym. Sci., Polym. Phys. Edn.* 1984, **22**, 721
Van Gisbergen, J.G.M., Proefschrift Technische Universiteit Eindhoven, 1991
9. De door Huang et al. gepresenteerde dynamisch mechanische thermische analyse van ionomeren gebaseerd op poly(2,6-dimethyl-1,4-phenyleen ether) is van twijfelachtige kwaliteit aangezien de pers-stap bij de monstervoorbereiding beneden de glasovergangstemperatuur van het ionomeer plaatsvindt.
Huang, Y., Cong, G. and MacKnight, W.J. *Macromolecules* 1986, **19**, 2267
10. Een vergelijking van het huidige maximale aantal netwerkpunten van kunstmatige neurale netwerken met het aantal cellen in de hersenen van een regenworm is typerend voor de lange weg welke de wetenschap nog heeft af te leggen voordat het menselijke niveau van intelligentie kunstmatig benaderd zal worden.
Egberts, J., De Graaf, J. en Ruigt, G. *Chemisch Magazine* 1993, **9**, 387
11. Door het toenemende gebruik van computers is de betekenis van het woord 'experiment' in sterke mate uitgebreid.